THERMODYNAMICS AND REACTION KINETICS DURING MECHANOCHEMICAL SYNTHESIS AND ENVIRONMENTAL TESTING OF LANTHANIDE AND ACTINIDE REFRACTORY MATERIALS

by

Gordon Andrew Alanko

A dissertation

submitted in partial fulfillment

of the requirements for the degree of

Doctor of Philosophy in Materials Science and Engineering

Boise State University

May 2014

BOISE STATE UNIVERSITY GRADUATE COLLEGE

DEFENSE COMMITTEE AND FINAL READING APPROVALS

of the dissertation submitted by

Gordon Andrew Alanko

Dissertation Title: Thermodynamics and Reaction Kinetics During Mechanochemical Synthesis and Environmental Testing of Lanthanide and Actinide Refractory Materials

Date of Final Oral Examination: 08 May 2014

The following individuals read and discussed the dissertation submitted by student Gordon Andrew Alanko, and they evaluated his presentation and response to questions during the final oral examination. They found that the student passed the final oral examination.

Darryl P. Butt, Ph.D.	Chair, Supervisory Committee
Dmitri Tenne, Ph.D.	Member, Supervisory Committee
Janelle Wharry, Ph.D.	Member, Supervisory Committee
Paul A. Lessing, Ph.D.	External Examiner

The final reading approval of the dissertation was granted by Darryl P. Butt, Ph.D., Chair of the Supervisory Committee. The dissertation was approved for the Graduate College by John R. Pelton, Ph.D., Dean of the Graduate College.

DEDICATION

This dissertation is dedicated to my wife, Bethany, and my little daughter Corinne. Beth, you have always stood by your vow to support me in my interests and to grow and learn alongside me. I was happy to share this time with you, and perhaps now I will have more time to share. Corinne, you may not know it yet, but your love of learning and discovery helped to drive me as I worked to finish this dissertation. You have so much left to learn and discover, and I hope you will always find the same joy that you experience in it now.

ACKNOWLEDGEMENTS

Each graduate student builds but few bricks upon the foundation constructed by their predecessors. Here I wish to acknowledge the foundation on which rests the last several years of study and research, and some of the key individuals who inspired, encouraged, challenged, and supported me along the way.

Dr. Alex Punnoose and Aaron Thurber were the first to pique my interest in fundamental scientific research. Dr. Will Hughes encouraged my decision to enter graduate study, and gave of his valuable time as a mentor and proof reader as I applied to graduate programs and fellowships.

My committee members, Dr. Dmitri Tenne, Dr. Janelle Wharry, and Dr. Paul Lessing were generous of their time and advice as I pursued many topics of interest to me. Under my advisor Dr. Darryl Butt, my graduate experiences have covered a range from armor to anthropology to nuclear materials. I could not have imagined the future scope of my studies at their outset, and the space of a single dissertation would not do justice to the breadth and depth of inquiry to which I have been exposed.

Much of the research described in the following pages grew out of a collaborative project between Boise State University, the University of Wisconsin-Madison, the Idaho National Laboratory, and Westinghouse Electric Company, funded by the Department of Energy (NEUP #00120690). Many individuals at these and associated institutions made important contributions to this work, especially Dr. Mitch Meyer, Dr. Jason Harp, and

Dr. Paul Lessing (INL), Dr. Rob O'Brian (INL-CSNR), Brian Jaques, Bryan Forsmann and Daniel Osterberg (BSU), Dr. Peng Xu and Dr. Edward Lahoda (Westinghouse), and Kolton Urso and Dr. Beata Tyburska-Püschel (UW-M), and I would like to thank each of these individuals for their time and involvement in my research.

Finally, I'd like to thank my wife and the rest of my family and close friends for their support. You made this journey both easy and enjoyable.

ABSTRACT

High energy ball milling is a broad family of well-known techniques for materials processing that includes mechanochemical synthesis, in which the milled materials react during milling. The latter may involve components reacting in the solid, liquid, or gas phases, and the operative kinetics have hardly been studied. Several manufacturers of high energy ball mills have recently made available instrumented milling vessel lids. These lids are able to monitor the temperature of the lid and the gas pressure within the vessel *in situ* during milling experiments. This ability is a significant improvement over the ad hoc instrumentation setups sometimes discussed in literature, and enables a level of precision in investigating milling processes not available previously.

This dissertation describes work done investigating the mechanochemical synthesis and compound formation in the Ce-Si, Ce-S, U-Si, and Dy-N systems, including the thermodynamic and kinetics processes that govern mechanochemical synthesis of these materials. Particular attention is devoted to two distinct mechanochemical phenomena. The first process is a fast reaction that occurs after a characteristic milling time, termed mechanically-induced self-propagating reaction (MSR). This behavior is sometimes observed during milling of the elemental constituents of compounds with a high enthalpy of formation. The second process is compound formation during milling of elemental metals in reactive gasses such as oxygen, nitrogen, or hydrogen. Mechanochemical synthesis experiments have been conducted while

monitoring the temperature and pressure of the milling vessel *in situ* to gain insight into the reaction kinetics. A new approach to analyzing this data in conjunction with simple physical models of the milling mechanics has been developed.

The effects of compound formation on the system geometry and energy transfer were assessed by experiment. The kinetics model explicitly considers milling energy and energy transfer to form chemically active surface site generation, and should be applicable to many systems involving gas reactions with ductile solids. Furthermore, the model allows for the incorporation of thermally activated kinetics if appropriate experimental data is available.

The results discussed in this dissertation are drawn from four research papers submitted or accepted by peer-reviewed journals. Several unique phenomena are observed due to a recently developed capability for in situ monitoring of temperature and pressure during milling. As such, this dissertation represents several significant steps forward in the understanding of the processes occurring during mechanochemical synthesis.

TABLE OF CONTENTS

LIST OF TABLES

LIST OF FIGURES

LIST OF ABBREVIATIONS

EDS	Energy-dispersive Spectrometry
HEBM	High energy ball milling
MSR	Mechanically-induced Self-propagating Reaction
RM	Reactive milling
SEM	Scanning Electron Microscopy
XRD	X-ray Diffraction

CHAPTER ONE: INTRODUCTION

This dissertation is composed of four papers accepted by or in the submission process to four journals. Chapter Two has been accepted by the Journal of Nuclear Materials and describes the preparation of uranium silicides by mechanochemical means. Chapter Three has been submitted to the Journal of Alloys and Compounds and describes the preparation of cerium silicides by mechanochemical means, provides a model to predict phase formation, and describes silicide powder densification by spark plasma sintering. Chapter Four has been accepted as a rapid communication by the Journal of the American Ceramics Society and describes the preparation of cerium monosulfide, an important refractory, by mechanochemical means. Chapter Five has been submitted to the Journal of Alloys and Compounds and describes the development of a milling kinetics model to describe the reactive gas-solid milling of dysprosium nitride. An additional paper appears in Appendix A and describes the experimental preparation of dysprosium nitride and the data reduction procedure employed to obtain the data discussed in Chapter Five. Each of the following chapters in this dissertation was written as a journal publication intended to stand alone on its merits. However, each chapter is connected by the common theme of mechanochemical synthesis conducted with in situ monitoring of the reaction conditions.

Mechanochemical synthesis involves the initiation or rate acceleration of chemical reactions by applied mechanical energy, and has been practiced now for

thousands of years [1]. More recently, higher energies and more frequent applications thereof through high velocity impacts have been obtained during high energy ball milling (HEBM). The technique of HEBM was developed in the 1960s as a means of mixing steel powders with ultrafine oxide particles to aid in strengthening the steel, and has from there developed into a common synthesis technique for large numbers of materials ranging from binary oxides, metal alloys and composites to highly non-equilibrium metastable compounds [2]. Mechanochemical or reactive milling, in which chemical reactions occur, is an extension of the technique. The varying applications of HEBM are attractive from a manufacturing standpoint, as they are commonly self-contained, low-temperature, and relatively environmentally friendly processes [3, 4] as well as capable of developing sought-after properties such as high hardness and the corresponding small grain size [5] and in situ formation of composite reinforcements [6].

One highly interesting feature of some mechanochemical synthesis systems is the occurrence of mechanically-induced self-propagating reaction (MSR) behavior [7, 8] which shares common features with a synthesis technique termed self-propagating high-temperature synthesis (SHS) [9]. Indeed, HEBM is commonly used as an “activation” step prior to SHS as doing so reduces the ignition temperature because of the stored deformation energy and size reduction in the milled powders [10]. The milling time required to initiate an MSR event has been investigated in several systems and seems to depend on the input energy [11] or equivalently on the reduction of a critical dimension between discrete layers of reactants. The reduction of dimension is in many cases proportional to input energy [12].

The mechanochemical synthesis of U3Si2 described in Chapter Two illustrates a case in which an existing prediction [9] for self-propagating behavior apparently fails. Instead of forming USi2 in an MSR event, the mechanochemical reaction proceeds through the intermediate state USi3.

Chapter Three describes a similar chemical system with very different behavior. In the Ce-Si system, mechanochemical reactions were observed to have self-propagating components in all compositions investigated from Ce5Si3 – CeSi2¬ with a composition-dependent initiation time explained in terms of an effective heat of formation model.

Using the knowledge and techniques developed in preparing the metal silicides discussed in Chapters Two and Three, Chapter Four describes the synthesis of CeS by mechanochemical processing. CeS is an important refractory material [13]. Although the synthesis of many sulfides have been reported by HEBM [14, 15], the Ce-S system was essentially unexamined despite the attractive properties of the Ce-S compounds. As in the Ce-Si system, the reaction of Ce and S was found to involve MSR behavior. Uniquely in the MSR literature, milling CeS results in two MSR events. In the first, CeS partially forms. In the second, CeS forms Ce2S3 and the remaining sulfur is consumed to form CeS.

Chapter Five draws from a series of experiments performed by milling Dy metal in Ar and N2 to develop a milling kinetics model. The effects of compound formation on the system geometry and energy transfer were assessed by experiment. Improving on the only model of reactive milling nitriding kinetics found in the literature [16], the kinetics model developed in Chapter Five explicitly considers milling energy and energy transfer to form chemically active surface sites. The model is predicted to be applicable to many

systems involving gas reactions with ductile solids. Furthermore, the model allows for incorporation of thermally activated kinetics if appropriate experimental data is available.

Taken together, the four publications that compose this dissertation represent significant steps towards understanding the processes governing mechanochemical synthesis as illuminated by the Ce-Si, Ce-S, U-Si, and Dy-N systems. Beyond the fundamental scientific interest, this research has demonstrated the synthesis of compounds such as DyN and CeS that were previously difficult or expensive to prepare [17, 18].

References

[1] Takacs L. Chemical Society Reviews 2013;42:7649.

[2] Suryanarayana C. Progress in Materials Science 2001;46:1.

[3] James SL, Adams CJ, Bolm C, Braga D, Collier P, Friscic T, Grepioni F, Harris KDM, Hyett G, Jones W, Krebs A, Mack J, Maini L, Orpen AG, Parkin IP, Shearouse WC, Steed JW, Waddell DC. Chemical Society Reviews 2012;41:413.

[4] Kaupp G. Crystengcomm 2009;11:388.

[5] Fecht HJ, Hellstern E, Fu Z, Johnson WL. Metallurgical Transactions a-Physical Metallurgy and Materials Science 1990;21:2333.

[6] Sabooni S, Mousavi T, Karimzadeh F. Journal of Alloys and Compounds 2010;497:95.

[7] Takacs L. Progress in Materials Science 2002;47:355.

[8] Takacs L. Mechanically Alloyed, Metastable and Nanocrystalline Materials, Part 2 1998;269-2:513.

[9] Munir Z, Anselmi-Tamburini U. Materials Science Reports 1989;Volume 3:Pages 279.

[10] Anselmi-Tamburini U, Maglia F, Spinolo G, Doppiu S, Monagheddu M, Cocco G. Journal of Materials Synthesis and Processing 2000;8:377.

[11] Gotor FJ, Achimovicova M, Real C, Balaz P. Powder Technology 2013;233:1.

[12] Thomas A, Filippov LO. International Journal of Mineral Processing 1999;57:285.

[13] Eastman ED, Brewer L, Bromley LA, Gilles PW, Lofgren NL. Journal of the American Ceramic Society 1951;34:128.

[14] Takacs L. Journal of Solid State Chemistry 1996;125:75.

[15] Urakaev FK. Combustion Science and Technology 2013;185:1281.

[16] Bab MA, Mendoza-Zelis L. Scripta Materialia 2004;50:99.

[17] Gibbard KB, Allahar KN, Kolman D, Butt DP. Journal of Nuclear Materials 2008;378:291.

[18] Mazumder B, Hector AL. Journal of Materials Chemistry 2009;19:4673.

CHAPTER TWO: MECHANOCHEMICAL SYNTHESIS OF URANIUM SESQUISILICIDE

Mechanochemical Synthesis of Uranium Sesquisilicide

Gordon A. Alanko[1]

Darryl P. Butt[1,2]

Department of Materials Science and Engineering, College of Engineering
Boise State University, 1910 University Drive, Boise, ID, 83725

Center for Advanced Energy Studies
995 University Boulevard, Idaho Falls, ID 83401

Abstract

Uranium sesquisilicide (U_3Si_2) has been prepared by high energy ball milling of the elemental powders. Starting materials were combined in a planetary ball mill and milled with a 10:1 ball-to-powder charge for varying times between 0 and 24 hours. Temperature and pressure of the milling vial were monitored to gain insight into reaction kinetics. The development of USi_3 as an intermediate phase is discussed. Starting materials and as-milled powders were characterized by X-ray Diffraction (XRD), Scanning Electron Microscopy (SEM), and Energy Dispersive Spectroscopy (EDS), demonstrating the viability of mechanochemical synthesis for U_3Si_2.

2.1 Introduction

Uranium sesquisilicide (U_3Si_2) is a qualified fuel for research and test reactors. Uranium silicides, including U_3Si_2, are potentially of interest as monolithic advanced fuels or as environmental barriers in accident-tolerant fuels [1]. Table 2.1 lists the compounds in the U-Si system that are relevant to the temperature range of ball milling, along with heats of formation [2] and crystallographic information [3]. Current commercial scale production of uranium silicide typically involves repeated vacuum induction melting and subsequent annealing. Research scale production is typically arc melting followed by annealing [4], although laborious production of ultrafine uranium via the hydride-dehydride route can yield highly phase-pure U_3Si_2 directly from the arc melt. Essentially phase-pure material can also be prepared by a powder metallurgy route [5]. In contrast to previous work, the present study concerns the production of uranium silicides by high-energy ball milling (HEBM) in a planetary ball mill. HEBM has been used to synthesize many materials including ODS alloys [6] and many intermetallics [7]

including Ti, Mn, Mg, and Mo silicides [8-13]. HEBM has also been evaluated for the synthesis of nuclear materials such as uranium nitride and nuclear surrogates, such as dysprosium nitride [14].

Table 2.1 Thermodynamic and Crystallographic Data for the U-Si System

Species	Unit cell	Space Group	mass (g/mol)	ρ (g/cm^3)	V (cm^3/mol)	$\Delta V/V_0$ (%)	ΔH_f^{298} (kJ/mol atom)
USi_3	Cubic	Pm-3m	322.3	8.0	40.3	-20.7	-32.9
USi_2	Tetragonal	$I4_1/amd$	294.2	9.0	32.8	-11.6	-43.33
$USi_{1.88}$	Tetragonal	$I4_1/amd$	290.8	9.1	31.9	-10.3	No data
$USi_{1.67}$	Hexagonal	P6/mmm	284.9	9.1	31.6	-3.1	-42.9
USi [a]	Orthorhombic	Pnma	266.1	10.4	25.6	3.9	-41.18
USi [b]	Tetragonal	I4/mmm	266.1	11.0	24.1	-1.9	No data
U_5Si_4	Hexagonal	P6/mmm	1302.5	11.6	111.9	1.1	No data
U_3Si_2	Tetragonal	P4/mbm	770.3	12.2	63.1	2.4	-34.32
β-U_3Si	Tetragonal	I4/mcm	742.2	15.59	47.62	-4.03	-24.93
γ-U_3Si	Cubic	Pm-3m	742.2	15.0	49.4	-0.20	-24.93

a. Oxygen stabilized
b. Oxygen-free

Key advantages of the HEBM technique include the ease of formation of in situ composites, low processing temperatures and power requirements, and the self-contained nature of the process. The latter is especially beneficial in smaller research labs, while the potential cost savings realized by scaled-up techniques may appeal to commercial producers.

A challenge in HEBM synthesis is that some impurity content is generally introduced by the milling tools. This may be minimized by the appropriate choice of charge size, by matching milling vessel and media materials, and by reducing milling time and energy to the minimum required. There is an ongoing interest in the way of formation of intermetallic compounds during high-energy ball milling. This work presents some results of in situ temperature and pressure monitoring along with

microstructural observations in an attempt to gain insight into the dynamic process of ball milling.

2.2 Materials and Methods

The starting materials were atomized depleted uranium powder (50 mesh, Idaho National Laboratory, USA) and silicon powder (1-20 μm, 99.9995%, Alfa Aesar, USA). X-ray diffraction analysis showed the atomized DU to be phase pure α-U to within the detection limit of the XRD, while the silicon was phase pure with a low amorphous background. For this initial process study, no purification of the precursors such as acid washing was attempted.

Initial milling parameters were chosen following previous studies on the HEBM of silicides [10, 15]. A planetary ball mill (Retsch PM100, Germany) and a 250 mL hardened steel milling vessel were used for all experiments. Most milling experiments were performed with ceria-stabilized zirconia milling (CSZ) media. Hardened steel media was used for the remainder of the milling experiments.

The milling tools were cleaned thoroughly between experiments by milling in air to oxidize adhered silicide followed by scrubbing with steel wool and 800 grit SiC paper to remove the resultant oxide. Media were cleaned by sonication in acetone. Experiments conducted after cleaning in this fashion will be referred to as being performed in a “clean vessel.” To gain insight into milling impurity pickup and process yield, a few experiments were performed in which the adhered silicide from the previous run was not removed. These experiments will be referred to as being performed in a “conditioned vessel” or with “conditioned tools.”

For several experiments, the pressure and temperature within the milling vessel were monitored during milling by sensors mounted in the milling vessel lid. The pressure sampling rate was 2 Hz and temperature sampling rate was 1 Hz. The ambient pressure and temperature near the mill was sampled by a benchtop datalogger at 10 minute intervals in order to separate any effect of the ambient conditions on the data collected in situ during milling. After each milling run in which pressure and temperature were monitored, the vessel was allowed to cool to ambient temperature. The milling run was then repeated without opening the jar. This allowed for the separation of reaction effects from process variables such as mechanical heating of the milling jar.

2.3 Experimental

In a typical synthesis, 5 g of the starting materials were added to the milling vessel under argon atmosphere in a glovebox along with a 10:1 mass charge of media in the ratio 3x (10 mm) : 2x (5 mm). Milling was conducted at 500 rpm for between 5 minutes and 24 hours.

The jar filling ratio (V_{charge}/V_{vial}) of 0.035 was much lower than the limit of 0.20 empirically determined for non-hindering media motion [16]. The primary energy transfer during the milling process is therefore predicted to be impact driven [17] in which ball-powder-wall interactions are both frequent and possess high effective energy. The oxygen content of the glovebox was $10 < P_{O2} < 30$ ppm but elementary calculations show that the trapped oxygen in a milling vessel should result in no more than ppm levels of UO_2 impurity in the milled product.

The starting materials and as-milled powder crystallite size and phases were characterized by X-ray diffraction in parallel-beam geometry (Bruker AXS D8 Discover,

Germany). To avoid excessive oxidation samples were mounted on steel slides and covered with a layer of PVDC film affixed by vacuum grease. Characteristic XRD peaks for the film were noted at 21° and 23° 2θ; this region is therefore omitted from the XRD results. Phase identification was performed by comparison to the Inorganic Crystal Structure Database.

Microstructure and morphology of the precursor and as-milled powders were investigated by scanning electron microscopy and stoichiometry by energy dispersive spectroscopy (Hitachi 3400-N, Japan). Samples were mounted on double-stick carbon tape or in conductive resin for analysis. Resin mounted samples were polished to reveal a cross-section.

2.4 Results

2.4.1 Milling Results

The desired silicide phase of U_3Si_2 was synthesized with less than 12 hours of milling time. Samples were taken at different milling times for X-ray diffraction and microstructural analysis. Representative microstructures at different milling times are shown in Figure 2.1, while representative diffraction plots are shown in Figure 2.2. A high amount of UO_2 can be noted in Figure 2.2, and the peak intensity is especially pronounced for samples milled for 8 hours or longer. All of the samples in Figure 2.2 were milled with CSZ media in a clean vessel. In experiments with a conditioned vessel and either CSZ or steel media, very little oxide contamination is noted, as shown in Figure 2.3. Additional experiments with a clean vessel and steel media also had very little oxide contamination (not shown).

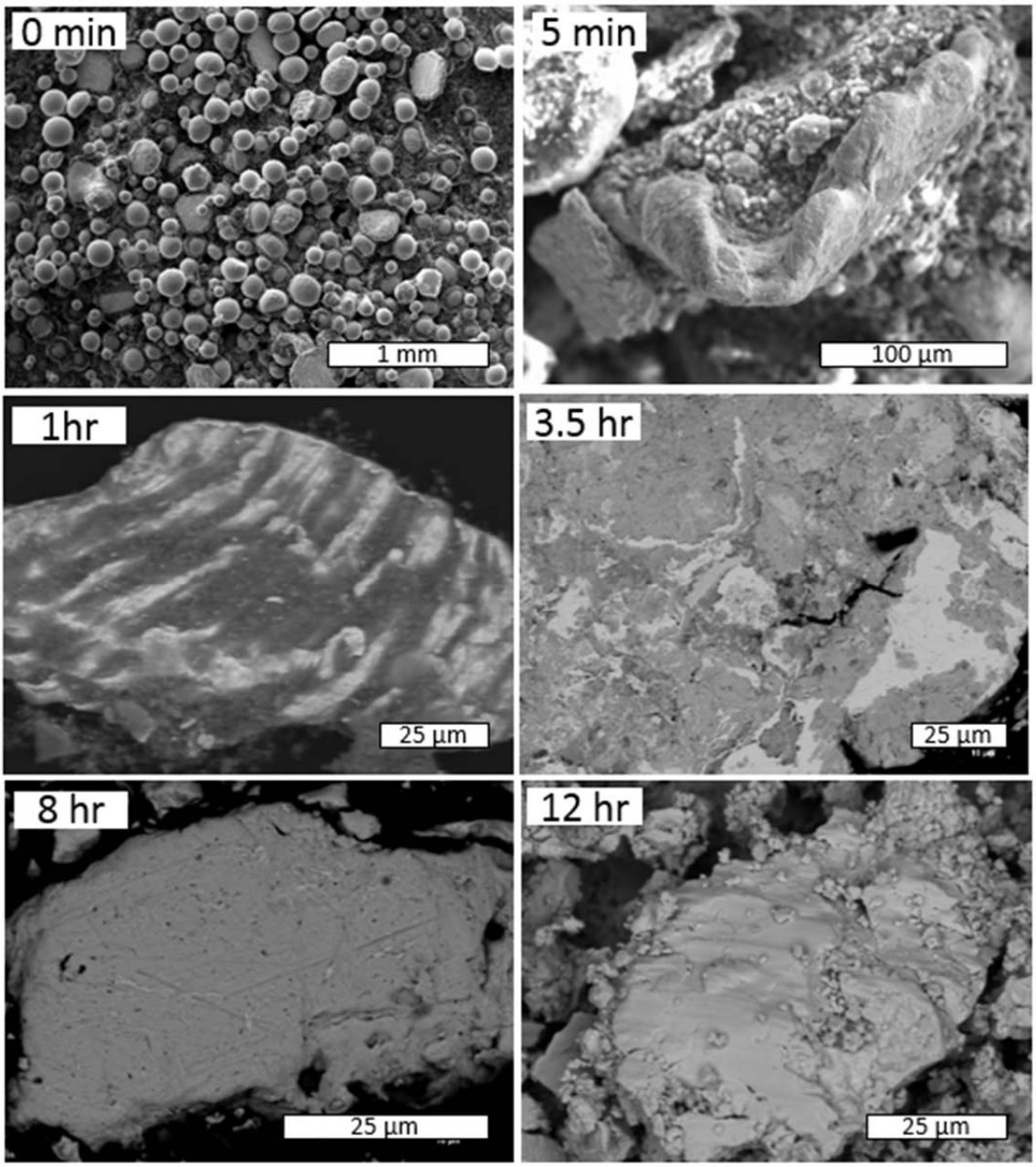

Figure 2.1 Representative micrographs from the specified milling times show microstructure development with increasing milling time. 0 and 5 minute images are SE micrographs, while 1-12 hour images show phase contrast with BSE micrographs.

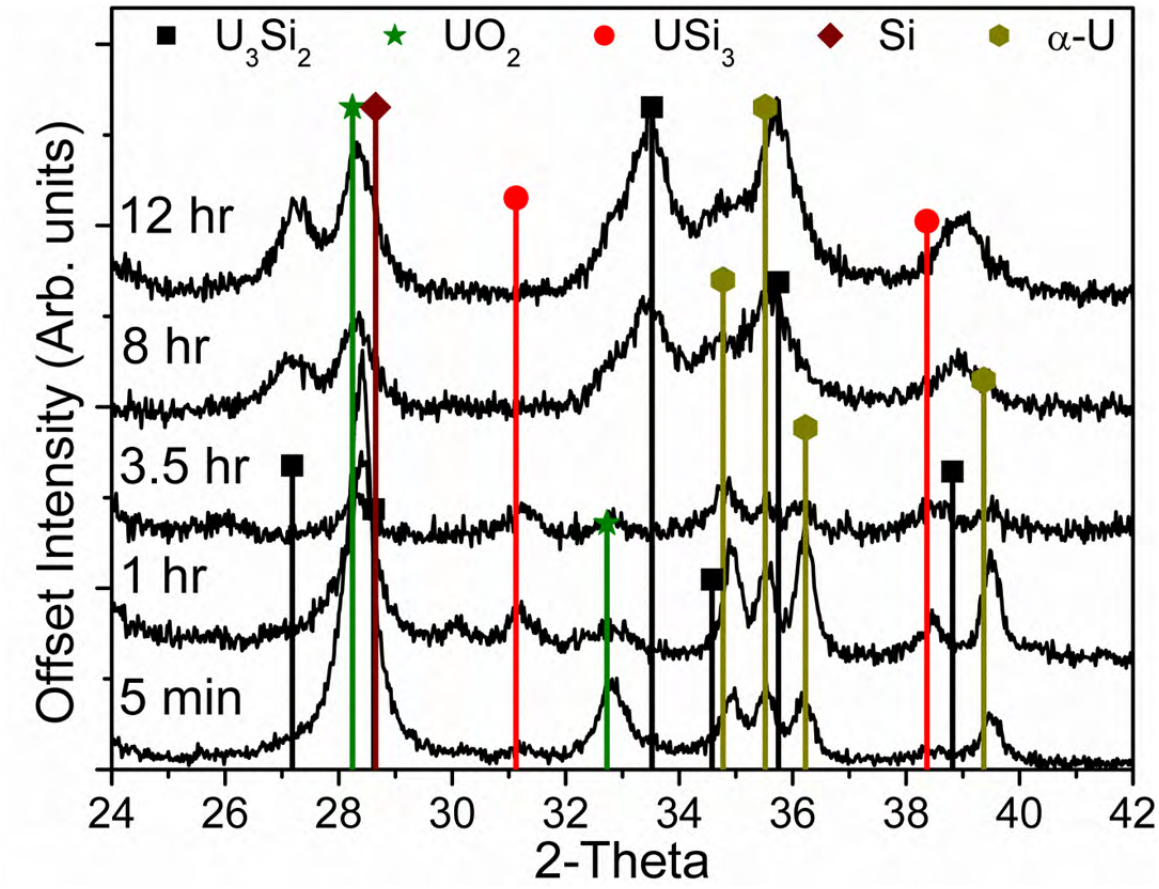

Figure 2.2 Representative XRD 2θ scans for U_3Si_2 milled in clean vessels with CSZ media for times from 5 minutes – 12 hours (indicated on plot). Droplines correspond to possible phases: black squares are the desired U_3Si_2, green stars are UO_2, red circles are USi_3, and wine diamonds and gold hexagons are the starting materials silicon and uranium, respectively. All data is displayed on the same scale.

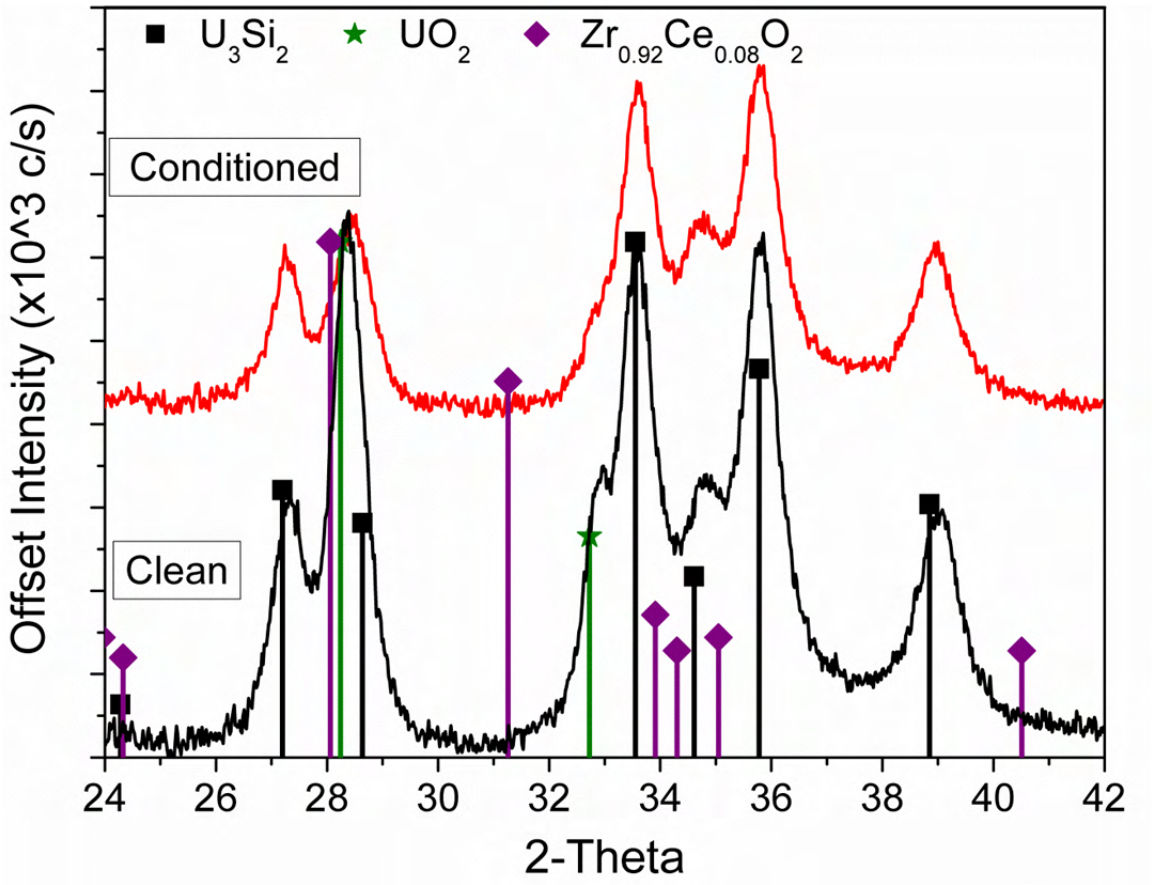

Figure 2.3 Representative XRD 2θ scans for U_3Si_2 milled for 12 hours in clean and conditioned vessels (indicated on plot) show a pronounced UO_2 peak near 28 and shoulder near 33. Droplines correspond to possible phases: black squares are the desired U_3Si_2, green stars are UO_2, and purple diamonds are 8% CSZ (not observed – see Discussion).

The phase content and relevant data on the milling process are summarized in Table 2.2 along with calculated amounts of ZrO_2 impurity resulting from media wear.

Table 1.2 Data for U_3Si_2 milled in clean vessels with CSZ media

Milling Time	**0 hr**	**5 min**	**1hr**	**3.5 hr**	**8 hr**	**12 hr**	**24 hr**
Phase content[a]	U+Si	U+Si+USi_3	U+USi_3+minor	U+USi_3+minor	U_3Si_2+minor	U_3Si_2	U_3Si_2
Free powder (g)	5	5	5	4.99	3.93	3.89	3.76
Free powder (%)[b]	100	100	100	98.3	70.2	--	64.4
Particle size (μm)	100	100	50-200	50-200	10-300	10-50	10-50
Particle morphology	Spherical	Spherical	Laminate	Platelet	Irregular	Equiaxed	Equiaxed
Δm_{media} (g)	0	--	--	-0.076	-0.60	--	-0.84
$\Delta m_{media}/m_{media}$ (%)	0	--	--	0.15	1.16	--	1.65
$m_{ZrO2}/(m_{ZrO2}+m_{U3Si2})$ (%)	0	--	--	1.54	10.70	--	14.63

a. All samples contain minor amounts of UO_2

b. Non-adhered powder mass normalized by $m_{powder}/(m_{U3Si2} - \Delta m_{media})$

The percentage of free powder in the milling vessel and the percentage mass loss of the milling media are plotted versus milling time in Figure 2.4, inset. An additional experiment was performed in which U_3Si_2 previously produced by milling in a conditioned vessel for 12 hours (Figure 3, top) was milled for an additional 12 hours with conditioned steel media and 15% mass monoclinic ZrO_2. This amount of ZrO_2 corresponds to the highest impurity content calculated in Table 2.2. After 12 hours of milling, a slight monoclinic ZrO_2 peak was observed by XRD (Figure 2.4), along with greatly increased cubic oxide peaks near 28 and 33° 2θ.

The data in Table 2.2 indicate the adhesion of approximately 1 g powder to the milling tools starting between 3.5 and 8 hours of milling. This mass of U_3Si_2 corresponds to a silicide coating layer with an average thickness of < 10 μm on the media and jar wall. Milling with “conditioned” tools (in which the adhered layer was not removed between runs) results in > 98% free powder recovery regardless of milling time.

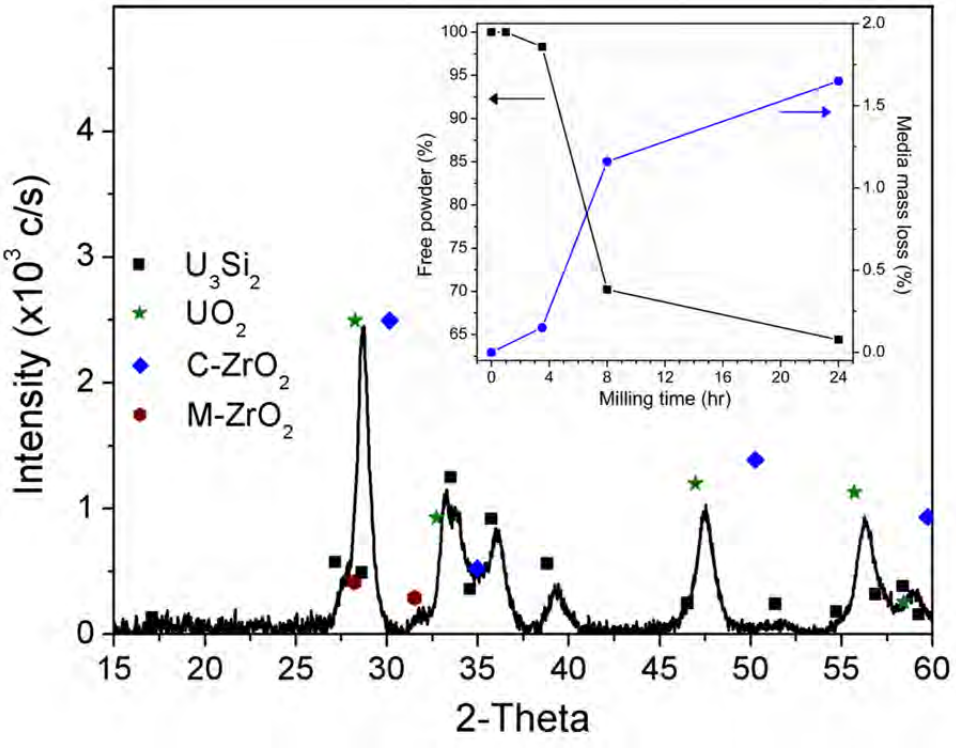

Figure 2.4 This plot shows the result of milling high purity U_3Si_2 (Figure 3, top) and ZrO_2 with steel media for 12 hours. Scatter points correspond to possible phases: black squares and maroon circles are the U_3Si_2 and monoclinic ZrO_2 starting materials, respectively, green stars are UO_2, and blue diamonds are cubic ZrO_2. The plot demonstrates that ZrO_2 and U_3Si_2 react during milling (see Discussion). The inset shows the variation in the amount of powder free in the milling vessel (black squares) and the change in media mass (blue circles) as a function of time during the milling of U_3Si_2 in clean vessels with CSZ media. Arrows indicate the reference axis.

2.4.2 Pressure/Temperature Monitoring Results

Pressure and temperature data collected in a milling vessel that was scrupulously cleaned before milling was repeatable to within 10% absolute error from run to run. Experimental results with a conditioned mill jar were repeatable to within 1%. Representative results are shown in Figure 2.5a-c.

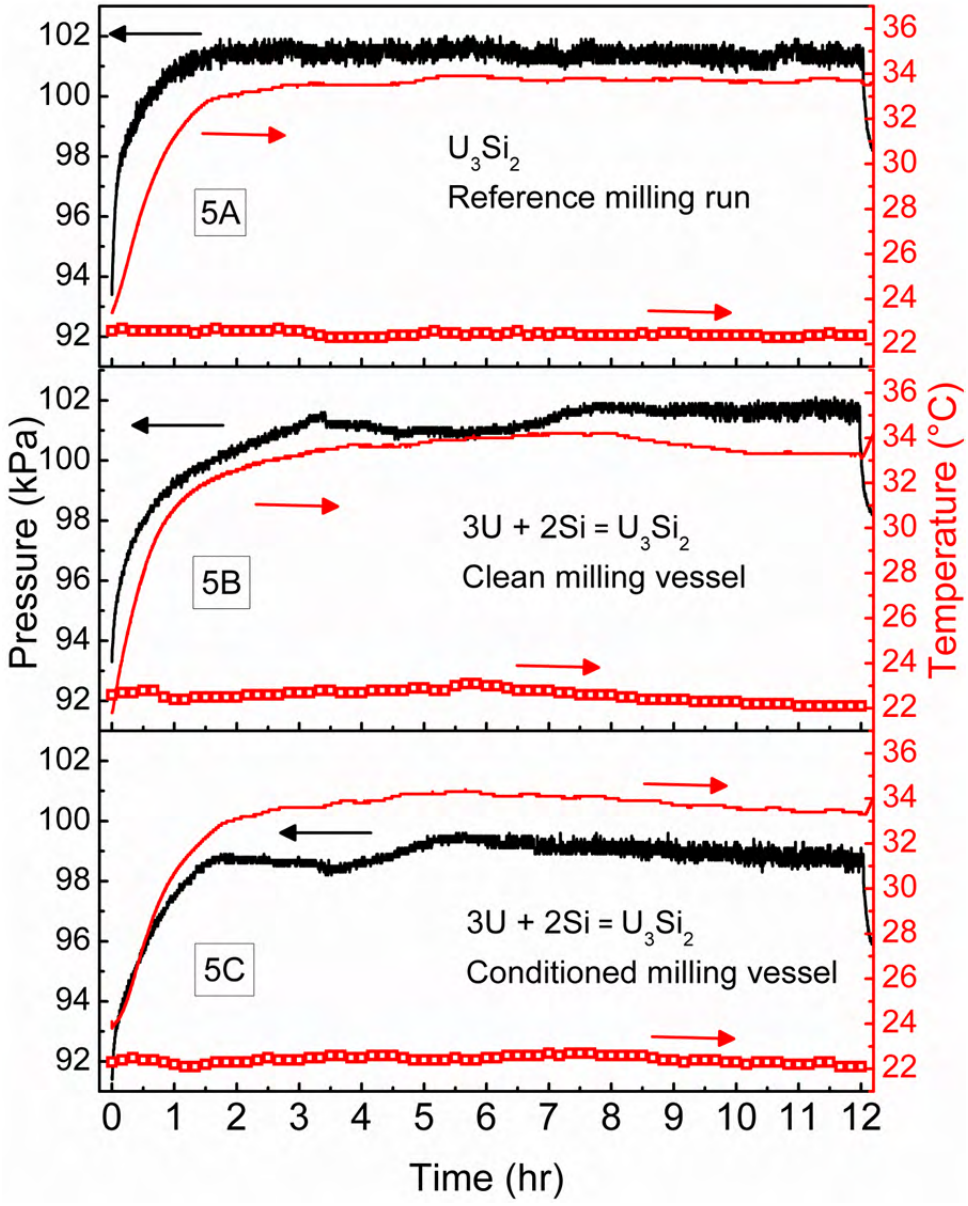

Figure 2.5 Typical P-T-t traces for 12 hour milling runs of U_3Si_2. In each pane, the black trace is milling vessel pressure, the red trace is milling vessel temperature, and the red boxes the room ambient temperature (arrows indicate proper axis). From top to bottom, the panes show typical data from A) reference data produced by milling U_3Si_2 for 12 hours, B) uranium and silicon milled in a clean milling vessel with CSZ media, and C) uranium and silicon milled in a conditioned vessel with CSZ media. Axis scales are self-consistent.

2.5 Discussion

Examination of Figures 2.2, 2.4, and 2.5 reveal a series of interesting correlations. When milling with CSZ media in clean vessels, U and Si react very quickly to form $U+USi_3$, followed by the reaction of $U+USi_3$ to form U_3Si_2 between 3.5 and 8 hours of milling time. Between 3.5 and 8 hours of milling time, approximately 1 g of the milled powder becomes adhered to the media. The milling media simultaneously loses approximately 0.5 g or 1% of the starting mass, which corresponds to approximately 10% of the total powder load of 5 g. The UO_2 content qualitatively appears to increase from 1 to 12 hours of milling time when milling was conducted with clean vessel and media. The pressure in the milling vessel has a local maximum near 3.5 hours of milling time, and decreases to a local minimum near 6 hours before increasing to the maximum near 8 hours of milling time. All of these observations are reproducible.

2.5.1 Phase Formation During Milling

The phase content and particle morphology of milled U_3Si_2 proceeds in a manner typical of ductile-brittle systems:

1. 5 minutes: Uranium is plastically deformed from ≈100 μm spheres into ≈10 μm thick sheets.
    a. USi_3 initially forms in the contact region between silicon and highly strained uranium.
2. 1 hour: System develops laminar structure of $U/USi_3/U$ sheets in irregularly shaped particles.
    a. Minor amounts of an unidentified USi_x phase observed in XRD.
3. 3 hours: U/USi_3 particle shape changes to roughly 10-30 x 100-300 μm platelets.
4. 8 hours: Reaction to U_3Si_2 is nearly complete in 10-50 μm, roughly equiaxed particles.
    a. Spherical inclusions of higher-silicon silicide and fillets of uranium, both ≈200 nm in size.
5. 12 hour: Fracturing/cold welding increases in essentially pure U_3Si_2.

The first bulk phase that formed under these milling conditions was USi_3, regardless of the nominal stoichiometery of the starting materials. In contrast to the present case, USi_2 is the first phase observed in thin-film reactions between γ-U (8% Mo) and Si at elevated temperatures [18]. It could be that the USi_3 phase has a low energy barrier for nucleation and is therefore easier to form during low temperature solid-state processing compared to the other uranium silicides.

2.5.2 Impurity Content

The milling results discussed in Section 2.4.1, above, reveal increased UO_2 contamination in those samples milled in clean vessels with CSZ media compared to those samples milled in conditioned vessels with CSZ media or in either clean or conditioned vessels with steel media. Three possibilities immediately offer themselves as potential sources of oxygen contamination:

1. Environmental contamination such as oxide films on starting materials or O_2 in vessel
2. Native oxide on the vessel or incomplete removal of oxidized silicide from the vessel
3. Reduction of the milling media by uranium or uranium silicide

Systemic environmental sources of oxygen should result in similar levels of oxide impurity in similar milling runs. Because oxide contamination was reliably found at high levels in milling runs with clean tools and CSZ media and at low levels in milling runs with conditioned tools or steel media, possibilities 1 and 2 are discounted as a cause of the observed high levels of oxide impurity.

Reduction of ZrO_2 from the milling media could be responsible for the observed oxide contamination. In this case, a loss in media mass should be observed and no

zirconia should be observed in the synthesized powders. From Table 2.2, 5 g of powder milled for 12 hours with clean CSZ media should contain at least 10% ZrO_2, but Figure 2.3 shows that no x-ray diffraction peaks that would indicate the presence of 10% CSZ are observed. To test the hypothesis, U_3Si_2 was milled with pure zirconia powder as described in Section 2.4.1. Figure 2.4 clearly demonstrates a reduction in U_3Si_2 and monoclinic ZrO_2 peak intensity and consequent development of a cubic XRD diffraction pattern intermediate to the UO_2 and ZrO_2 cubic oxide peaks. This implies the formation of a $(U,Zr)O_2$ cubic solid solution known to exist at high temperature. Thermodynamic modeling does not predict a stable cubic solid solution near room temperature [19] so the ZrO_2-UO_2 system may be another example of metastable solid solution formation during ball milling [7]. Analysis of the U-Si [1], Zr-Si [20], and U-O/Zr-O [21] system thermodynamics indicates that the U-ZrO_2 couple should be stable at temperatures relevant to ball milling. However, all Zr-Si compounds have significantly lower free energies than any U-Si compounds. This implies that the equilibrium U-Zr-Si-O quaternary system will include a $ZrSi_x$ compound, which in the present case requires the formation of UO_2 as observed in Figure 2.4. Thus, by thermodynamic data and a key experiment, it is argued that the observed UO_2 contamination in clean jars occurs by the reduction of ZrO_2 from the unconditioned milling media wear products

2.5.3 Pressure/Temperature Monitoring

There are at least three sources of heat in the milling vessel: 1) conduction from the mill motor and drive assembly, 2) chemical heat of reaction of the milled material, and 3) mechanical heat generated by media impact and friction. Heat loss is primarily

convective transfer to the air surrounding the spinning vessel and should therefore vary to some small extent if the ambient temperature changes.

The energy released by the formation of 5 g of U_3Si_2 is -1.1 kJ. Treating the mill jar as a bomb calorimeter and referring to Table 2.1, the maximum temperature rise possible would be on order 0.5 °C if all the material reacted simultaneously to form U_3Si_2. This is not the case, as Figure 2.2 shows that USi_3 is the first phase to form and is followed several hours later by reaction of $U+USi_3$ to form U_3Si_2. Referring to Table 2.1, 0.57 kJ is released by the reaction of 5 g of material with a nominal U_3Si_2 stoichiometry to form $U+USi_3$. The remaining 0.53 kJ of reaction heat is released slowly during the reaction of $U+USi_3$ to form U_3Si_2 over several hours of milling. The maximum pressure increase due to the heat of reaction is on the order of 0.1 kPa, determined by applying the ideal gas law. Both the calculated pressure and temperature increases due to the chemical reaction are below the signal-to-noise ratio caused by the ambient temperature change as seen in Figure 2.5a.

However, Figure 2.5b and 2.5c show an initial stable pressure after approximately 3 hours of milling followed by a pressure change of approximately 3 kPa. The data in Table 2.2 and Figure 2.5 show that the adhesion of milled material to the media greatly increases between 3.5 and 8 hours of milling. One would intuitively expect powder adhesion to change the dynamic coefficients of friction in the system. Given that the heat from friction has been shown to be at least on the order of the reaction heat [22], and taking the data of Figures 2.4 and 2.5 into account, it seems plausible to suggest that the observed variation in pressure at consistent, reproducible milling times is due to

increased mechanical heating. This heating is in turn caused by an increase in the dynamic coefficient of friction as milled material coats the surface of the milling media.

2.6 Conclusions

The uranium silicide U_3Si_2 has been successfully prepared by high-energy ball milling of elemental silicon and uranium starting materials. Short milling times at 500 rpm quickly consume all the free silicon to form USi_3, while extended milling times of 4-12 hours slowly form U_3Si_2 by reaction of USi_3 with the remaining U. Qualitative analysis of in situ pressure and temperature measurements suggest that the mechanical alloying of $U+USi_3$ is accompanied by increased powder adhesion to the milling tools and a change in dynamic coefficient of friction. The as-milled powder after 12 hours consists mainly of fractured and cold-welded agglomerates 10-50 μm in size. Milling with steel vessels and media with a 10 μm silicide "conditioned" coating greatly reduces the impurity content derived from the milling tools and increased the free powder yield of the milling process. These results suggest that mechanochemical synthesis is a viable technique for production of U_3Si_2 and U_3Si_2-based composites.

2.7 Acknowledgments

This project was supported by the Department of Energy under NEUP award #00120690. Mitch Meyer, Jason Harp, and Paul Lessing at the Idaho National Laboratory, Brian Jaques and Daniel Osterberg at Boise State University, and Peng Xu and Edward Lahoda at Westinghouse Electric Company engaged in helpful discussion. Mitch Meyer and Doug Toomer at the Idaho National Laboratory provided the depleted

uranium used in this project. SEM studies were supported by the Department of Energy [National Nuclear Security Administration] under Award Number DE-NE0000338.

2.8 Author Justification

The research presented in this publication was carried out by Gordon Alanko in partial fulfillment of the requirements for a Doctoral degree in Materials Science and Engineering at Boise State University, under the advisement and supervision of Dr. Darryl P. Butt. Dr. Darryl Butt contributed greatly in terms of financial support, discussion of processing routes, and critical review of the article throughout the writing process.

2.9 References

[1] P.A. Lessing, INL/EXT-12-24974 (2012)

[2] A. Berche, C. Rado, O. Rapaud, C. Gueneau, and J. Rogez, *J. Nucl. Mater.*, 389[1] (2009) 101-07

[3] S. Yagoubi, S. Heathman, A. Svane, G. Vaitheeswaran, P. Heines, J. C. Griveau, T. Le Bihan, M. Idiri, F. Wastin, and R. Caciuffo, *J. Alloy. Compds.*, 546 (2013) 63-71

[4] H. Shirnizu, NAA-SR-10621 (1965)

[5] V. P. Sinha, G. P. Mishra, S. Pal, K. B. Khan, P. V. Hegde, and G. J. Prasad, *J. Nucl. Mater.*, 383[1-2] (2008) 196-200

[6] S. Pasebani, I. Charit, Y.Q. Wu, D.P. Butt, and J.I. Cole, *Acta Mater.*, 61[15] (2013) 5605-5617

[7] C. Suryanarayana, *Prog.Mater. Sci.*, 46[1-2] (2001) 1-184

[8] C. S. Byun, S. Bopark, D. K. Kim, W. Lee, C. Y. Hyun, and P. J. Reucroft, *J. Mater.Sci.* 36[2] (2001) 363-69

[9] I. Dezsi, C. Fetzer, L. Bujdoso, J. Brotz, and A. G. Balogh, *J. Alloy. Compds.*, 508[1] (2010) 51-54

[10] T. Itoh and M. Yamada, *J. Electron. Mater.*, 38[7] (2009) 925-29

[11] M. Loannou, E. Hatzikraniotis, C. Lioutas, T. Hassapis, T. Altantzis, K. M. Paraskevopoulos, and T. Kyratsi, *Powder Technol.,* 217 (2012) 523-32

[12] R. B. Schwarz, S. R. Srinivasan, J. J. Petrovic, and C. J. Maggiore, *Mater. Sci. Eng. A,* 155[1-2] (1992) 75-83

[13] L. Takacs, *J. Solid State Chem.,* 125[1] (1996) 75-84

[14] B. J. Jaques, B. M. Marx, A. S. Hamdy, and D. P. Butt, *J. Nucl. Mater.,* 381[3] (2008) 309-11

[15] P. Z. Feng, X. H. Wang, Y. H. Qiang, and X. H. Qu, *Powder Metall.,* 51[4] (2008) 298-302

[16] M. Magini, C. Colella, A. Iasonna, and F. Padella, *Acta Mater.,* 46[8] (1998) 2841-50

[17] P. P. Chattopadhyay, I. Manna, S. Talapatra, and S. K. Pabi, *Mater. Chem. Phys.,* 68[1-3] (2001) 85-94

[18] A. Leenaers, S. Van den Berghe, and C. Detavernier, *Solid State Sciences,* 14 (2012) 1133-1140

[19] M. Yashima, T. Koura, Y. Du, and M. Yoshimura, *J. Am. Ceram. Soc.,* 79[2] (1996) 521-24

[20] C. Wang, M. Zinkevich, and F. Aldinger, *CALPHAD,* 28 (2004) 281-292

[21] C. Colinet, R. Viennois, and J.C. Tedenac, *CALPHAD,* 36 (2012) 118-126

[22] F. K. Urakaev, *Combust. Sci.Tech.,* 185[5] (2013) 723-34

CHAPTER THREE: MECHANOCHEMICAL SYSNTHESIS OF THE CERIUM SILICIDES

Mechanochemical Synthesis of the Cerium Silicides

Gordon A. Alanko[1]

Brian Jaques[1]

Allyssa Bateman[1]

Darryl P. Butt[1,2]

2. Department of Materials Science and Engineering, College of Engineering
Boise State University, 1910 University Drive, Boise, ID, 83725

3. Center for Advanced Energy Studies
995 University Boulevard, Idaho Falls, ID 83401

Abstract

The cerium silicides, Ce_5Si_3, Ce_3Si_2, CeSi, Ce_3Si_5, and $CeSi_2$, have been prepared from the elements by mechanochemical processing in a planetary ball mill. Temperature and pressure of the milling vial were monitored *in situ* to gain insight into the mechanochemical reaction kinetics, which include a mechanically-induced self-propagating reaction (MSR). Some prepared powders were consolidated by spark plasma sintering to high density. Starting materials, as-milled powders, and consolidated samples were characterized by x-ray diffraction, scanning electron microscopy, and energy dispersive spectroscopy. The results obtained help elucidate key questions in mechanochemical processing of intermetallics, showing first phase formation similar to thin films, MSR ignition times that are composition- and milling speed-dependent, and sensitivity of stable compound formation on the impact pressure. The results demonstrate mechanochemical synthesis as a viable technique for rare earth silicides.

3.1 Introduction

Rare earth silicides have been studied for many years because of their interesting electromagnetic properties, utility in semiconductor devices, refractory nature, and for the ability of some silicides to form oxidation resistant protective silica films. Cerium is well known among the rare earths for forming compounds with complicated magnetic behavior, and binary and ternary compositions near $CeSi_2$ have received considerable attention for their magnetic properties [1, 2]. Ce_3Si_2 is isostructural with U_3Si_2[3], and may be a potential surrogate for studies of processing techniques, oxidation, corrosion, and transport properties in this important compound. Meanwhile, CeSi, Ce_5Si_4, and ternary compounds based on Ce_5Si_4 have been studied as magnetocaloric materials for

refrigeration [4, 5]. The compounds of cerium with silicon are commonly prepared by arc melting the elements, with the cast buttons used as-is or as master alloys for single crystal growth[2]. This process may dissolve oxygen or volatilize cerium or silicon as MO species, resulting in off-stoichiometric products.

Here we describe the preparation of the entire range of cerium silicides by high energy ball milling (HEBM), which is a self-enclosed processing technique that can limit oxygen contamination and cerium or silicon loss. The HEBM technique has been used to synthesize many materials including oxide dispersion strengthened steel alloys[6] and many intermetallics[7]. The preparation of silicides by HEBM was first reported nearly thirty years ago [8, 9], and the technique has since been applied to many silicide systems. Some silicides with a high enthalpy of formation, such as $MoSi_2$, exhibit a sudden reaction during HEBM in a process termed mechanochemically-induced self-propagating reaction (MSR) [10]. Takacs adapted the criterion[11] for self-propagating high-temperature synthesis to predict MSR to occur in systems with an adiabatic reaction temperature > 2000 K. The adiabatic temperature is given by $T_{AD} = \Delta H_f (T_{rxn})/ C_P(T_{rxn})$, where ΔH_f and C_P are the respective reaction enthalpy and heat capacity of the formed compound at the temperature of the reaction. The ratio $\Delta H_f^{298} / C_P$ is assumed to be a close approximation to the high temperature value $\Delta H_f (T_{rxn})/ C_P(T_{rxn})$ as high temperature properties are not well known in many systems. A similar condition requires T_{AD} to exceed the melting temperature of at least one constituent. The Ce-Si system is uncommon in the fact that all line compounds have $\Delta H/Cp$ > 2000 K, as shown in Table 3.1, making the Ce-Si system ideal for investigating MSR-type behavior in systems with multiple intermetallic compounds.

Table 3.1 lists the compounds in the Ce-Si system that are relevant to the temperature range of ball milling, along with heats of formation ΔH_f^{298} [12, 13], calculated adiabatic reaction temperatures T_{AD}, effective heats of formation $\Delta H_f'$ [14], and crystallographic information[3]. Heats of formation are used rather than free energies because the product $-T\Delta S$ is small for solid state reactions near room temperature and the free energy may thus be approximated by ΔH_f. The effective heat of formation is defined as $\Delta H_f' = \Delta H_f (x'/x)$ where x is the limiting reactant at the nominal composition, and x' is the limiting reactant at the composition of the lowest melting eutectic. For the crystallographic data, we adopt a formalism in which $CeSi_{2-x}$ denotes the silicon deficient α-$ThSi_2$ prototype compound spanning the composition range $CeSi_{1.81}$-$CeSi_2$[2]. Likewise, $CeSi_{2-y}$ denotes the α-$GdSi_2$ prototype, which melts congruently at $CeSi_{1.81}$ but has been reported to have a greatly increased homogeneity range when equilibrated in the range 800-1100°C[15, 16].

Table 3.1 Thermodynamic and Crystallographic data for the Ce-Si system

Species[3]	$CeSi_{2-x}$	$CeSi_{2-y}$	CeSi	Ce_5Si_4	Ce_3Si_2	Ce_5Si_3
Formation[3]	Peritectic	Congruent	Congruent	Peritectic	Peritectic	Peritectic
Unit cell[3]	Tetragonal	Orthorhombic	Orthorhombic	Tetragonal	Tetragonal	Tetragonal
Space Group[17]	$I4_1/amd$	Imma	Pnma	$P4_12_12$	P4/mbm	I4/mcm
Prototype[17]	α-$ThSi_2$	α-$GdSi_2$	FeB	Zr_5Si_4	U_3Si_2	W_5Si_3
Volume (cm^3/mol)[17]	36.21	36.3	29.42	143.56	79.77	129.05
$\Delta V/V_0$ (%)	-24.4	-13.5	-12.2	-6.5	-9	-9.2
ΔH_f [12, 13] (kJ/mol atom)	-62.7	-68.1	-70.5	-65.7	-60.9	-57.2
T_{AD} ($\Delta H/C_P$ (K))	2829	3033	3017	2764	2529	2359
$\Delta H_f'$ (kJ/mol atom)	-16.0	-16.0	-15.5	-14.8	-11.1	-9.9

3.2 Materials and Methods

The starting materials were cerium filings (99.9%, ESPI Metals, USA) and silicon powder (1-20 μm, 99.9995%, Alfa Aesar, USA). The cerium filings were supplied at -40 mesh, and were further graded to +60 (corresponding to screened particle sizes of 420 - 250 μm) before conducting experiments. X-ray diffraction (XRD) analyses showed the cerium to be phase pure to within the detection limit of the XRD, while the silicon was phase pure with a low amorphous background. All experiments were performed with a planetary ball mill (Retsch PM100, Germany) with a 250 mL hardened steel milling vessel and ceria-stabilized zirconia milling (CSZ) media of 5 and 10 mm diameter. Before beginning experiments, the volume of the milling vessel after sealing the attached lid was calculated to be 274 mL by measuring the amount of deionized water required to completely fill the assembly. The pressure and temperature within the vessel during milling were monitored *in situ* by sensors mounted in the milling vessel lid. The pressure sampling rate was 2 s^{-1} and temperature sampling rate was 1 s^{-1}. The ambient pressure and temperature near the mill was sampled by a benchtop datalogger at 10 minute intervals in order to separate any effect of the ambient conditions on the data collected in situ during milling.

After each milling run in which pressure and temperature were monitored, the vessel was allowed to cool to ambient temperature. The milling run was then repeated without opening the jar to allow for the separation of the effects of chemical reaction(s) from that of mechanical heating of the milling jar. Milled silicides with higher cerium contents than that of CeSi tended to adhere to the milling vessel walls. To clean the vessel when changing from one nominal composition to another, the milling vessel

volume was filled 2/3 full with CSZ media and 20 mL isopropyl alcohol and milled for 5 minutes at 500 rpm. This treatment was sufficient to removed gross deposits of silicide. Media were cleaned of adhered silicide between milling experiments of identical compositions by another 5 minute milling in isopropyl alcohol, and fresh media were substituted when changing compositions. As-milled powders were screened to -120 mesh and stored in an argon-atmosphere glovebox. Some as-milled powder was consolidated into dense pellets by spark plasma sintering (SPS) (Dr. Sinter SPS-550, Fuji Corp., Japan) for further experiments and microstructural characterization of the monolithic product.

3.3 Experimental

In a typical milling experiment, 5 g of the elemental starting materials were weighed and added to the milling vessel along with fifteen 10 mm and ten 5 mm media in an argon atmosphere glovebox with $P_{O2} < 30$ ppm. Different sized media were used in order to randomize milling media trajectories and help ensure that no portion of the vessel contained unmilled material. Milling was conducted at 500 rpm for between 5 minutes and 8 hours. At least two experiments were conducted at the nominal composition of each line compound in Table 3.1, as well as at the nominal compositions identified as the middle eutectic (55% Si, $CeSi_{1.23}$) and near the Si-poor boundary of the $CeSi_{2-y}$ phase (61% Si, $CeSi_{1.56}$).

In a typical SPS experiment, 4 g of milled powder was loaded into a graphite die (I-85, Electrodes Inc, USA) in a nitrogen atmosphere glovebox with $P_{O2} < 200$ ppm. Samples were cold pressed at 5 kN in the die and then transported to the SPS in a polyethylene bag. The graphite dies had a 21 mm bore and 15 mm thick wall and were

lined with grafoil (99.8%, Alfa Aesar, USA). Samples were heated at 100°C/min to 1000-1300°C with a 5-15 minute hold. Process temperature was controlled by a pyrometer focused in a 5 mm bore hole drilled to within 5 mm of the sample. Samples were pre-loaded at 5kN in the SPS apparatus and held at 5 kN throughout the temperature ramp until cooldown. Sintered samples of $CeSi_{2-x}$, CeSi, and Ce_3Si_2 were prepared in this manner.

The crystallite size and phase of starting materials, as-milled powder, and sintered pellets were characterized by XRD in Bragg-Brentano geometry (Rigaku Miniflex, Japan). To avoid excessive oxidation, powder samples were mixed with a small amount of vacuum grease under argon before loading the XRD sample holder. A single peak was noted at 28.1° 2θ when characterizing a blank slide containing only vacuum grease. Phase identification was performed by comparison to the Inorganic Crystal Structure Database[17]. Microstructure and morphology were investigated by scanning electron microscopy and stoichiometry by energy dispersive spectroscopy (Hitachi 3400-N, Japan). EDS spectra were collected with an accelerating voltage of 10 kV to improve surface selectivity and sensitivity to silicon content.

3.4 Results

3.4.1 Pressure/Temperature Monitoring Results

The *in situ* monitoring of temperature and pressure revealed a small spike in pressure between 30 minutes and 150 minutes of milling at 500 rpm. The exact location depended on the composition, and the occurrence, height, and timing of the spike was repeatable to within 10% relative error from run to run. Representative data for four

different compositions are shown in Figure 3.1, with details of the ΔT calculation given in the discussion section. The inset shows a very nearly linear dependence of milling time before reaction on milling speed for the CeSi composition.

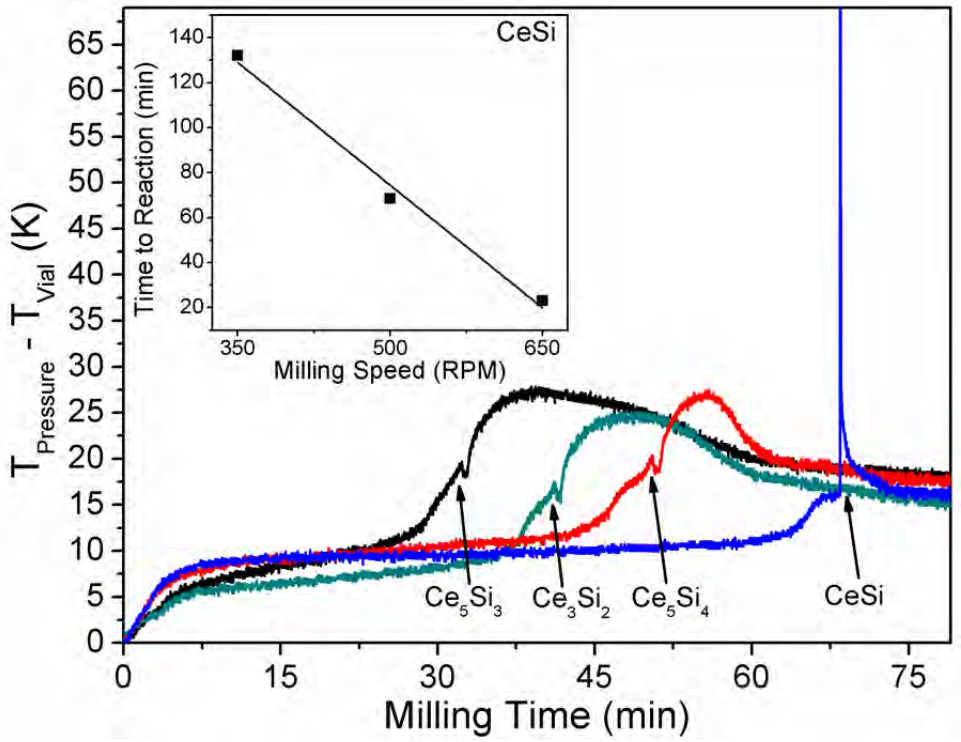

Figure 3.1 This figure shows ΔT (calculated from vessel parameters and measured P and T, see text) versus milling time for the indicated compositions. The arrow points to sharp peaks in the data indicative of MSR events. The inset shows the milling time to MSR ignition for CeSi at different milling speeds.

3.4.2 Milling Results

All of the line compounds in the Ce-Si system except Ce_5Si_4 were successfully synthesized by high-energy ball milling at 500 rpm. Representative diffraction plots for the each composition are shown in Figure 3.2.

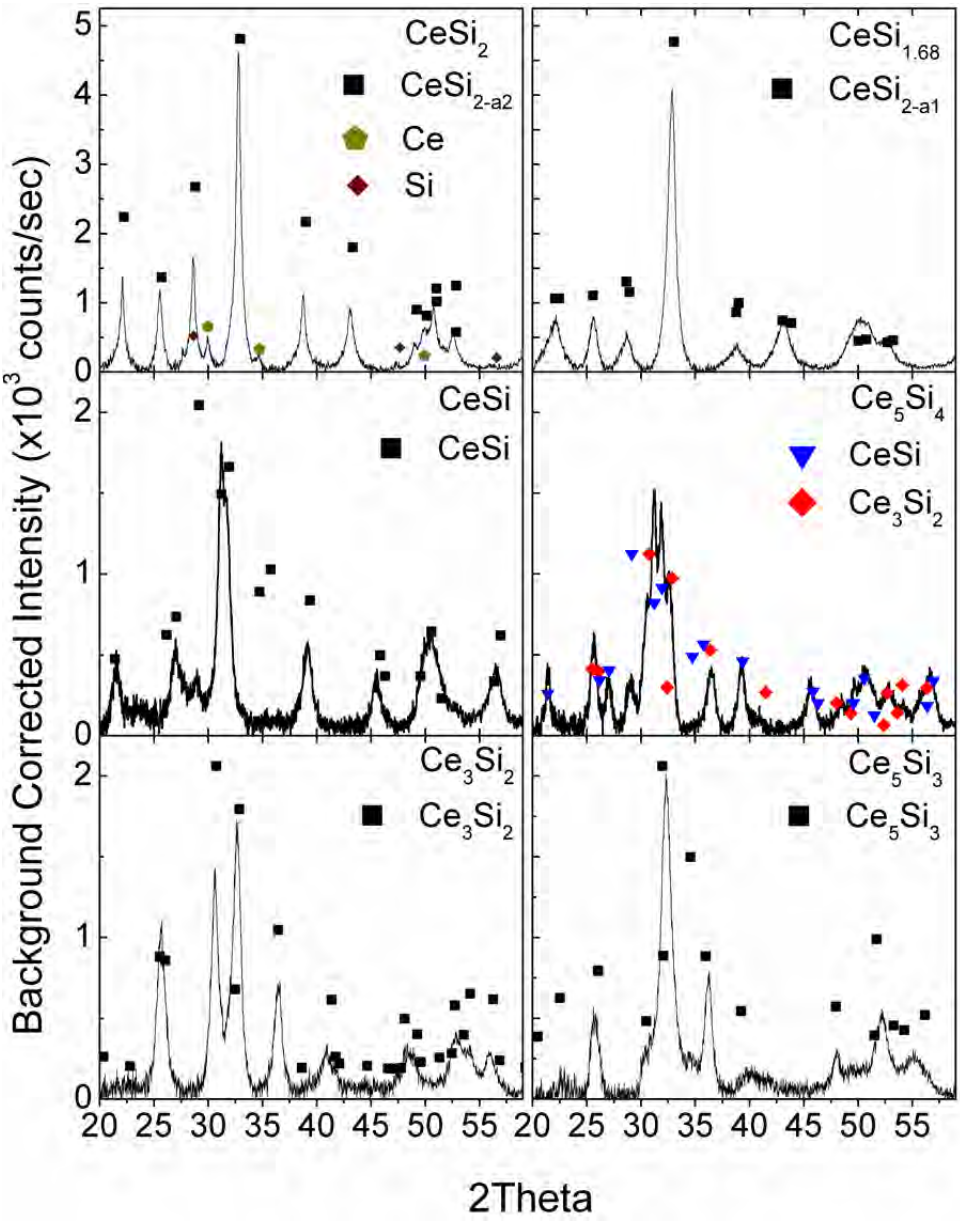

Figure 3.2 This figure displays the XRD 2θ spectra of cerium silicides synthesized by milling. The nominal composition is denoted in the top-right corner of each pane, and the experimentally observed phases denoted below the nominal composition. The desired phase was obtained in all cases except Ce_5Si_4.

XRD analysis of $CeSi_2$ showed a small amount of unreacted cerium, which was determined to be a consequence of a small amount of material that became trapped in the vessel lid seal during milling. No impurity phase was detected in XRD of $CeSi_{1.68}$, Ce_3Si_2 and Ce_5Si_3. The XRD pattern for CeSi matched the peak locations in the database but not

intensities, implying a change in structure from the Pbma orthorhombic phase commonly observed when cooling from the melt. There is precedence for formation of low-temperature (LN)Si phases in the lanthanides, although none have yet been reported for CeSi. The nominal composition Ce_5Si_4 showed the presence of CeSi and Ce_3Si_2 phases with little to no Ce_5Si_4. EDS investigation found minimal contamination of < 1% Zr and Fe from the milling media and vessel, respectively, after 6 hours of milling at 500 rpm. Figure 3 shows material with nominal composition Ce_3Si_2 as sampled just before (Figure 3c) and just after (Figure 3a,b) the P/T spike shown in Figure 1.

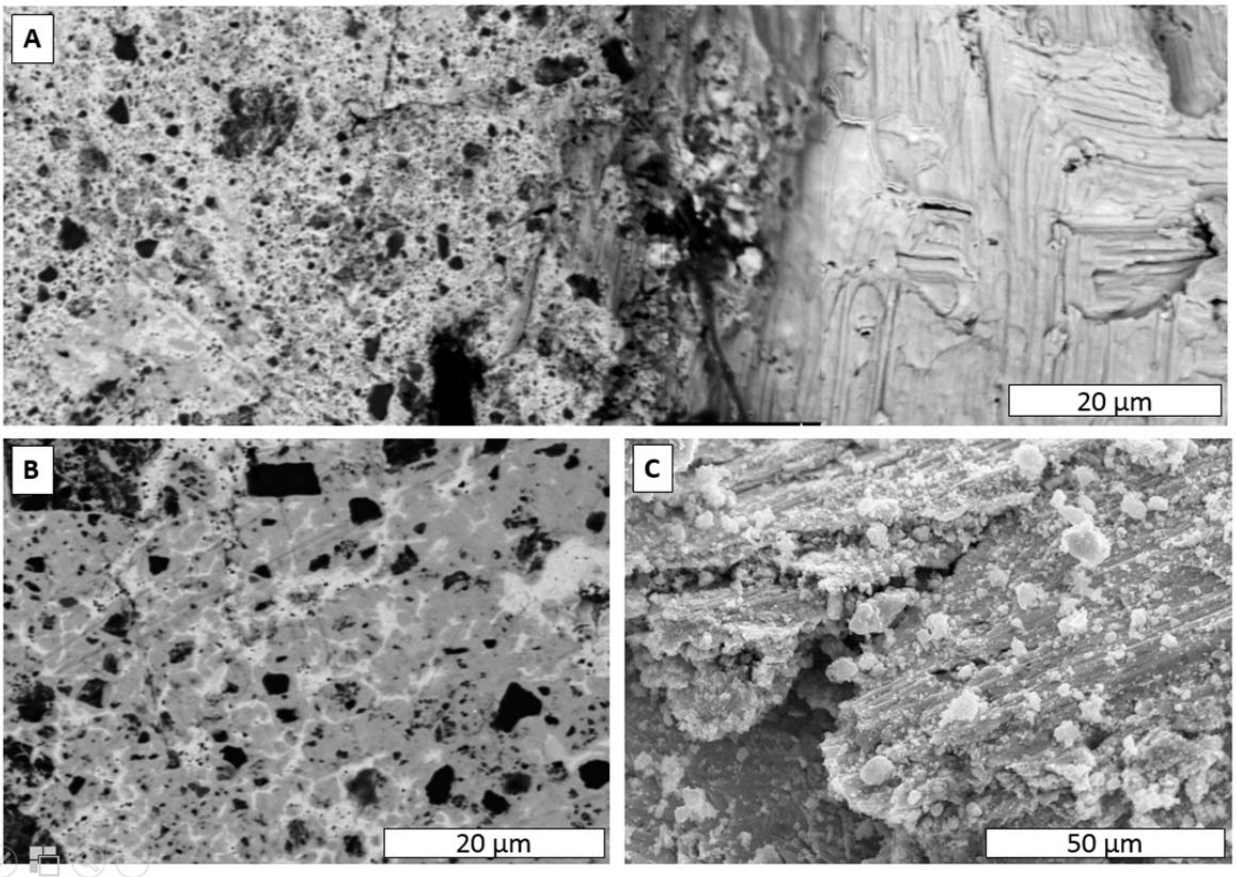

Figure 3.3 This figure shows SEM micrographs just before and after MSR in the Ce_3Si_2 composition. A) BSE panorama from a sectioned and polished fragment recovered directly after the MSR event. On the right side, a smooth Ce exterior implies melting during reaction, while moving toward the left reveals the

inhomogeneous interior. B) BSE micrograph of a Ce, Ce_2Si_3 and Si three-phase region from the same sample as A. C) SE micrograph prior to MSR event shows Si particles layered with Ce sheets.

3.4.3 Spark Plasma Sintering Results

A representative plot of the sintering temperature, pressure, and punch displacement during densification of a Ce_3Si_2 powder milled for 4 hr at 500 rpm is shown in Figure 3.4. Densification was nearly complete by 1000°C, indicated by the decrease in densification rate near the end of the temperature ramp. Spark plasma sintered samples, phase pure by XRD, were found to be greater than 95% of the theoretical density by the Archimedes method. Samples had a thin interaction layer with the grafoil liner (not shown) that was easily removed by polishing. A representative SEM micrograph of a fracture surface is shown in Figure 3.5, demonstrating the high density and very fine grain structure of the sintered material

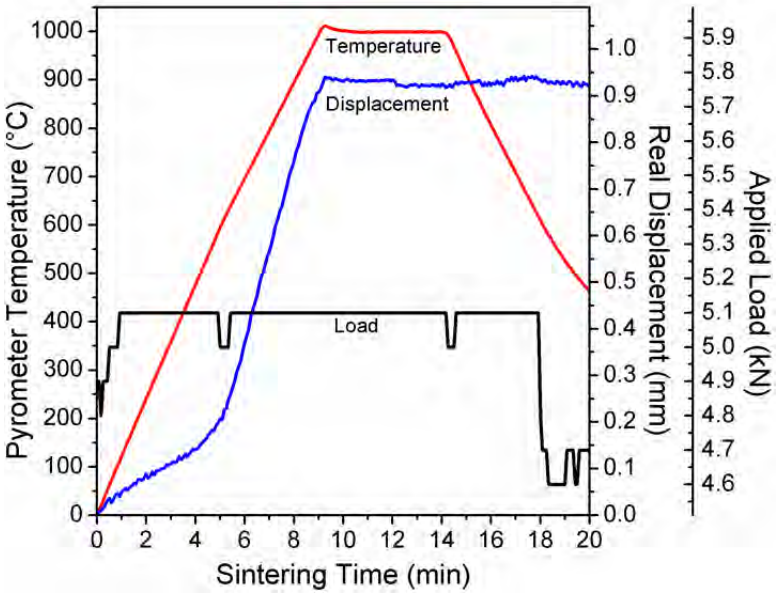

Figure 3.4 This figure shows a typical Spark Plasma Sintering experiment conducted with as-milled Ce_3Si_2 powder. The temperature was quickly raised to 1000°C at a constant 5kN load and held for 5 minutes before cooling to 600°C and releasing pressure.

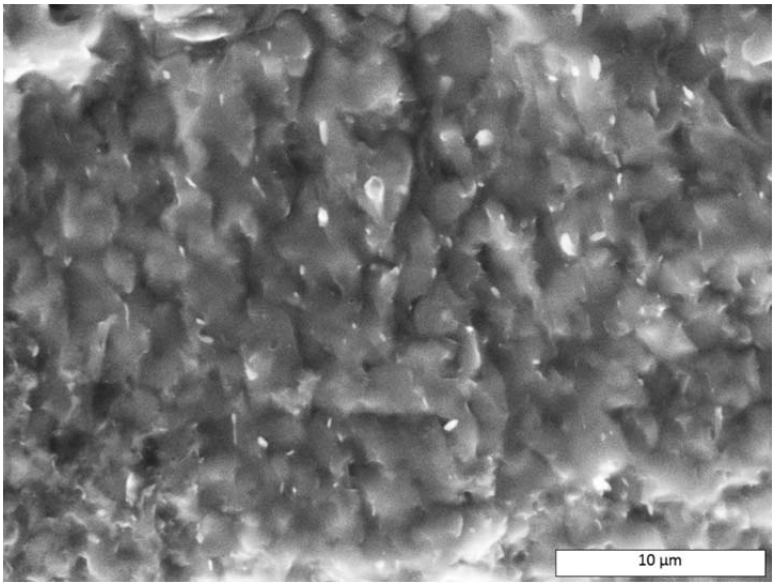

Figure 3.5 SEM micrograph of a fracture surface in a Ce_3Si_2 sample prepared by ball milling followed by SPS at 1000 C shows fine grain structure with a few small rounded pores at grain boundaries.

3.5 Discussion

3.5.1 In situ Pressure and Temperature Monitoring

For each milling run, the equilibrium temperature and pressure prior to the start of milling was used to calculate the constant P/T = nR/V for each experiment, where P and T are the measured pressure and temperature, V and n are the volume of the milling vessel and the moles of gas contained within, and R is the gas constant. This constant was then used to calculate the instantaneous temperature from the measured pressure throughout the milling experiment. The primary heat loss is convective cooling, which means that both the measured pressure and temperature are sensitive to the ambient temperature. However, the quantity ΔT calculated by subtracting the measured temperature from that calculated from the pressure is not particularly sensitive to the ambient T. Converting the P-T data to ΔT data in this manner is particularly convenient

as it allows for estimation of the energy flux through the system, which may be used to identify transient energy supplied by chemical reactions.

Table 3.2 presents data on the mass of powder both free in the vessel and adhered to media or vessel walls. These data demonstrate that the adhesion of milled material to the media is minimal prior to the MSR event for the Ce_3Si_2 composition (it is also minimal in the other compositions, not shown). This implies that the MSR events indicated by arrows in Figure 3.1 occur in the free volume of the milling vessel. However, some cerium should be expected to adhere to the milling media, resulting in a silicon-rich free powder. A reaction propagating through powder filling free space in the vessel would then produce a silicon-rich composition there, and a cerium-rich composition on the surface of the media and vessel. In fact, in no composition did the MSR event result in complete formation of the expected compound. The furthest extent was reached for the CeSi composition, in which the products directly after MSR were Ce_5Si_3 and $CeSi_{2-x}$. Other compositions display quenching behavior in which the MSR reaction is initiated, resulting in a brief spike in pressure, but the excess reactant absorbs more energy than the reaction can supply. In these cases, the MSR peak is followed by a broad hump in ΔT as the system components continue to react in the solid state.

Table 3.2 Phase and powder habit during milling of nominal composition Ce_3Si_2

Milling Time	0 min	30 min	35 min (MSR)	60 min	90 min	120 min	360 min
Phase content[a] (from XRD and EDS)	Ce, Si	Ce, Si	Ce, Ce_2Si_3, minor Si, Ce_5Si_3	Ce, Ce_3Si_2, CeSi, Ce_2Si_3	Ce, Ce_3Si_2, CeSi	Ce, Ce_3Si_2, minor CeSi	Ce_3Si_2
Free powder (g)	5	4.60	0.57	1.40	2.16	2.45	2.55
Free powder (%)	100	92	11	28	43	49	51
Powder on media (g)	0.00	0.10	2.83	1.49	0.44	0.34	0.39
Powder on media (%)	0	2	57	30	9	7	8
Powder on vessel (g)[b]	0.10	0.30	1.60	2.11	2.40	2.21	2.06
Powder on vessel (%)	3	6	32	42	48	44	41
Particle size (μm)	480	--	>1000	--	--	--	10
Particle morphology	Filings	Sheets	Adherent coating	--	--	--	Equiaxed

a. All contain ppm CeO_2 from O_2 exposure as well as < 0.1% ZrO_2 and < 0.1% Fe from milling
b. Powder on vessel calculated from Initial – Free – Media = Vessel

3.5.2 Phase Formation During Milling

The Effective Heat of Formation (EHF) model has proven quite successful at predicting the first phase formation in interfacial or thin film reactions involving silicon[14]. The effective heat of formation is found as $\Delta H_f' = \Delta H_f (x'/x)$ where (x'/x) is the number of moles of the nominal composition $A_{1-x}B_x$ that formed if the reaction proceeds to completion at the composition of the lowest melting eutectic $A_{1-x'}B_{x'}$. The predicted first phase is the congruent melting compound with the most negative ΔH_f' at the eutectic composition. There are three eutectic points in the Ce-Si system, with the lowest melting of these observed at 10.5 at % Ce[3]. EDS data (from the sample shown in Figure 3a, b) shows silicide grains surrounded by cerium metal containing approximately 10 atom % silicon. This data supports the assumption that a eutectic phase is formed during the MSR event. Therefore, the limiting element x' is assumed by the EHF model is Si = 10.5 at % for all compositions and the effective heat of formation for each compound is given by:

$$\Delta E_f'\left(Ce_xSi_y\right) = \Delta H_f^{298}\left(Ce_xSi_y\right)\mathbf{0.105}\left(\frac{x+y}{y}\right) \quad (3.1)$$

The first formed phase predicted by the EHF model is has the most negative ΔH_f'. . However, the existing literature reports $CeSi_{2-y}$ ($y \approx 0.3$) for thin Ce films in contact with silicon[18, 19]. , and in the present case $CeSi_{2-y}$ ($y \approx 0.5$) is observed as the first phase. The first formation of a phase with the silicon-deficient $CeSi_{2-y}$ orthorhombic crystal structure appears to be a failure of the EHF model in this case, which may indicate errors in the literature heats of formation. Despite the shortcomings of the model in this case, the calculated values of ΔH_f' listed in Table 3.1 correlate remarkably well with the experimentally observed time of MSR ignition at each composition as shown in Figure 3.6.

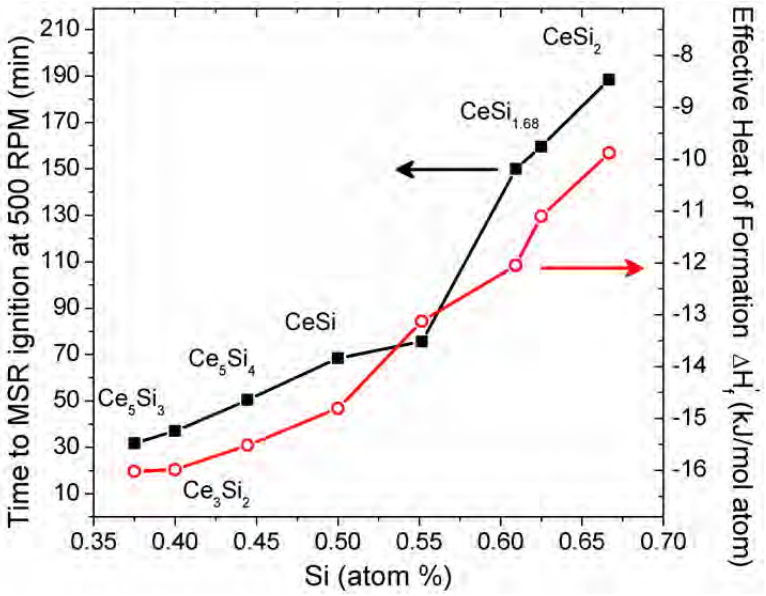

Figure 3.6 This figure shows the correlation of MSR ignition time at 500 RPM for 5 g loads of all compositions studied (left axis) and the effective heat of formation of each composition at the $Ce_{0.895}Si_{0.105}$ eutectic (right axis)

We therefore suggest that the EHF model, which was developed for thin films, is also an effective tool for predicting the behavior of milled material systems with multiple binary compounds.

All milling experiments examined in SEM/EDS after an MSR event contained a phase with approximate composition Ce_2Si_3. Cerium-rich compositions contained inhomogeneous regions of elemental silicon and what appeared to be a Ce-Si eutectic phase with 10-20 atom % Si Si (Figure 3 shows an example for the Ce_3Si_2 composition). The CeSi composition was found to consist of Ce_5Si_3 and Ce_2Si_3 directly after the MSR event. This may be explained by the presence of local inhomogeneity within the milling vessel. Some cerium will always stick to the milling media and will form a cerium rich phase during any nearly complete reaction. This in turn results in the formation of a Si-rich phase in the free volume of the milling jar, followed by a relatively quick mechanochemical reaction of the two phases to form the desired compound. In compositions further from CeSi with its nearly complete MSR behavior, the total amount of off-stoichiometric compounds formed is larger, leading to an increase in width of the post-MSR humps observed in Figure 3.1. Table 3.2 lists some data versus milling time for the Ce_3Si_2 composition, showing the phase progression with increasing milling time as well as the physical location of the milled material within the vessel.

3.5.3 Thermodynamics of Ce_5Si_4 Formation

All cerium silicide line compounds *except* Ce_5Si_4 were prepared by milling for 6 hours or less at 500 rpm. The inability to easily form Ce_5Si_4 is interesting and may be explained in terms of the molar volumes found in Table 3.1. The free energy of formation is commonly written as $\Delta G = \Delta Hf - T\Delta S$. In high-energy ball milling, the entropy term is

often neglected as both T and ΔS are small compared to ΔH. However, under high pressure conditions or in systems with large volume changes, the free energy of formation must account for these terms[20].

The solid state reaction $Ce_3Si_2 + 2CeSi = Ce_5Si_4$ has ΔG_f = -4.97 kJ/mol at reference temperature and pressure, and a volume change of + 4.95 cm^3/mol. With a negative free energy of formation, this reaction is thermodynamically likely to proceed. However, the reaction is driven by the milling media impacts, with an impact pressure estimated from closed form hertzian milling modeling[21] to be approximately 5 GPa. Under these conditions, the large volume expansion associated with the formation of Ce_5Si_4 from the bordering line compounds CeSi and Ce_3Si_2 results in a positive free energy of formation for pressures exceeding $\Delta H_f/\Delta V$ = 950 MPa. The given reaction $Ce_3Si_2 + 2CeSi = Ce_5Si_4$ at 5 GPa has a modified $\Delta G_f^{298K, 5GPa}$ = +18.31 kJ/mol, which provides a thermodynamic argument for the experimental difficulty in forming Ce_5Si_4 in the impact-driven milling system studied

3.5.4 Time to MSR Ignition Since MSR behavior was observed for the CeSi composition, CeSi was investigated further by milling at different speeds and at different powder loads. Changing the volume of milled powder produced a linear change in the time required for MSR ignition, which is in line with the recent results of Gotor, *et al.* [22], who studied the Zn-Se system. However, milling Ce-Si at different speeds *also* resulted in a linear change in the ignition time, as shown in Figure 3.4, inset. This indicates MSR kinetics that depend only on the number of milling media impacts[21, 23], which at first seems to contradict the rpm^3 dependence described by Gotor, *et al.* as being proportional to the mechanical dose absorbed by the powder.

However, this discrepancy may be resolved by considering the particle sizes involved. Gotor milled Zn and Se at -325 mesh, while we have milled Ce and Si at -40/+60 mesh. If we assume that the phenomenon of atomic level mixing during milling is driven by grain size refinement in the milled material, resulting in a mechanical dose dependence, then we may make use of the well-known empirical laws of grinding summarized by Hukki[24] to estimate the actual dependence of grain refinement on mechanical dose. Huuki proposed a "solomnic settlement," a combined law of form

$$\boldsymbol{dE = -C\frac{dx}{x^{f(x)}}} \tag{3.2}$$

where x is the critical dimension of a comminuted material, C is a material constant, and f(x) describes some dependence of dE on the current size. Rittinger's law predicts the energy required for particle size reduction in very small (< 10 μm) particles to be proportional to the new surface created and requires f(x) = 2 in Equation 3.2. The relationship observed by Gotor, *et al.* for Zn-Se involves milling kinetics that depend on the energetic dose as in Rittenger's Law. Another form of Equation 2 with f(x) = 1 is known as Kick's Law and covers the range of somewhat larger (100-1000 μm) particles. In this regime, fracture, sheet thinning, and other forms of dimension reduction depend only on the number of times the particle is struck with an appropriate force, and this is the relationship observed in the Ce-Si system.

A caveat to note is that Hukki's combined law is empirically derived for brittle materials, and while work has been done to consider elastic deformation and fracture in terms of a combined law[25], it does not appear that a satisfactory model currently exists to describe grain refinement in ductile materials during milling. That should not detract from the general applicability of the model in this instance, as the central point is that

particle size reduction or grain refinement during milling is not inversely proportional to milling dose for relatively large starting particle size.

3.5.6 Phenomenological Model

The phase content and particle morphology of milled cerium and silicon proceeds in a manner typical of ductile-brittle systems with the added complexity of an intermediate MSR event. When milling at 500 rpm, the system follows well-defined steps:

1. 0-30 minutes: Cerium is plastically deformed from > 100 μm filings into < 10 μm sheets
    a. Formation of cerium / silicon laminate structure (Figure 3.3c)
2. 30-70 minutes: Cerium and silicon undergo incomplete reaction in an MSR event (Figure 3.1)
    a. Ignition time linearly dependent on milling speed (Figure 3.1, inset)
    b. Ignition time correlated to effective heat of formation at nominal composition (Figure 3.6)
3. MSR: Cerium and silicon react to form an intermediate compound
    a. Ce-rich compositions contain silicide and free silicon surrounded by cerium (Figure 3.3a, b)
    b. XRD indicates $CeSi_{2-y}$ defect orthorhombic structure
    c. EDS indicates Ce_2Si_3 MSR product as well as $Ce_{0.895}Si_{0.105}$ eutectic
4. MSR-2 hours: Cerium quickly reacts with the silicide formed during the MSR
    a. Broad peak in heat release by solid state reaction (Figure 3.1)

3.6 Conclusions

All cerium silicide line compounds save Ce_5Si_4 were successfully synthesized by mechanochemical processing of elemental cerium and silicon. The nominal composition Ce_5Si_4 could not be synthesized in this manner and remained a two phase mixture of CeSi and Ce_3Si_2 after 6 hours of milling at 500 rpm. The synthesis proceeded by means of a mechanically-induced self-propagating reaction to form a phase with the orthorhombic $CeSi_{2-y}$ crystal structure and nominal composition Ce_2Si_3. The MSR event took place after a characteristic induction time that was shown to correlate with the effective heat of formation for each composition at the lowest melting eutectic. Microstructural evidence

suggests that the reactants were partially or totally melted during MSR events. The MSR event was followed by a rapid solid state diffusion reaction between the Ce_2Si_3 compound and excess Ce and/or Si to form an essentially single phase product with the nominal starting composition. Some Ce_3Si_2, CeSi and $CeSi_{2-x}$ powders were consolidated by spark plasma sintering, resulting in pellets of 95% or higher theoretical density and fine, equiaxed grain structure.

3.7 Acknowledgments

This project was partially supported by the Department of Energy under NEUP award #00120690. Paul Lessing at the Idaho National Laboratory, Dan Osterberg and Bryan Forsmann at Boise State University, and Kolton Urso and Beata Tyburska-Püschel at University of Wisconsin-Madison all contributed helpful discussion during this project.

3.8 Author Justification

The research presented in this publication was carried out by Gordon Alanko, Brian Jacques, Allyssa Bateman, and Dr. Darryl P. Butt. Gordon Alanko designed and conducted milling experiments in discussion with Dr. Darryl P. Butt. Brian Jaques and Allyssa Bateman assisted in material characterization. The work done by Gordon Alanko was in partial fulfillment of the requirements for a Doctoral degree in Materials Science and Engineering at Boise State University, under the advisement and supervision of Dr. Darryl P. Butt. Dr. Darryl P. Butt contributed greatly in terms of financial support, discussion of processing routes, and critical review of the article throughout the writing process.

3.9 References

[1] M. Kohgi, T. Satoh, K. Ohoyama, M. Arai, Competition Between the Kondo Effect and RKKY Interactions in $CeSi_x$, Physica B 169 (1991) pp. 501-502.

[2] D. Souptel, G. Behr, W. Loser, A. Teresiak, S. Drotziger, C. Pfleiderer, CeSi2-delta single crystals: growth features and properties, J Cryst. Growth 269 (2004) pp. 606-616.

[3] M.V. Bulanova, P.N. Zheltov, K.A. Meleshevich, P.A. Saltykov, G. Effenberg, Cerium-silicon system, J. Alloy. Compd. 345 (2002) pp. 110-115.

[4] L.C. Wang, Q.Y. Dong, J. Lu, X.P. Shao, Z.J. Mo, Z.Y. Xu, J.R. Sun, F.X. Hu, B.G. Shen, Low-temperature large magnetocaloric effect in the antiferromagnetic CeSi compound, J. Alloy. Compd. 587 (2014) pp. 10-13.

[5] H. Zhang, Y. Mudryk, Q. Cao, V.K. Pecharsky, K.A. Gschneidner, Y. Long, Phase relationships, and structural, magnetic, and magnetocaloric properties in the Ce_5Si_4-Ce_5Ge_4 system, J. Appl. Phys. 107 (2010) pp. 10.

[6] S. Pasebani, I. Charit, Y.Q. Wu, D.P. Butt, J.I. Cole, Mechanical alloying of lanthana-bearing nanostructured ferritic steels, Acta Mater. 61 (2013) pp. 5605-5617.

[7] C. Suryanarayana, Mechanical alloying and milling, Prog. Mater. Sci. 46 (2001) pp. 1-184.

[8] R.K. Viswanadham, S.K. Mannan, S. Kumar, Mechanical Alloying Behavior in Group-V Transition-Metal Silicides, Scripta Metall. 22 (1988) pp. 1011-1014.

[9] Le Caër, E. Bauer-Grosse, A. Pianelli, E. Bouzy, P. Matteazzi, Mechanically Driven Syntheses of Carbides and Silicides, J. Mater. Sci. 25 (1990) pp. 4726-4731.

[10] L. Takacs, Self-sustaining reactions induced by ball milling, Prog. Mater. Sci. 47 (2002) pp. 355-414.

[11] Z. Munir, U. Anselmi-Tamburini, Self-propagating exothermic reactions: The synthesis of high-temperature materials by combustion, Mater. Sci. Rep. 3 (1989) pp. 279–365.

[12] S.V. Meschel, O.J. Kleppa, Standard Enthalpies of Formation of Some Carbides, Silicides and Germanides of Cerium and Praseodymium, J. Alloy. Compd. 220 (1995) pp. 88-93.

[13] A. Shukla, Y.B. Kang, A.D. Pelton, Thermodynamic assessment of the Ce-Si, Y-Si, Mg-Ce-Si and Mg-Y-Si systems, Int. J. Mater. Res. 100 (2009) pp. 208-217.

[14] C.C. Theron, O.M. Ndwandwe, J.C. Lombaard, R. Pretorius, First phase formation at interfaces: Comparison between Walser-Bene and effective heat of formation model, Mater. Chem. Phys. 46 (1996) pp. 238-247.

[15] P. Schobingerpapamantellos, K.H.J. Buschow, 2-Step Ferromagnetic Ordering of Ce_2Si_3-Delta, J. Alloy. Compd. 198 (1993) pp. 47-50.

[16] E. Houssay, A. Rouault, O. Thomas, R. Madar, J.P. Senateur, Metallurgical Reinvestigation of the Rare Earth Silicides, App. Surf. Sci. 38 (1989) pp. 156-161.

[17] Inorganic Crystal Structure Database, FIZ Karlsruhe, icsd.fiz-karlsruhe.de, Accessed 4/2014.

[18] C.C. Hsu, J. Ho, J.J. Qian, Y.T. Wang, Cerium Silicide Formation in Thin Ce-Si Multilayer Films, J. Vac. Sci. Tech. A 9 (1991) pp. 998-1001.

[19] R.D. Thompson, B.Y. Tsaur, K.N. Tu, Contact Reaction Between Si and Rare-Earth Metals, Appl. Phys. Lett. 38 (1981) pp. 535-537.

[20] E. Brosh, R.Z. Shneck, G. Makov, Explicit Gibbs Free Energy Equation of State for Solids, J. Phys. Chem. Solid. 69 (2008) pp. 1912-1922.

[21] P.P. Chattopadhyay, I. Manna, S. Talapatra, S.K. Pabi, A mathematical analysis of milling mechanics in a planetary ball mill, Mater. Chem. Phys. 68 (2001) pp. 85-94.

[22] F.J. Gotor, M. Achimovicova, C. Real, P. Balaz, Influence of the milling parameters on the mechanical work intensity in planetary mills, Powder Technol. 233 (2013) pp. 1-7.

[23] A. Iasonna, M. Magini, Power measurements during mechanical milling. An experimental way to investigate the energy transfer phenomena, Acta Mater. 44 (1996) pp. 1109-1117.

[24] R.T. Hukki, Proposal for a Solomnic Settlement between the Theories of von Rittinger, Kick, and Bond, Trans. Am. Inst. Min. Metall. Eng. 220 (1961) pp. 403-408.

[25] A. Thomas, L.O. Filippov, Fractures, fractals and breakage energy of mineral particles, Int. J. Miner. Process. 57 (1999) pp. 285-301

CHAPTER FOUR: MECHANOCHEMICAL SYNTHESIS OF CERIUM MONOSULFIDE

Mechanochemical Synthesis of Cerium Monosulfide

Gordon A. Alanko[1] and Darryl P. Butt[1,2,*]

1. Department of Materials Science and Engineering, College of Engineering
Boise State University, Boise, ID, 83725

2. Center for Advanced Energy Studies
Idaho Falls, ID 83401

Abstract

Cerium sulfides were prepared by high-energy ball milling of high purity Ce and S powders. Starting materials were milled while monitoring the temperature and pressure *in situ* to observe the reaction kinetics. Starting and mechanically alloyed powders were further characterized by x-ray diffraction, electron microscopy, and energy dispersive spectroscopy. For the first time, it is demonstrated that cerium monosulfide, which has historically been produced only at very high temperatures using both toxic and flammable gases, can be produced from a stoichiometric mixture of the elemental powders at near room temperature. It is shown that the formation of the monosulfide involves a very rapid reaction of intermediate compounds consistent with a mechanochemically-induced self-propagating reaction (MSR).

4.1 Introduction

The rare earth chalcogenides have potential for use as refractories[1] and possess other interesting and valuable properties[2, 3] Cerium monosulfide, CeS, is a particularly interesting rare earth compound with a number of highly desirable refractory properties, including the highest melting point (2450°C) of the sulfides, and an extremely high thermal conductivity. Under inert atmosphere or vacuum, CeS has a very low vapor pressure below 1900°C. CeS also has outstanding compatibility with highly electropositive metals, such as the alkaline earths, lanthanides, actinides, and transition metals,[1] and has even been shown to be non-wetting in contact with some molten metals.[4] Consequently, CeS is an outstanding crucible material for the melting and casting of reactive metals. Table 4.1 lists the refractory compounds in the Ce-S system along with

heats of formation,[5] crystallographic information,[5] and values for selected thermophysical properties.[6, 7]

Table 4.1 Summary of crystal structures and selected properties, where available, of known refractory compounds in the Ce-S system

Phase	**γ-Ce_2S_3**	**$Ce_{3-x}S_4$**	**Ce_3S_4**	**CeS**
Unit cell	Cubic	Cubic	Cubic	Cubic
Space Group	I-43d	I-43d	I-43d	Fm-3m
Prototype	Th_3P_4	Th_3P_4	Th_3P_4	NaCl
Molar mass (g/mol)	376.43	--	548.61	172.2
Density (g/cm^3)	5.15	--	5.68	5.93
Formation Reaction	Unknown	Peritectoid	Congruent	Congruent
ΔH_f^{298} (kJ/mol atom)	1154.35	--	1652.91	456.48
Heat Capacity (J mol/K)	126	--	--	50
Thermal Expansion (1/K)	10.5-13.2	--	12.3	9.8-12.4
Thermal conductivity (W/m K)	--	--	3.8	16.3[a]

a. Sample with 13% porosity and unspecified impurity content

The reported methods for synthesizing CeS, recently summarized by Gibbard *et al.*[8] require the use of hazardous gases (H_2 and H_2S), high temperatures (>2000°C), and multiple processing steps. All of these factors contribute to an environmentally unfriendly process with a very high production cost, and in fact we are unaware of any current commercial availability of CeS at this time.

Here we describe a new means for preparing CeS by high-energy ball milling. High-energy ball milling is in effect a mechanochemical process in which the driving force for chemical reaction is at least partially supplied by energetic milling media impacts. In contrast to the traditional methods for synthesizing CeS, mechanochemical processing is self-contained, very amenable to alloying or doping, uses no hazardous chemicals such as CeH_2 or gases such as H_2S, and requires minimal infrastructure. The

method has been used to synthesize a variety of compounds including chalcogonides of Sn, Zn, Zr, Hf, and Ti.[9, 10] Tsuzuki and McCormick[11] prepared nanostructured Ce_2S_3 by ball milling, but did not report CeS formation. Successful mechanochemical synthesis of CeS will have low process cost and low environmental impact as primary advantages, which could enable wide scale production and expand the realized range of applications of CeS.

4.2 Materials and Methods

A planetary ball mill (Retsch PM100, Haan, Germany) with a 250 mL hardened steel milling vessel and hardened steel spherical media were used for all experiments. The pressure and temperature within the milling vessel were monitored during milling by sensors mounted in the milling vessel lid, transmitted to a nearby computer by wireless Bluetooth link and logged for analysis. The pressure sampling rate was 20 s^{-1} and temperature sampling rate was 1 s^{-1}; both are plotted at 1 s^{-1} . The ambient pressure and temperature near the mill were monitored at 10 minute intervals (Extech SD700, Nashua, NH, USA) during the milling process. The starting materials used to synthesize CeS included cerium metal filings (99.999%, -40 mesh, ESPI Metals, Ashland, OR, USA) and sulfur powder (99.999%, Acros Organics, Fair Lawn, NJ, USA). X-ray diffraction analyses showed both starting materials to be phase pure within the detection limit of the XRD. In a typical synthesis, 5 g of the starting materials were added to the milling vessel in an argon atmosphere glovebox with PO2 < 30 ppm. Two sizes of milling media were used to help randomize media trajectories and ensure than the full interior surface of the vessel would be struck by media during milling. A total of fifteen media of 10 mm

diameter and an additional ten of 5 mm diameter were added to the milling vessel, which was then sealed. Milling was conducted at 500 rpm for between 50 minutes and 12 hours.

Samples were taken at different milling times for x-ray diffraction (XRD) and microstructural analysis. The starting materials and as-milled powder crystallite size and phases were characterized by XRD in Bragg-Brentano geometry (Rigaku Miniflex, Tokyo, Japan). To avoid potential oxidation, powder samples were mixed with a small amount of silica vacuum grease under an argon atmosphere. A characteristic XRD peak for the grease was noted at 28.1° 2θ. Phase identification was performed by comparison to the Inorganic Crystal Structure Database.[12] Microstructure and morphology of the precursor and as-milled powders were investigated by optical microscopy (Leica DM6000M, Buffalo Grove, IL, USA). Microstructure and chemical composition were investigated by scanning electron microscopy (SEM) and energy dispersive spectroscopy (EDS), respectively (Hitachi 3400-N, Tokyo, Japan). Samples were mounted in resin and polished down to a 1 μm diamond finish to reveal particle cross sections as a function of milling conditions.

4.3 Results

All milling runs displayed at least two high-intensity pressure spikes with a corresponding rapid increase in the temperature of the milling vessel. A representative data set for a 12 hour milling run is shown in Figure 4.1, with the inset providing detail of the transient behavior. The sudden increases in the temperature of a milling vessel has been attributed to the initiation of a sudden reaction in the starting materials in a process termed mechanochemically-induced self-propagating reaction (MSR) by an early investigator of the phenomena.[13] The pressure and temperature spikes observed after

approximately one hour of milling are evidence of an MSR-type reaction in the Ce-S system. Pressure and temperature data collected during multiple milling runs of powder mixtures of fixed stoichiometry exhibited approximately the same induction time before the onset of the first MSR event with times being repeatable to within 10% absolute error from run to run.

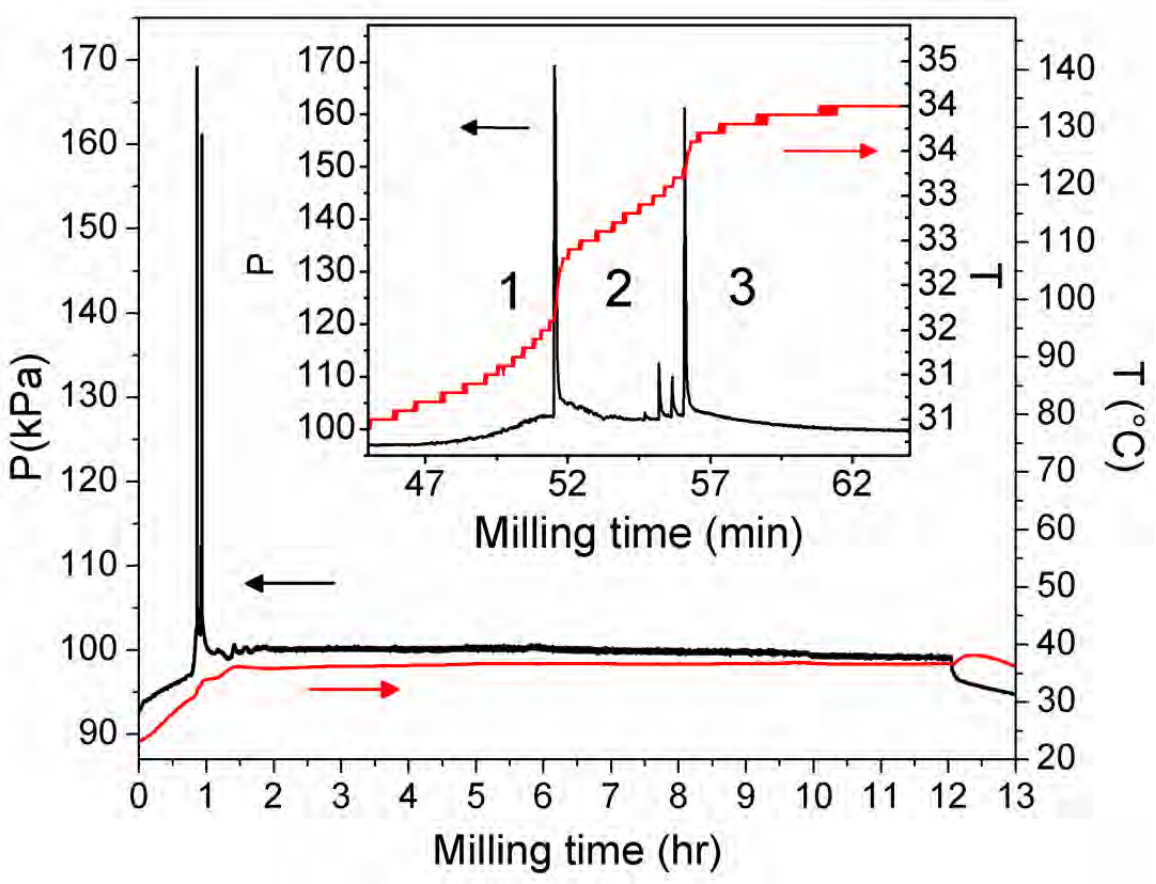

Figure 4.1 Plot of pressure (left axis) and temperature (right axis) versus time measured in situ during the milling of a stoichiometric mixture of Ce and S. The two major thermal events were repeatable and were associated with a self propagating reaction. In separate experiments, the reactions were terminated carefully during the stages of milling labled 1, 2, and 3 and powder samples taken for characterization of the phase and microstructural character (described in text).

Following the first MSR event, a second MSR event followed 5 ± 1 min later. Often one or more intermediate MSR events, small in magnitude, were observed just

before the second MSR event. This type of behavior has been previously observed and attributed to incomplete reaction or "hot spot" formation.[14]

Representative diffraction patterns are shown in Figure 4.2 from the milling time intervals labeled regions 1, 2, 3 in Figure 4.1. From these data, it is apparent that the milled materials remain as distinct cerium and sulfur until initiation of the first MSR reaction. Figure 4.2, region 1 shows diffraction data after 50 minutes of milling where the Ce and S peaks are strong and there is no evidence of solid solution or compound formation. Visual inspection of the milled materials revealed that the cerium remained in the form of coherent filings similar to that of the starting material and the sulfur was a grey-green finely dispersed powder. The diffraction data from the intermediate region 2 shows the formation of CeS and minor amounts of a cubic sulfide with the generic formula $Ce_{3-x}S_4$. A significant percentage of both cerium and sulfur remained unreacted at this intermediate stage in the overall reaction, and most of the powder charge is adhered to the milling media and vessel walls. After several more minutes of milling, the powder charge is removed from the walls and media through collision events and subsequently reacts in the second major MSR event. The diffraction data from region 3, just after the second MSR event, shows the remaining free sulfur is almost entirely consumed to form more CeS and $Ce_{3-x}S_4$, while some free cerium remained in the material at this stage and was shown to gradually react with the $Ce_{3-x}S_4$ compound with further milling. Diffraction analysis at 3, 4, 6, and 12 hours of milling show a gradual reduction in free cerium and $Ce_{3-x}S_4$ with the consequent formation of additional CeS. This final stage is classic mechanical alloying behavior for a ductile (CeS, Ce) – brittle ($Ce_{3-x}S_4$) system.[9]

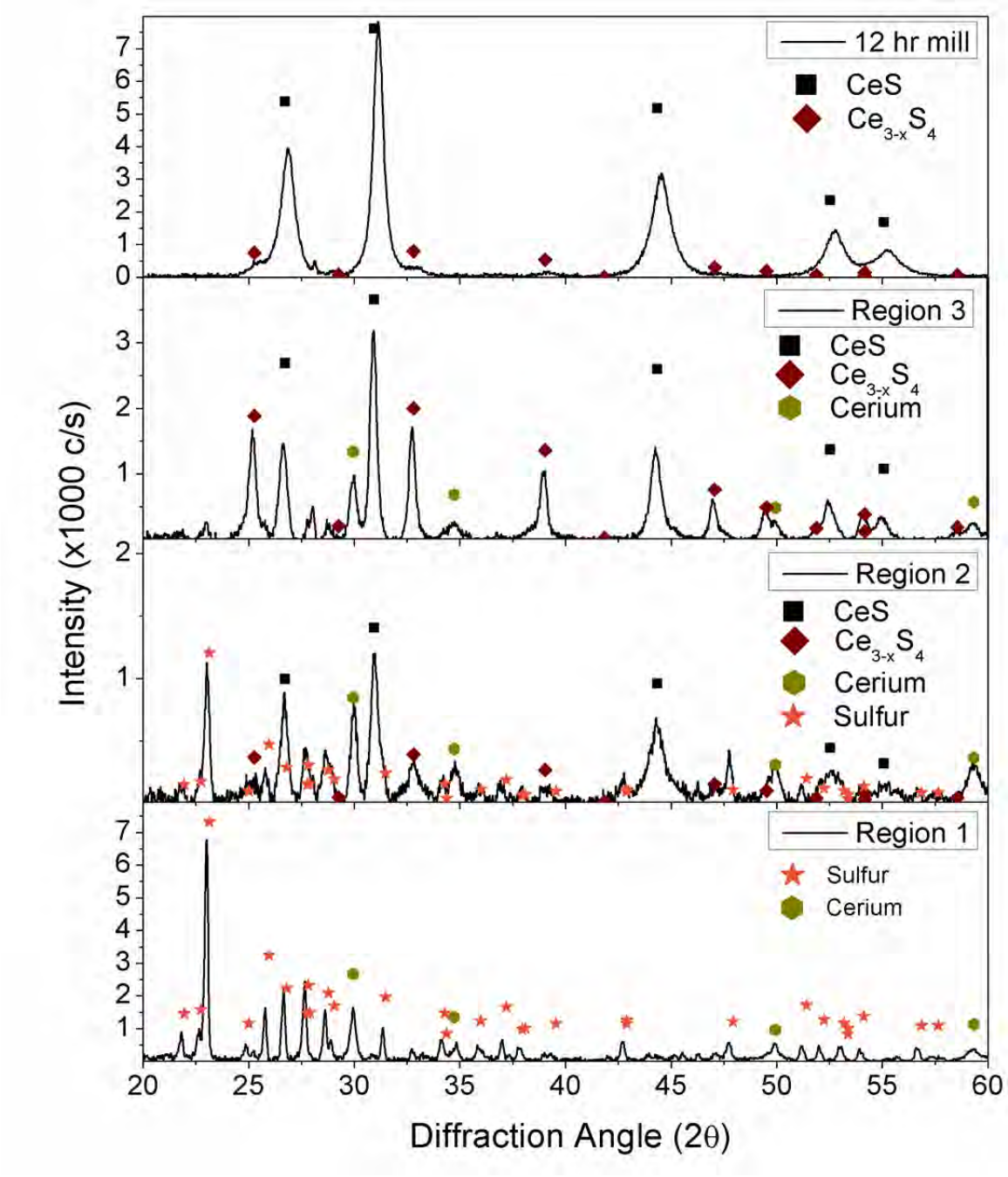

Figure 4.2 The plot shows x-ray diffraction 2θ scans from the marked regions in Figure 4.1 as well as a 12 hr milling run (labeled in plot). Also shown are expected peak positions for cerium (gold hexagons), sulfur (orange stars), $Ce_{3-x}S_4$ (red diamonds), and CeS (black squares).

No oxide or oxysulfide was produced during milling at levels detectable by XRD. Inspection of Figure 4.2 reveals a small amount of Ce_2S_3 remaining in the powder milled

for 12 hours at 500 rpm. This is believed to be the result of the tendency of the milling vessel and lid assembly to trap small amounts (0.2-0.4 g) of milled material at the seam of the lid. After every milling run, the material removed from this area contained metallic flakes of cerium along with some $Ce_{3-x}S_4$. This material is knocked into the seam during both of the pressure spikes during milling, and a better seal in the milling vessel should remove this source of non-stoichiometry in the finished material. In many applications, however, minor percentages of Ce_2S_3 would not be deleterious.

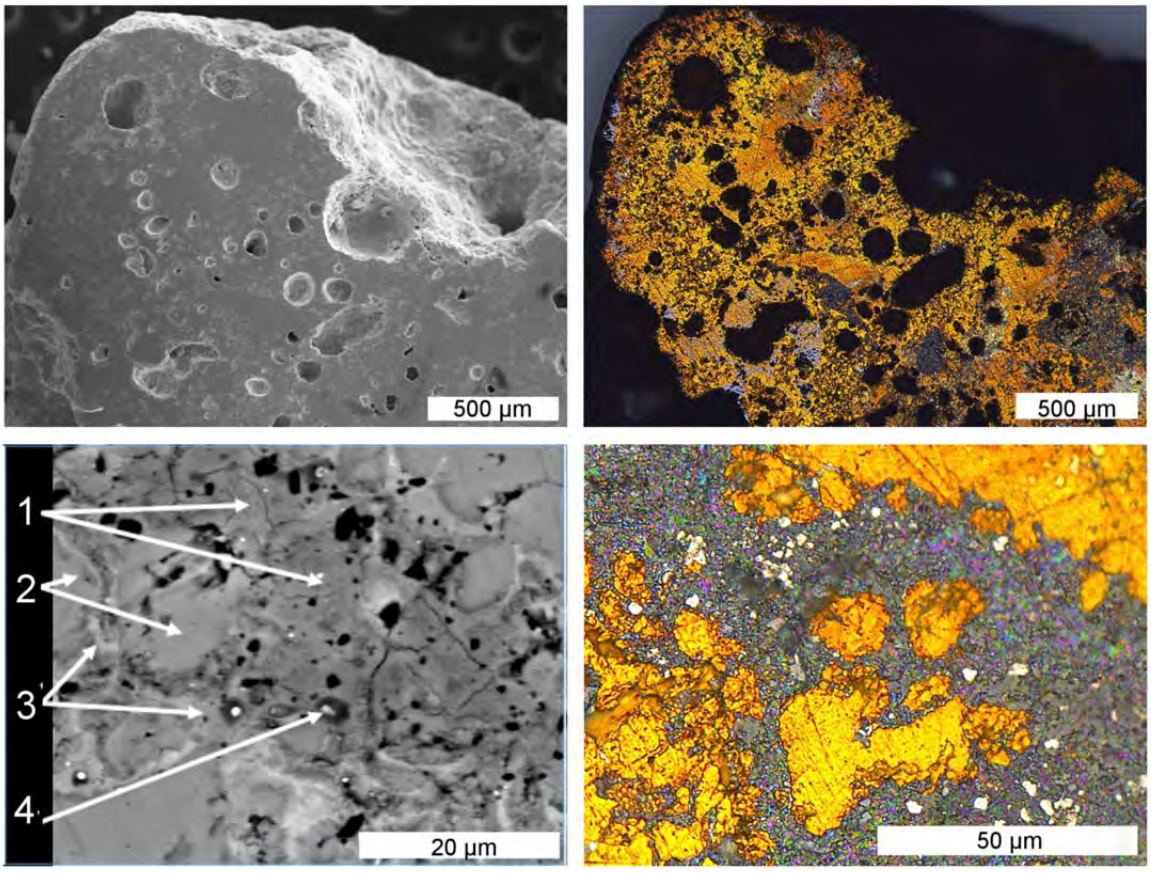

Figure 4.3 Comparisons of backscattered electron images (left column) with bright-field optical images (right column) at increasing magnification (top to bottom). Panel (e) shows phases identified by EDS, where 1=$Ce_{3-x}S_4$, 2= CeS, 3=Ce and 4=S.

A representative particle was sampled in Region 3, just after the second MSR event. The particle was cross-sectioned and polished for microstructural characterization, and optical and electron micrographs are shown in Figure 4.3. The material had some internal porosity with spherical or rounded features, possibly indicative of the evolution of high-temperature entrapped gas. The CeS grains tended to have rounded surfaces as well. Backscatter imaging and EDS analyses indicated that the CeS grains were generally coated with a thin (<1 μm) layer of cerium metal at this stage. The experimental quantity of 5 g of cerium forms 0.0357 moles of stoichiometric CeS with an enthalpy of formation of 18.3 kJ. By conducting dummy milling runs without reaction, we understand that the heat production during an MSR event is dominated by the Ce-S reaction rather than mechanical heat generated by the mill. The measured pressure spikes represent significant energy released into the milling vessel by quick reaction of the starting materials. This energy can be estimated by the well known relationship $E \approx RT_{rxn} = \Delta P_{rxn} V/n$, where ΔP_{rxn} is the measured pressure spike associated with the MSR event and the system constant V/n, calculated from the ideal gas law and free milling vessel volume, is equal to 0.026 m^3/mol. If the pressure spike is assumed to be close to adiabatic, then the energy absorbed by the milling vessel may be neglected and the minimum energy released at each major pressure spike is estimated to be 1.5-2 kJ. This is more than the approximately 1 kJ required to raise the starting materials from 25°C to their respective melting points under adiabatic conditions. Thus, even though direct observation was not possible in the present experimental configuration, it is hypothesized that melting of the starting materials occurred during the observed MSR events. The hypothesis is supported by analyzing the microstructural features presented in Figure 4.3,

such as large spherical voids in the reacted material and the thin cerium layer that coats rounded particles of sulfide. Regardless of whether or not melting actually occurs, the energy release during the MSR reaction is substantial and must be accounted for when scaling up the production of CeS. For example, it may be necessary during high-energy ball milling to dilute the reaction mixture with some reaction product[14] or an inert filler[11] or to externally cool the milling vessel.

4.4 Conclusions

The compound CeS was successfully synthesized by high-energy ball milling of the elemental powders. The ball milling synthesis was shown to proceed by two distinct mechanochemically-induced, self-propagating reactions. To the best of our knowledge, double MSR events, as observed here, have not been previously reported for any material system. In the first reaction, CeS is formed from Ce and S but the reactants are not completely consumed. In the second reaction, the formation of Ce_2S_3 from existing CeS consumes the remaining sulfur. Finally, prolonged milling reacts Ce_2S_3 to CeS by consuming the remaining free Ce. Since CeS is the first observed product phase, it is possible that better control of the processing parameters, such as starting material size, will facilitate formation of CeS by total consumption of the reactants in a single MSR event. The CeS produced contained a small percentage of Ce_2S_3 impurity that is due to the design of the milling vessel-lid interface but is otherwise was free of common, detrimental impurities such as carbon, CeO_2 or $Ce_2O_{2-x}S_x$. These results clearly demonstrate the utility of mechanochemical synthesis of CeS and may enable more widespread use of this interesting material, which has a remarkable variety of combined useful refractory, electrical, and optical properties.

4.4 Author Justification

The research presented in this publication was carried out by Gordon Alanko in partial fulfillment of the requirements for a Doctoral degree in Materials Science and Engineering at Boise State University, under the advisement and supervision of Dr. Darryl P. Butt. Dr. Darryl Butt contributed greatly in terms of financial support, discussion of processing routes, and critical review of the article throughout the writing process.

4.5 References

1. E. D. Eastman, L. Brewer, L. A. Bromley, P. W. Gilles, and N. L. Lofgren, "Preparation and Tests of Refractory Sulfide Crucibles," *J. Am. Ceram. Soc.,* **34** [4] 128-34 (1951).
2. P. Maestro and D. Huguenin, "Industrial Applicationf of Rare-Earths – Which Way Forward for the End of the Century," *J. Alloy. Compd.,* **225** [1-2] 520-28 (1995).
3. P. N. Kumta and S. H. Risbud, "Rare-Earth Chalcogenides – An Emerging Class of Optical Materials," *J. Mat. Sci.,* **29** [5] 1135-58 (1994).
4. G. Geirnaert, "Ceramics-Liquid Metals, Compatibilities and Angles of Wetting," *B. Soc. Fr. Ceram.,* [106] 7-50 (1975).
5. E. D. Eastman, L. Brewer, L. A. Bromley, P. W. Gilles, and N. L. Lofgren, "Preparation and Properties of Refractory Cerium Sulfides," *J. Am. Chem. Soc.,* **72** [5] 2248-50 (1950).
6. I. A. Smirnov, "Thermal Properties of Rare-Earth Chalcogenides," *Phys. Status Solidi A,* **14** [2] 363-404 (1972).
7. V. P. Zhuze, A. V. Golubkov, E. V. Goncharova, and V. M. Sergeeva, "Electrical Properties of Rare-Earth Monochalcogenides (Cerium Subgroup)," *Sov. Phys. Solid State,* 6[1] 205-12 (1964).
8. K. B. Gibbard, K. N. Allahar, D. Kolman, and D. P. Butt, "Kinetics of thermal synthesis of cerium sulfides," *J. Nucl. Mat.,* **378** [3] 291-98 (2008).
9. C. Suryanarayana, "Mechanical alloying and milling," *Prog. Mat. Sci.,* **46** [1-2] 1-184 (2001).
10. P. Balaz and E. Dutkova, "Mechanochemistry of sulphides," *J. Therm. Anal. Calorim.,* **90** [1] 85-92 (2007).

11. T. Tsuzuki and P. G. McCormick, "Mechanochemical synthesis of metal sulphide nanoparticles," *Nanostruct. Mater.,* **12** [1-4] 75-78 (1999).

12. "Inorganic Crystal Structure Database." in. FIZ Karlsruhe, icsd.fiz-karlsruhe.de, 2014.

13. L. Takacs, "Ball milling-induced combustion in powder mixtures containing titanium, zirconium, or hafnium," *J. Solid State Chem.,* **125** [1] 75-84 (1996).

14. L. Takacs, "Self-sustaining reactions induced by ball milling," *Prog. Mat. Sci.,* **47** [4] 355-414 (2002).

CHAPTER FIVE: REACTIVE MILLING OF DYSPROSIUM NITRIDE: A KINETICS EVALUATION

Reactive Milling of Dysprosium Nitride: A Kinetics Evaluation

Gordon Alanko[1]

Daniel Osterberg[1]

Brian Jaques[1,2]

Mike Hurley[1,2]

Darryl P. Butt[1,2]

3. Department of Materials Science and Engineering, College of Engineering

Boise State University, 1910 University Drive, Boise, ID, 83725

4. Center for Advanced Energy Studies

995 University Boulevard, Idaho Falls, ID 83401

Abstract

Dysprosium nitride was synthesized by the reactive milling of the rare earth metal under 400 kPa nitrogen gas in a planetary ball mill. The nitrogen consumption rate was calculated from *in situ* temperature and pressure measurements to find the reaction extent as a function of milling time at milling speeds from 350-650 rpm. The results are analyzed in terms of a fundamental milling dynamics model in which the input milling energy is the primary driving force for reaction and the rate limiting step of the nitridation kinetics is the formation of chemically active surfaces. The model differs from traditional gas-solid reactions, which are often limited by diffusion of a species through a surface layer or by dissociation of the gas molecule. These results give fresh insight into reactive gas-solid milling kinetics.

5.1 Introduction

Reactive milling is an adaptation of the high-energy ball milling techniques that have been used for materials processing for some 50 years[1]. In reactive milling, sometimes termed mechanochemical synthesis, the system is designed to use the energy imparted by the milling tools to assist in driving a chemical reaction. The reaction may be solid-solid, solid-liquid, or solid-gas, with the latter being especially common in studies of hydrogen storage materials[2, 3]. There has been some work done describing the kinetics of gas-solid reactions during reactive milling[4, 5, 6], while many closed-form analytical models have been developed to describe the mechanical energy imparted during high energy milling[7, 8, 9, 10, 11, 12]. Reactive milling is interesting from both a fundamental standpoint and with a view to applications, as the self-contained, low temperature nature

of the process could enable the synthesis of many materials that are difficult or hazardous to prepare[13, 14, 15] as well as reducing the environmental impact of synthesis[16].

5.1.1 Dysprosium and Dysprosium Nitride

Dysprosium, like the other rare earth metals, displays extreme reactivity on fresh surfaces with most gasses [17, 18]. An X-ray photoelectron spectroscopy study of the reaction of nitrogen on clean dysprosium demonstrated that nitrogen dissociatively chemisorbs with the formation of one or two monolayers of nitride at 300 K[19]. Gas phase reactions arrested in frozen argon provide evidence for direct scisson of the N≡N bond by adjacent Dy atoms and do not indicate high complexation of the nitride by molecular nitrogen[20]. Similar behavior is observed for the early lanthanides[21] in contrast to the higher tendency of light transition[22] and some actinide[23] metals and nitrides to complex molecular nitrogen. Although the kinetics of the dysprosium nitridation reaction have not yet been reported in any detail, the demonstrated tendency for dissociative chemisorption over physisorption or dissolution of nitrogen suggests that the rate limiting step in the nitridation process will be either gas transport to the metal or through the nitride. This makes DyN an interesting model system for a reactive milling study: since milling is widely understood to break up and disperse surface films, nitride formation during reactive milling under a high nitrogen pressure might be expected to be kinetically limited by the formation of fresh chemically active surfaces rather than by transport mechanisms or nitrogen dissociation.

5.1.2 Ball Milling Modeling

The planetary ball milling model developed by Chattopadhyay *et al.*[12] was used as a starting point for analysis of milling mechanics. The model includes assumptions that limit the applicability to the stochastic process of ball milling. Modeled media move in a no-slip condition, being governed by the normal force while "attached" to the vessel wall, by rigid body mechanics while not attached, and stick without slip on impact. Modeled impact is described by Hertzian mechanics[24] and assumes perfectly elastic impacts rather than the elastic-plastic behavior found in real milling systems. Even considering these limitations, the milling model provides a helpful point of reference and was employed to extract the angular frequency dependencies of various process variables. These dependencies are provided in

Table 5.1, along with the physical constants of the planetary ball mill and milling media used. The kinetics analysis considered here is specific to counterrevolving planetary ball mills, although the analysis could be extended to other high-energy mill geometries by modifying the model.

Closed form milling theory based on Hertzian contact solutions generally assumes completely elastic impacts, although the obtained solutions are sometimes modified by a constant scalar to correct for an assumed value of the coefficient of restitution C_R. In the case of normal impact with negligible spin, the energy state of the media after impact may be described solely by $C_R = v_f/v_i$, $0 \leq C_R \leq 1$. A value of 1 indicates a completely elastic impact as described by Hertzian impact theory, while a value of 0 represents completely plastic impact. In high-energy milling, both theory and experiment call for values in the range 0.5-0.9. In general, the value of C_R for a given media at a given

moment depends on the thickness of material coating the media (and thus the volume available for plastic deformation).

Table 5.1 Mill and Media Constants and Derived Milling Model Dependencies

Mill parameters:				
Constant	**Symbol**	**Value**		**Units**
Vial/Disk speed	ω_v/ω_d	-2.00		
Disk radius	r_d	70.5		mm
Vial radius	r_v	37.5		mm
Corrected rv	$r_v' = r_v - r_b$	35.0		mm
Vial/Disk radius	r_v'/r_d	0.496		
Media parameters:				
Constant	**Symbol**	**Value**		**Units**
Radius	r_b	2.5		mm
Density	ρ_b	5.89		g/cm^3
Mass	m_b	0.3855		g
Poisson's ratio	υ_b	0.31		
Elastic modulus	E_b	234.8		GPa
Angular Frequency Dependencies				
Variable	**Symbol**	**Coefficient**	**ν^x**	**Units**
Deflection	δ_h	1.267	$\nu^{0.8}$	µm
Hertz radius	a_h	0.056	$\nu^{0.4}$	µm
Net velocity	v	0.286	ν^1	m/s
Impact Energy	$E_b(\nu)$	0.056	ν^2	mJ/hit

The constant input of energy during milling media impacts leads to crystallite size reduction. The exact mechanism is debated and probably varies from system to system. In brittle materials, fracture is assumed to be dominant, while in ductile materials there is probably dislocation coalescence leading to dynamic recrystallization of new subgrains[25] that asymptotically approach a limiting size of 10-20 nm. This limit condition is different for each material and thought to be related to the cohesive strength and to the maximum dislocation stacking density[26]. Unfortunately, very few studies on ball milling of pure

metals have reported the particle size as a function of milling time[27, 28], while most studies report only ending particle size.

The reduction of dimension with increasing milling energy dose is a well known relationship in mineral processing typically represented by the empirical laws of Rittinger, Kick or Bond[29]. Hukki proposed that all such empirical laws are approximations to a size-dependent energy consumption of the general form:

$$dE = -C\frac{dx}{x^{f(x)}} \tag{5.3}$$

where x is the critical dimension of a comminuted material, C is a material constant, and f(x) describes some dependence of dE on the current size. Rittinger's law makes the approximation f(x) = 2 in Eq. 1 and predicts the energy required for particle size reduction in very small (< 10 μm) particles to be proportional to the area of new surface created. Fractal analysis has suggested f(x) = 2.3 + x ln(x) with x measured in micrometers [30]. If we assume that the phenomenon of atomic level mixing during milling is driven by grain size refinement in the milled material, then a mechanical dose dependence that falls somewhere on the curve of Eq. 1 should result.

5.2 Materials and Methods

Milling experiments were conducted on a planetary ball mill (Retsch PM100, Haan, Germany) in a hardened steel vessel with a 250 mL nominal volume. The actual volume of the vessel + lid was calculated to be 269.7 mL by measuring the amount of deionized water required to completely fill the vessel along with the gas ports in the milling lid. In a typical experiment, 5 g of metal filings were added to the milling jar along with 184 yttria-stabilized 5 mm milling media, resulting in a ball-to-powder charge

of 14:1. The vessel was then sealed and purged with nitrogen before pressurizing to 400 kPa nitrogen. Milling was conducted at speeds ranging from 350-650 rpm for between 5 min – 24 hr. Nitrogen consumption was monitored by pressure and temperature sensors mounted in the milling lid. As-milled powders were checked for phase purity by x-ray diffraction (Rigaku Miniflex, Tokyo, Japan). Full details of these experiments are currently being published[31].

Two experiments were performed on milling media coated by pure metals milled under argon for 0-24 hours and for media coated by metal-metal nitride composites formed by milling metal under nitrogen for 0-1 hours. The coefficient of restitution C_R was measured by removing media from the milling vial and dropping media 40 cm onto a milling jar lid. Vacuum tweezers were used to hold the media before dropping to avoid imparting spin. The rebound height was measured and the value of C_R calculated by assuming that the relationship $mgh = 0.5mv^2$ held such that $C_R = (H_i / H_f)^{0.5}$. At least 20 trials were performed for each combination of system and milling time. In addition, the amount of material coating the media and vessel walls was calculated for each system and milling time by weighing the free powder in the vessel, weighing the media, and calculating the quantities adhered to the media and vessel walls. The average thickness and roughness of the starting and coated media was also measured by laser micrometery.

5.3 Results

Reactive milling for a period of 6 hours at all milling speeds from 350-650 rpm was found to be sufficient for complete reaction of dysprosium with nitrogen to form DyN. Faster milling speeds required considerably less time. A representative XRD plot is

shown in Figure 5.1, showing the formation of phase pure DyN to within the detection limit of the XRD.

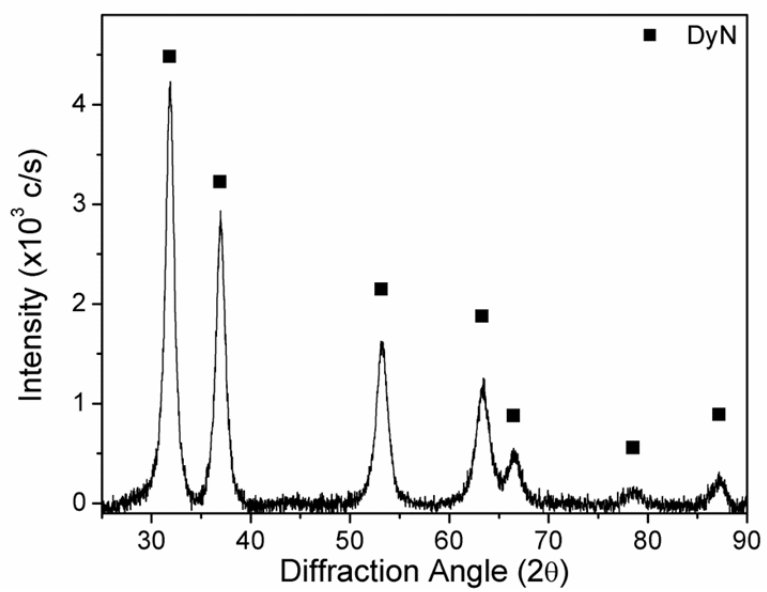

Figure 5.1 This representative x-ray diffraction plot shows phase pure DyN after milling dysprosium in nitrogen for 6 hours at 500 rpm. The scatter points mark the expected peak positions and intensities for DyN.

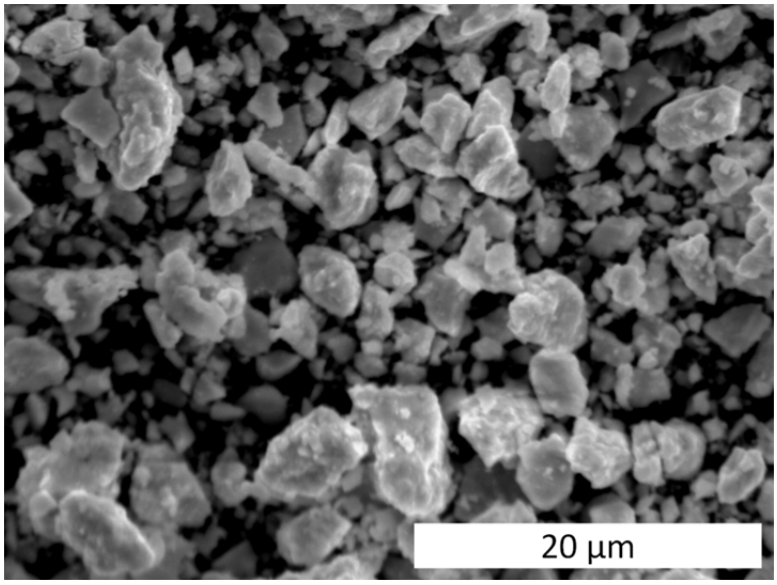

Figure 5.2 This SEM micrograph shows a secondary electron image of DyN formed by milling dysprosium for 6 hours at 500 rpm in nitrogen.

Shortly after the start of milling, dysprosium metal was found to quickly adhere to the vessel walls and media. During reactive milling with nitrogen, adhered metal is reacted and breaks off as powder, as shown in Figure 5.2. X-ray diffraction analysis (not shown) of the partially nitrided powders showed that the free powder at any point was primarily DyN with slight Dy, and the material adhered to the media and vessel walls was primarily Dy with slight DyN.

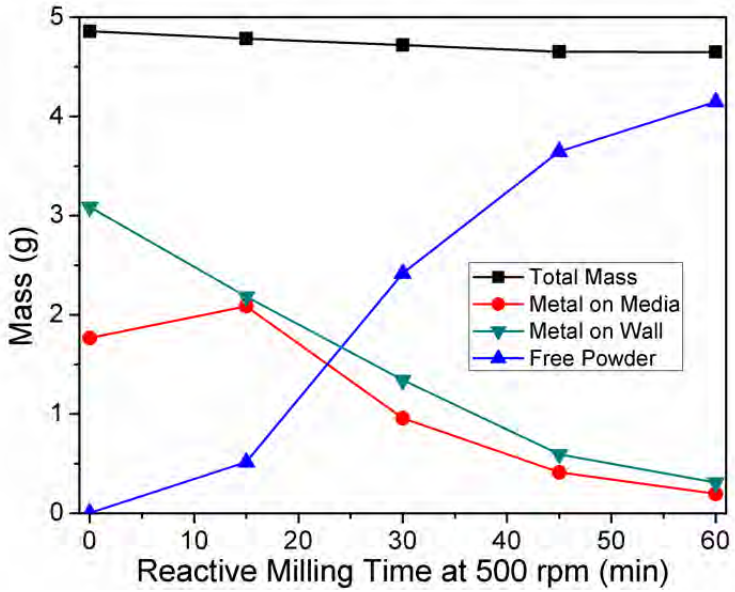

Figure 5.3 This plot tracks the disposition of Dy and DyN during reactive milling at 500 rpm. Before the start of RM, ductile Dy was coated onto the media and walls by premilling in argon. The media and wall traces (red circles and green down arrows) show consumption of Dy and formation of free DyN powder (blue up arrows). Total mass in the vessel (black squares) decreases as coated media are removed for further characterization.

The value of C_R for fresh 5 mm hardened steel balls is 0.96-0.98 when impacting a hardened steel plate at 1-4 m/s, and is 0.90-0.94 for fresh 5 mm zirconia balls under the same conditions. When media were coated with dysprosium, C_R was found to decrease to 0.60-0.65. The value of C_R was found to depend on the thickness of the dysprosium layer, and with prolonged milling under argon the media were found to transfer significant

quantities of dysprosium to the vessel walls and lid resulting in an increase in C_R towards a limiting value of 0.82-0.85 for less than 20 μm thickness of metal. A similar behavior was found when milling dysprosium in nitrogen as shown in Figure 5.3, except that in this case metal was consumed to form nitride and the value of C_R increased more rapidly during milling. As the metal was consumed, the media mass decreased to the starting media mass as shown in Figure 5.3.

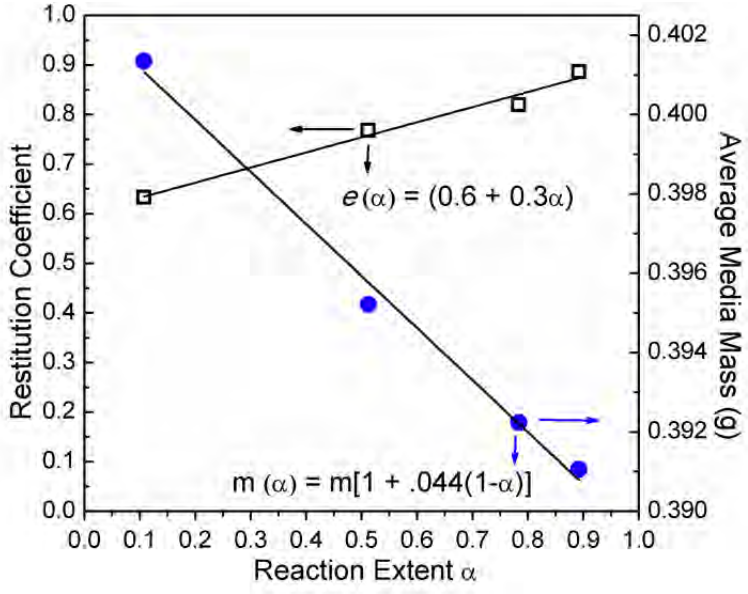

Figure 5.4 This plot shows the variation of the coefficient of restitution C_R (black open squares) and media mass m (blue circles) with extent of reaction α during reactive milling of Dy in nitrogen. Equations for the best fit lines are shown.

5.4 Discussion

The ideal gas law was applied to the raw pressure and temperature data to calculate the moles of nitrogen contained within the milling vessel and the consumption of nitrogen during milling. A slight gas leak rate was observed during milling for times longer than those required for the complete formation of nitride by XRD. The calculated moles data was corrected for this leak rate as well as for a temperature/pressure

equilibration lag caused by mechanical heating from media impact and friction. The details of these corrections are described in more detail elsewhere. Finally, the theoretical moles of nitrogen required to form stoichiometric nitrides was calculated for each milling run and used to normalize the moles consumed data as a measure of the extent α.

Free dysprosium had a slight tendency to segregate to the vessel lid during milling where it was infrequently struck by media. This results in a pronounced knee in the plot of nitrogen consumption during milling. This material is still converted into nitride eventually, but the process is much slower as a result of the infrequent media impacts. Because of this complicating geometry, reaction extents of $\alpha > 0.7$ were not considered during the kinetics analysis described below. In beginning a discussion of the milling kinetics, a summary of the key experimental milling results is helpful.

When a milling run begins, metallic dysprosium quickly coats the milling media, increasing their mass as well as decreasing their coefficient of restitution. The increase in mass makes media impacts more energetic, while the decrease in $\mathbf{C_R}$ increases the energy transfer during an impact. As milling progresses, nitrogen reacts with the metal coating the media and vessel to form metal nitride powder that is not adhered to either media or vessel. The reaction speed increases with milling speed and appears to accelerate at least up to 70% of theoretical completion. After several hours of reactive milling, high purity DyN is the only compound detected by XRD.

5.5 Kinetic Analysis

The mole consumption data calculated from *in situ* temperature and pressure monitoring of the experiments described above is expressed as functions of time at

different milling speeds. In a generalized approach to kinetics analysis, one often begins by parameterizing the functional dependence of α in terms of separated variables [32]:

$$\frac{d\alpha}{dt} = \boldsymbol{f(\alpha)h(P)\,k(T)} \tag{5.4}$$

In the present analysis, the gas-solid reaction is assumed to be primarily driven by milling media impacts with a rate related to the energy of an impact, in accordance with previous investigations [4, 33]. In addition, the experimental work completed to date holds P_{N2} in large excess, limiting pressure effects, and varies the average milling temperature over only a small range in which thermally activated diffusion is assumed to be small. Thus, Eq. 1 is rewritten to include the effects of mechanical work and to reduce pressure and temperature effects to a constant:

$$\frac{d\alpha}{dt} = A\, f(\alpha)\, M(E),\ A = \ k(T)h(P_{N_2}) \tag{5.5}$$

As the experimental data is in the integral form α(t), we find the integral form of Eq. 3:

$$\int_0^{\alpha} \frac{d\alpha}{f(\alpha)} = g(\alpha) = \ A\, M(E)t \tag{5.6}$$

Here, *M(E)* describes the time-dependent effects of the mechanical energy from milling and *g(α)* is a reaction model that takes into account the time-independent effects of the extent of reaction

5.5.1 Empirical Reaction Model

The reaction model g(a) in Eq. 4 describes the manner in which the geometrical changes introduced by the chemical reaction affect the continuing propagation of the reaction. Without a physical motivation for choosing one model over another, a good

description of the reaction model cannot be obtained by statistical methods alone. Thus, in order to proceed with analysis, an empirical stand-in was developed for the reaction model g(α) by fitting the α(t) reaction extent data calculated from the gas consumption over the range $0 < \alpha < 0.6$ with a power law:

$$\alpha(t) = A_0 + Bt^m = A_0 + [A\, M_a(E)]t^m \tag{5.7}$$

A_0 is employed solely as a fitting parameter to reduce the effect of experimental noise near the origin on the fit. Fits to the data are shown in Figure 5.4. Rearranging Equation 5.5:

$$\alpha^{1/m}(t) = [A\, M_a(E)]^{1/m}\, t \tag{5.8}$$

Substituting Eq. 6 into Eq. 4 produces the empirical reaction model:

$$g'(\alpha) \cong \alpha^{1/m}(t) = [A\, M_a(E)]^{1/m}\, t \tag{5.9}$$

Eq. 7 allows the graphical evaluation of the mechanical rate dependence of the reactive milling kinetics by plotting $B^{1/m} = A\, M_a$ versus milling speed as shown in Figure 5.5:

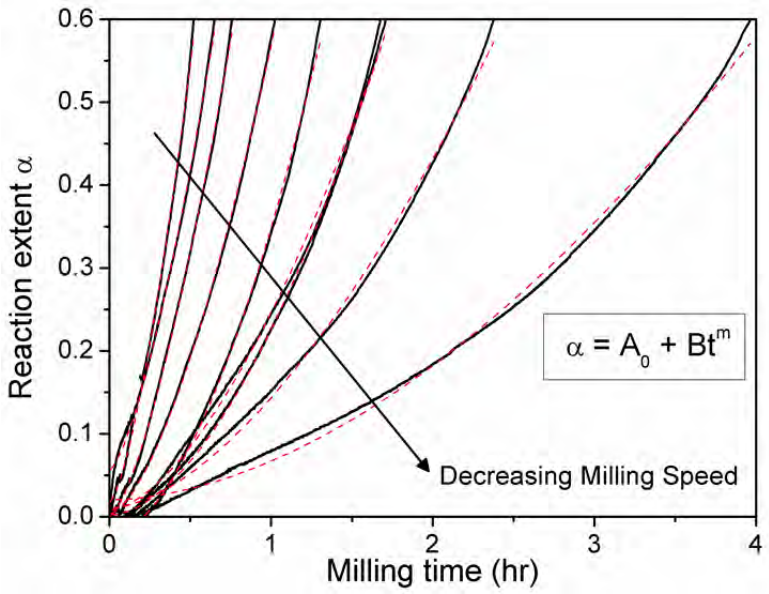

Figure 5.5 This figure shows plots of reaction extent data (black traces) fit to the formula $\alpha = A_0 + Bt^m$ (red traces). The adjusted r^2 value is > 0.98 for all fits.

5.5.2 Dependence of Reaction Rate on Milling Energy

The values of m and B obtained from the data fitting shown in Figure 5.4 are both plotted versus the angular frequency of the mill in Figure 5.6 along with best fit lines. The value of m apparently decreases slightly with increasing milling speed, while M_a depends on the cube of the angular frequency:

$$A\,M_a(E) \;=\; A\,M_0\,\nu^3 \tag{5.10}$$

Relationships linear in ν^3 have been previously observed in high energy ball milling[33], and together with the dimensional analysis presented in Table 5.2, the data suggest that the mechanical rate constant for nitridation is directly proportional to the milling intensity $I = \nu E_b$ (J/s). A plot of this relationship is shown in Figure 5.7, which gives a value of $A\,M_0 = 9.16 \pm 0.31$ (s/mJ N) where N is the total number of media.

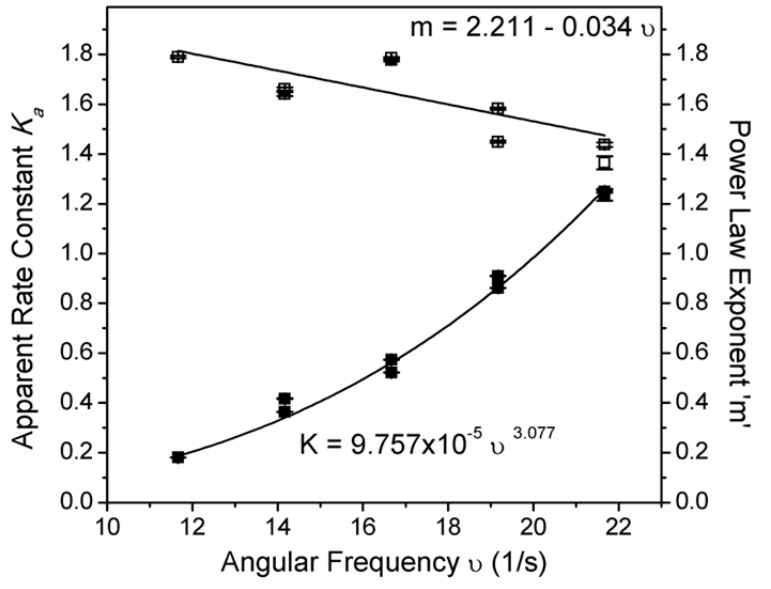

Figure 5.6 This figure plots the power law fit coefficients K and m versus the angular frequency of the milling vessel. Equations for the best fit lines are shown.

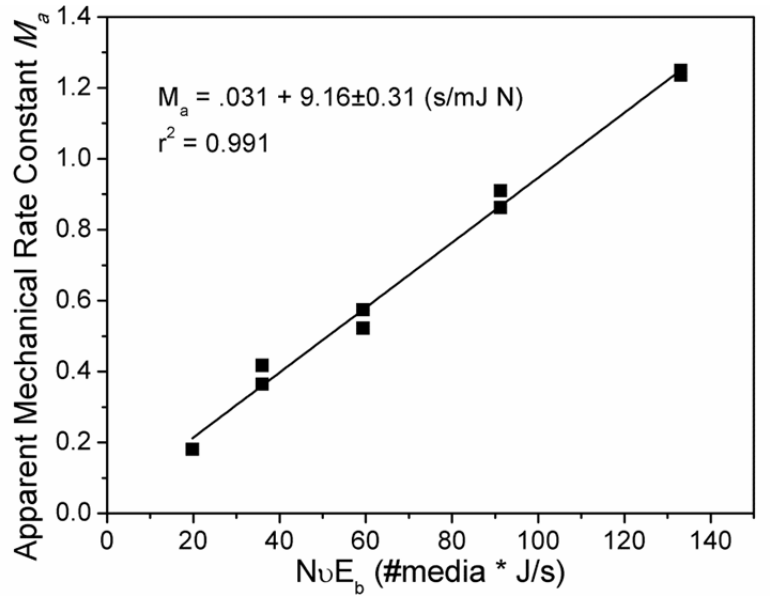

Figure 5.7 This figure shows fitted values for Ma plotted versus the milling intensity per media vEb/N. The equation for the best fit line is shown, and the very good correlation indicates a reaction rate that depends on the milling intensity.

Having demonstrated that M_a is linear in νE_b, it is appropriate to consider the effects that changing reaction extent could have on the impact energy. This in turn will allow insight into the physical parameters underlying the reaction model on the left side of Equation 5.7.

5.4.3 Effects of Reaction Extent α on Restitution C_R

As shown in Figure 5.3 and 5.4, the thickness of metal coating the media decreases with increasing reaction extent. Almost immediately after the start of milling, metal adheres to the media and the mass of each media is increased by the amount of metal Δm_{Dy} adhered to them, which may be approximated by:

$$\Delta m_{Dy} \cong \frac{m_c}{N_b} \frac{A_b}{A_v + A_b} \tag{5.11}$$

where A_b is the cumulative media surface, A_v the area of the vessel wall, m_c the mass of the milled charge of metal, and N_b the total number of media. As shown in Figure 5.4, the Dy system with the present experimental conditions has $\Delta m = 0.044\ m_b$ where m_b is the media mass. As metal reacts during milling, the media mass decreases from $m_b + \Delta m$ down to the original value of m, which in turn linearly decreases the impact energy:

$$E_b'(\alpha) = E_b \left[1 + \frac{\Delta m}{m_b}(1 - \alpha)\right] \tag{5.12}$$

5.4.4 Effects of Reaction Extent α on Media Mass

The data in Figure 5.4 demonstrate that C_R depends nearly linearly on the thickness of the media coating. As discussed previously, dysprosium is the major component of the material adhered to the media during reactive milling, while the nitride

is the primary component of the free powder. Thus, to a reasonable approximation, the value of C_R during reactive milling of dysprosium in nitrogen linearly increases with reaction extent. The effective energy transferred to the milled material during an impact event depends on the elasticity of the impact:

$$\Delta E(C_R) = E_b'(1 - C_R) \tag{5.13}$$

The fit of C_R vs α from Figure 5.3 is found to be:

$$C_R(\alpha) = (0.6 - 0.3\alpha) \tag{5.14}$$

Now Equation 5.12 may be substituted into Equation 5.11 to describe the dependence of the energy transferred during impact on the reaction extent:

$$\Delta E(\alpha) = E_b'\,(0.4 - 0.3\alpha) \tag{5.15}$$

Equation 5.13 describes the increase in the elasticity of media impacts with increasing reaction extent and the corresponding decrease in energy transferred to the impacted material. Substituting Equation 5.9 and Equation 5.10 into Equation 5.13 gives the change in energy transferred as a function of α:

$$\frac{\Delta E(\alpha)}{E_b} = \left[1 + \frac{m_c}{N_b m_b}\,\frac{A_b}{A_v + A_b}\,(1 - \alpha)\right](0.4 - 0.3\alpha) \tag{5.16}$$

5.4.5 Analytical Reaction Model

Having calculated the effects of changing reaction extent on the energetic of milling media impacts, an analytical reaction model may be found that accounts for both media energetics and reactant geometry. From Equation 5.13

$$g'(\alpha) = g(\alpha)\frac{\Delta E(\alpha)}{E_b} \cong \alpha^{1/m} \tag{5.17}$$

For the present system, from Equation 5.14 and using the mass equation from Figure 5.4, Equation 5.15 reduces to:

$$g'(\alpha) = g(\alpha)(1.044 - 0.044\alpha)(0.4 - 0.3\alpha) \cong \alpha^{1/m} \qquad (5.18)$$

Using Equation 5.16, we replace *g(α)* with reaction models representing a variety of physical situations. A fuller description of these models and their physical basis may be found elsewhere [34]. To narrow down the types of reaction models considered, we plot *g'(α)* vs. experimental values of α measured at 650 rpm. Figure 5.8 shows the various models plotted on normalized axes $g_i(\alpha)/g_i(\alpha_{max})$ and $t/t_{\alpha max}$ over the range $0 < \alpha < 0.7$. A necessary but not sufficient condition of a valid reaction kinetics model is linearization of α vs *g(α)* over a significant fraction of the range of α, which in Figure 5.8 occurs for the shrinking geometry models.

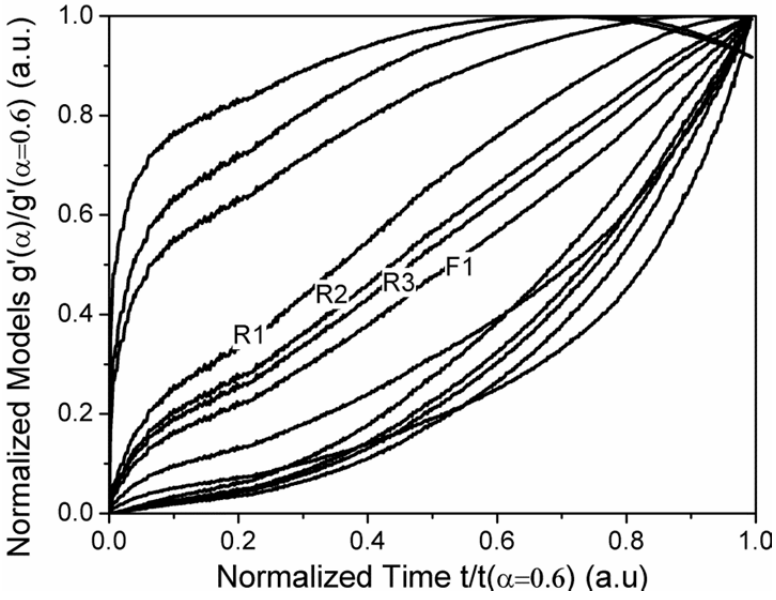

Figure 5.8 This figure shows normalized kinetics model output utilizing reaction extent data from a 650 rpm milling run. The initial jump in the data is a result of the temperature/pressure equilibration at the start of every milling run. Nearly linear slopes are observed for shrinking geometry models (marked R1-3 on plot) and a first-order model (marked F1).

These models are valid when nucleation is nearly instantaneous on the reactive surface, which is true of the rare earth metals as discussed in Section 5.1.1. Shrinking geometry models are generally recognized as being difficult to distinguish except at high reaction extent[35].

The data in Figure 5.7 shows that the reaction progresses at a rate that increases linearly with impact energy. This suggests that reactive surface area is formed during impact with some finite area [24] that decreases slightly (< 5%) with reaction extent as the effective radius and mass of the media decreases with subsequent formation of nitride. This process is illustrated schematically in Figure 5.9a-c, while Figure 5.9d diagrams the impact event.

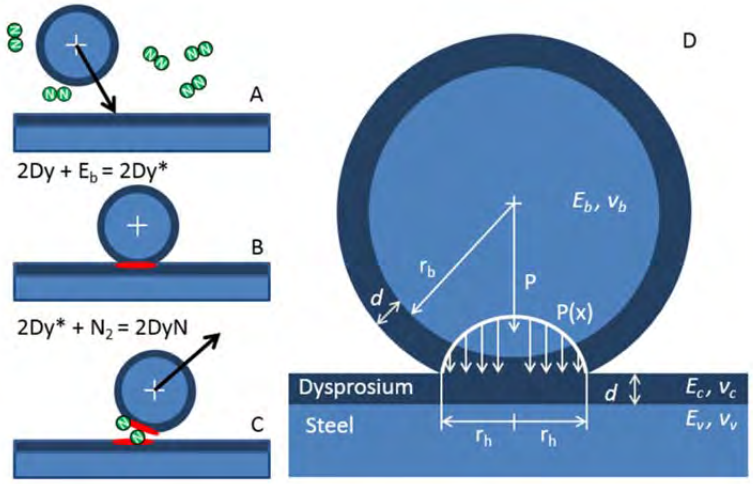

Figure 5.9 This figure (a-c) shows a schematic of an impact event renewing the reactive surface. (a) media approaches the vessel wall in nitrogen atmosphere (b) media impact transfers energy to the impact area πr_h^2, activating Dy (c) media rebound exposes activated surfaces on the wall and media that react to form nitride. Part (d) shows a schematic of the impact event.

Intuitively, as more reaction product accumulates in the free volume of the milling vessel, more of the product will be caught in ball-wall collisions. This will result in some impact energy dissipation by the trapped nitride powder and reduce the effective metal surface refinement. Thus, a reaction kinetics model based on a contracting area geometry is suggested:

$$g'(\alpha) = \left(1 - (1-\alpha)^{\frac{1}{2}}\right)(1.044 - 0.044\alpha)(0.4 - 0.3\alpha) \qquad (5.19)$$

Figure 5.10 shows the experimental data input into the reaction model of Equation 5.17.

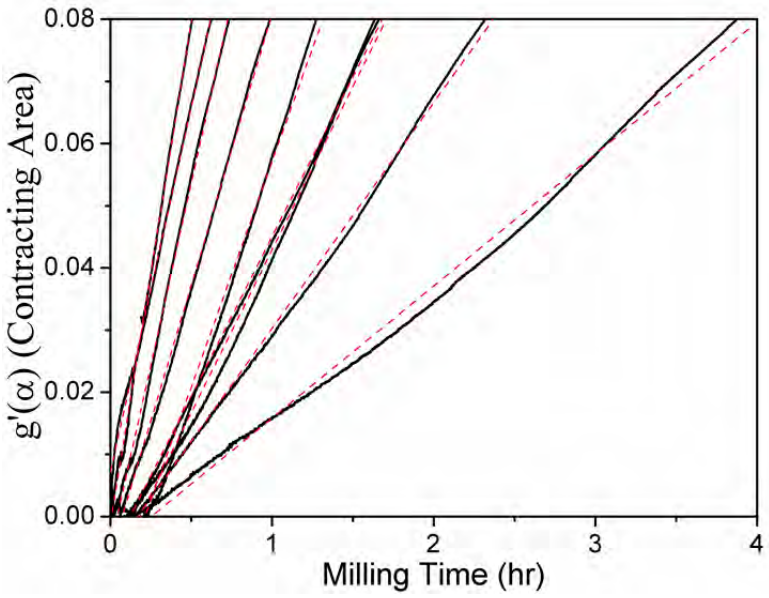

Figure 5.10 This figure shows the reaction model g'(a) from Equation 5.17 with experimental data from Figure 5.5. The dashed lines are best fits to the model.

These results may be interpreted as describing a reactive milling process in which ductile metal, adhered to the milling tools, is gradually consumed to form a powdered nitride. The reaction rate depends explicitly on the energy input, which acts on the Hertzian area of impact.

5.6 Conclusions

The reaction of dysprosium metal during high energy milling under nitrogen atmosphere has been quantized by monitoring the temperature and pressure in situ. A model of reactive milling kinetics for the formation of dysprosium nitride has been developed that predicts the rate of nitride formation in reactive milling to be limited by the areal energy input of media impacts. This novel result is explained in terms of generation of atomically rough chemically active sites within the hertizian impact area. Equivalently, impacts could be seen as comminuting thin films of nitride within the impact area to allow for fast diffusion to the surface. Gas-solid reactions during reactive milling of other rare earths are predicted to follow the model so long as the following conditions are met:

a. The solid is ductile and coats the milling tools
b. There is a low energy barrier for dissociative chemisorbtion on the solid
c. There is low solubility of the gas in the solid

These conditions should be met by many if not all of the lanthanides. These results help to demonstrate the reactive milling as a viable approach to synthesis of the rare earth and actinide nitrides, and provide a foundation for further study of the gas-solid reactions during high energy milling.

5.8 Author Justification

The research presented in this publication was carried out by Gordon Alanko, Dan Osterberg, Brian Jaques, Dr. Mike Hurley, and Dr. Darryl P. Butt. Dan Osterberg and Brian Jaques designed and performed milling experiments in discussion with Dr. Mike Hurley and Dr. Darryl P. Butt. Gordon Alanko verified earlier experimental results, conceived and performed coefficient of restitution experiments, and performed kinetics

and milling modeling in discussion with Brian Jaques, Dr. Mike Hurley, and Dr. Darryl P. Butt. Work done by Gordon Alanko was in partial fulfillment of the requirements for a Doctoral degree in Materials Science and Engineering at Boise State University, under the advisement and supervision of Dr. Darryl P. Butt. Dr. Darryl P. Butt contributed greatly in terms of financial support, discussion of processing routes, and critical review of the article throughout the writing process.

5.9 References

[1] Suryanarayana C. Prog. Mater. Sci. 2001;46:1.

[2] Bellosta von Colbe J, Felderhoff M, Bogdanovic B, Schuth F, Weidenthaler C. Chem. Comm. 2005:4732.

[3] Bab M, Baum L, Mendoza-Zelis L. Physica. B 2007;389:193.

[4] Bab M, Mendoza-Zelis L. Scripta Mater. 2004;50:99.

[5] Streletskii A, Butyagin P, Leonov A. Colloid J. 1996;58:238.

[6] Streletskii A, Leonov A, Butyagin P. Mater. Sci. Forum 1997;235-2:181.

[7] Yazdani A, Hadianfard M, Salahinejad E. J. Alloy. Compds. 2013;555:108.

[8] Iasonna A, Magini M. Acta Mater. 1996;44:1109.

[9] Magini M, Iasonna A, Padella F. Scripta Mater. 1996;34:13.

[10] Bellon P, Averback R. Phys. Rev. Lett. 1995;74:1819.

[11] Magini M, Colella C, Iasonna A, Padella F. Acta Mater. 1998;46:2841.

[12] Chattopadhyay P, Manna I, Talapatra S, Pabi S. Mater. Chem. Phys. 2001;68:85.

[13] Jaques B, Marx B, Hamdy A, Butt D. J. Nucl. Mater. 2008;381:309.

[14] Callahan P, Jaques B, Marx B, Hamdy A, Osterberg D, Butt DP. J. Nucl. Mater. 2009;392:121.

[15] Alanko G, Butt DP. J. Amer. Ceram. Soc. 2014;In Press.

[16] Kaupp G. Crys. Eng. Comm. 2011;13:3108.

[17] Netzer F, Matthew J. Rep. Prog. Phys. 1986;49:621.

[18] Bastl Z, Cerny S, Kovar M. Appl. Surf. Sci. 1993;68:275.

[19] Schreifels J, Deffeyes J, Neff L, White J. J. Electron Spectrosc. Relat. Phenom. 1982;25:191.

[20] Willson S, Andrews L. Journal of Physical Chemistry A 1999;103:1311.

[21] Willson S, Andrews L. Journal of Physical Chemistry A 1998;102:10238.

[22] Kushto G, Souter P, Chertihin G, Andrews L. J. Chem. Phys. 1999;110:9020.

[23] Kushto G, Souter P, Andrews L. J. Chem. Phys. 1998;108:7121.

[24] Johnson K. Contact Mechanics. Cambridge: Cambridge University Press, 1985.

[25] Huang J, Wu Y, Ye H. Mater. Sci. Eng. A. 1995;199:165.

[26] Fecht H, Hellstern E, Fu Z, Johnson W. Metall. Trans. A. 1990;21:2333.

[27] Butyagin P, Zhernovenkova Y, Povstugar I. Colloid J. 2003;65:141.

[28] Butyagin P, Streletskii A. Phys. Solid State 2005;47:856.

[29] Hukki R. Trans. Am. Inst. Min. Metall. Eng. 1961;220:403.

[30] Thomas A, Filippov L. Int. J. Miner. Process. 1999;57:285.

[31] Jaques B, Alanko G, Osterberg D, Tamrakar S, Smith C, Hurley M, Butt DP.Acta Mater. 2014;To be submitted

[32] Brown M, Maciejewski M, Vyazovkin S, Nomen R, Sempere J, Burnham A, et al. Thermochim. Acta 2000;355:125.

[33] Gotor F, Achimovicova M, Real C, Balaz P. Powder Technol. 2013;233:1.

[34] Brown W, Dollimore D, Galwey A. Reactions in the Solid State. New York, NY: Elsevier Scientific, 1980.

[35] Galwey A, Brown M. Thermochim. Acta 1995;269:1.

CHAPTER SIX: CONCLUSIONS

High-energy ball milling has been used to synthesize a vast number of materials ranging from composites such as oxide-dispersion strengthened steels and similar techniques, solid solutions of normally immiscible materials, and other metastable compounds. The related technique of reactive milling drives chemical reactions in the solid state, potentially involving components reacting in the solid, liquid, or gas phases, or all three, and the operative kinetics are not well understood.

Manufacturers of several common high-energy ball mills have recently made standardized accessories available for their mills that allow for *in situ* monitoring of the temperature and pressure of milling runs. This new capability has opened the door to detailed studies of the kinetics of high-energy milling. This dissertation was rooted in such studies of the in situ temperature and pressure during mechanochemical synthesis in the Ce-Si, Ce-S, U-Si, and Dy-N systems with the goal of beginning to understand the thermodynamic and kinetics processes governing mechanochemical synthesis.

In Chapter Two, the preparation of the uranium silicide U_3Si_2 from the elements is described. The reaction was found to proceed through USi_3 as an intermediate state rather than MSR reaction to USi_2 as some models predict. Analysis of in situ pressure and temperature measurements suggest that the mechanical alloying of $U+USi_3$ is accompanied by increased powder adhesion to the milling tools and increased energy

transfer in the system. These quantities are explored further in the non-radiological system described in Chapter Five.

A chemically similar system with remarkably different milling behavior is described in Chapter Three. Mechanochemical processing of Ce-Si compounds involves an MSR type reaction for all compositions from Ce_5Si_3 – $CeSi_2$. The initiation of the MSR event took place after a characteristic induction time for each composition that was shown to correlate well with an effective heat of formation model. Microstructural evidence suggests that the reactants were partially or totally melted during MSR events. The MSR event was followed by a quick solid state diffusion reaction between the Ce_2Si_3 compound and excess Ce and/or Si to form a mostly single phase product with the nominal starting composition.

Utilizing the knowledge and expertise gained in the course of experiments described in Chapter Two and Three, Chapter Four describes the successful preparation of the important refractory compound CeS by high-energy ball milling of the elemental powders. The reaction proceeds by two distinct MSR events, which has not been reported previously for any system. The first MSR forms CeS by partially consuming the reactants. The second reaction forms Ce_2S_3 from existing CeS, and enough CeS to consume the remaining sulfur. Prolonged milling reacts Ce_2S_3 to CeS by consuming the remaining free Ce.

Finally, Chapter Five details the derivation of a model of reactive milling kinetics for the formation of rare earth nitrides. The model predicts reaction rate in reactive milling to be a function of input energy. In addition, the model describes the reaction as taking place on the surface of the milling media, whose mass and elastic properties

change in time. Gas-solid reactions during reactive milling are predicted to follow the model so long as the milled solid is ductile and coats the milling tools, there is a low activation energy barrier for dissociative chemisorbtion on the solid, and there is low solubility of gas in the solid. These results help to demonstrate the reactive milling as a viable approach to synthesis of the rare earth and actinide nitrides, and provide a foundation for further study of the gas-solid reactions during high energy milling.

APPENDIX

Preparation of Dysprosium Nitride by Ball Milling

In Situ Characterization of the Nitridation of Dysprosium During Mechanochemical Processing

Brian J. Jaques[a,b]

Daniel D. Osterberg[a,b]

Gordon A. Alanko[a,b]

Sumit Tamrakar[a,b]

Cole R. Smith[a,b]

Michael F. Hurley[a,b]

Darryl P. Butt[a,b,1]

[a]Department of Materials Science and Engineering, Boise State University, 1910 University Dr., Boise, ID 83725, USA

[b]Center for Advanced Energy Studies, 995 University Blvd., Idaho Falls, ID 83401, USA

Abstract

Processing of advanced nitride ceramics traditionally requires long durations at high temperatures and, in some cases, in hazardous atmospheres. In this study, dysprosium mononitride (DyN) was rapidly formed from elemental dysprosium in a closed system at ambient temperatures. An experimental procedure was developed to quantify the progress of the nitridation reaction during mechanochemical processing in a high energy planetary ball mill (HEBM) as a function of milling time and intensity using *in situ* temperature and pressure measurements, SEM, XRD, and particle size analysis. No intermediate phases were formed. It was found that the creation of fresh dysprosium surfaces dictates the rate of the nitridation reaction, which is a function of milling intensity and the number of milling media. These results show clearly that high purity nitrides can be synthesized with short processing times at low temperatures in a closed system requiring a relatively small processing footprint.

A.1 Introduction

Interest in rare earth element production and management has increased significantly in the United States (US) in the past few years. Such “strategic materials” have substantially increased the US dependence on the Republic of China, which exported 99% of the approximately $186 million worth of rare earths to the US in 2008 for use in metallurgical applications and alloys, electronics, catalysts, and cathode ray tubes [1]. Compared to the light rare earth metals, relatively little published literature exists for praseodymium, promethium, thulium, lutetium, and dysprosium although scientific interest in these metals is on the rise. In the next forty years, Hoenderdaal *et al.* [2] project that the demand for dysprosia (Dy_2O_3) and other dysprosium compounds will

increase to between 7-25 times (to 14-50 ktons) the 2010 demand. This increase in projected demand largely stems from magnetic applications in electric motors due to dysprosium's exceptional magnetic moment of 10.6 Bohr magnetrons, which is second only to holmium, and its ability to induce coercivity as an alloying agent or dopant [3]. DyN has also been investigated as a material for ferromagnetic and semiconductor superlattice structures for spintronic applications [4-6]. Dysprosium's isotopes strongly absorb neutrons and could be applied as moderator materials in nuclear reactors. Additionally, due to its physical attributes and high vapor pressure, dysprosium mononitride (DyN) has been postulated as a suitable surrogate for americium mononitride (AmN) in studying its sintering and alloying effects in spent nuclear fuel reprocessing [7-12].

Traditional synthesis routes to advanced nitride ceramics are based on thermal treatments, which can require large amounts of infrastructure, long processing times, and can introduce excessive amounts of anion impurities. High energy ball milling (HEBM) is an alternative technique that can be used to synthesize high purity nitride ceramics in relatively short times in a sealed and controlled environment, which reduces exposure to unwanted atmospheres. HEBM is used in many processes that have been described in literature: Mechanical alloying (MA), mechanical milling (MM) and mechanical grinding (MG), mechanical disordering (MD), reactive milling (RM), reactive mechanical milling (RMM), cryomilling, mechanically activated annealing (M2A), double mechanical alloying (dMA), and mechanically activated self-propagating high-temperature synthesis (MASHS) [13, 14]. HEBM is a versatile processing technique that has demonstrated useful for producing nanometer-structured materials, crystalline and amorphous

materials, as well as equilibrium and metastable phases [13]. A ball milling process that is considered high energy is one that utilizes high media impact velocities and large media impact frequencies to efficiently mill the powder charge. This can be accomplished in numerous ways. Most notably, dynamic mechanical energy can be delivered to a powder charge using a few different milling techniques, including: horizontal ball milling, planetary ball milling (PBM) which is shown in Figure A.1, magneto ball milling, and shaker milling (SPEX) [13-16]. Different milling apparatuses vary in capacity, efficiency of milling, and spatial arrangements requiring each to be characterized independently when attempting to understand the mechanisms of the processes.

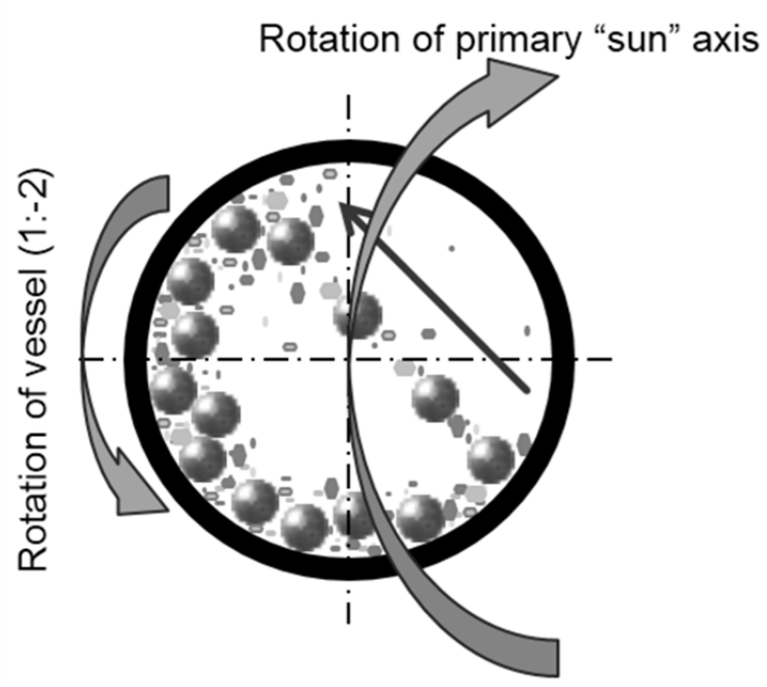

Figure A.1 Schematic showing the planetary ball milling process when efficient milling parameters are chosen. The rotation of the milling vessel in Retsch PBM has a ratio of 1:-2 with the sun axis of the mill.

Mechanical alloying has been used to synthesize oxide dispersion strengthened alloys since the 1960s and, approximately a decade later, the same process was shown to be useful as a ceramic synthesis method, later noted as RM [13]. For the past 40 years, RM has been investigated for the low temperature, solid state synthesis of advanced ceramics. According to Huot *et al.* [14], RM has been demonstrated on hydrogen storage materials using various milling techniques for the past 10 years, resulting in approximately one thousand publications. However, the study of RM in the synthesis of non-oxide and non-hydride materials has not been studied as extensively; there are fewer than 50 publications on the use of RM to form nitrides and fewer than 20 that used PBM. The limited number of studies that focused on producing nitride ceramics tended to investigate transition metals and class IIIA elements such as: Al, B, Cr, Fe, Ga, Nb, Si, Ta, Ti, V, and Zr [13, 17-33]. To the best of the authors' knowledge, the synthesis of lanthanide or actinide nitrides via RM has not been published other than the earlier work of this group [7-10]. In particular, to study nitridation reaction kinetics during RM in a PBM using *in situ* temperature and pressure data is very limited; there are no studies found in the literature on RM in a PBM to form nitrides with *in situ* temperature and pressure measuring capabilities. The only studies found that have demonstrated such capabilities during PBM are limited and stem from the research on hydrogen storage materials [34-40].

The work described here is part of a larger effort in the understanding of RM (also referred to as a mechanochemical synthesis or a mechanically induced gas-solid reaction) by high energy planetary ball milling elemental dysprosium in a nitrogen atmosphere to form dysprosium mononitride (DyN), as follows:

$$Dy + \frac{1}{2}N_2 \rightarrow DyN \qquad (1)$$

The mechanochemical reaction was monitored (as a function of milling intensity and time) using *in situ* temperature and pressure measurements to calculate the extent of the reaction. A more detailed kinetics study is presented on the nitridation of dysprosium in a PBM by Alanko *et al.* [41], where a fundamental milling dynamics model is used to describe the behavior of the RM process.

A.2 Experimental Details

To study the RM during PBM of the nitridation reaction, milling experiments were performed in ultra-high purity (UHP) nitrogen with high purity dysprosium filings (99.9% purity, ESPI) sieved through a 40 mesh (420 μm) sieve (Figure A.2). The filings had a surface area of 0.196 ± 0.058 m^2g^{-1}, as determined by nitrogen adsorption Brunauer-Emmett-Teller (BET) techniques. In order to gain insight into the reaction kinetics, the internal temperature and pressure of the milling vessel were monitored during milling in a Retsch planetary ball mill (PM100) at milling intensities varying from 350 – 650 rpm. Each milling run was completed using a Retsch 250 mL hardened steel milling vessel (85Fe, 12Cr, 2.2C, 0.45Mn, 0.4Si) and 5 mm diameter, spherical yttria stabilized zirconia media (Tosoh, Tokyo, Japan). According to the respective vendors, the milling vessel and milling media had a hardness of 62 HRC and 72 HRC, respectively.

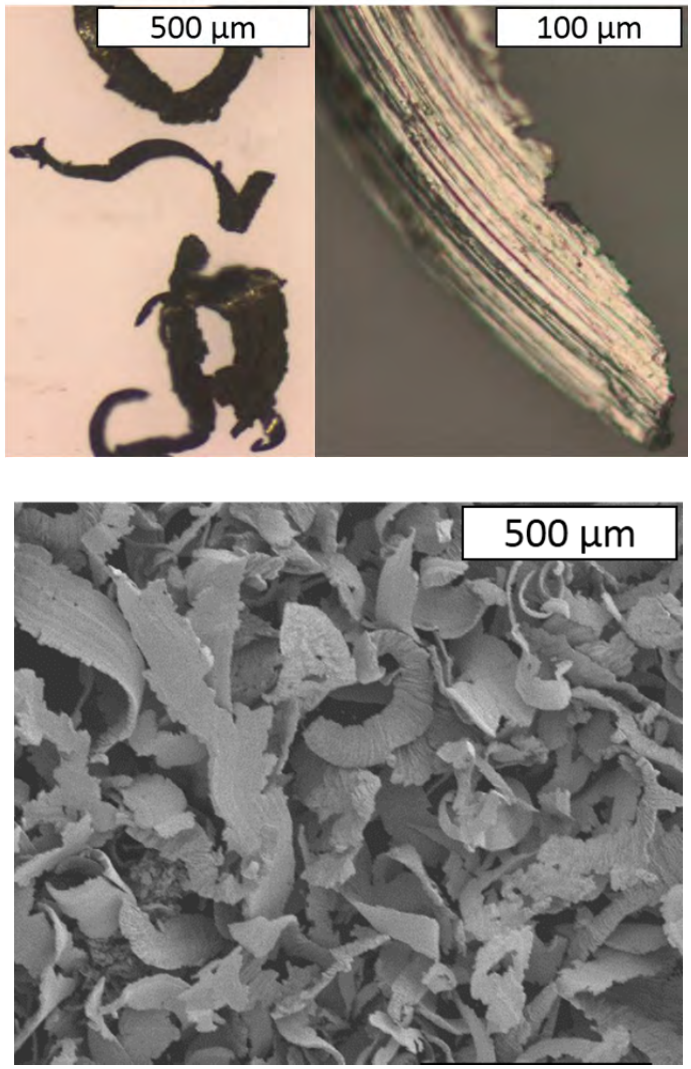

Figure A.2 Images of the dysprosium filings used as the starting materials for the kinetics study of the nitridation reaction to form DyN using a dry planetary ball milling process in nitrogen atmosphere. The filings have a surface area of 0.196 ± 0.058 m^2/g.

The ball to powder ratio (BPR) was held constant at 14:1 with a total dysprosium mass of 5 grams (70 grams of YSZ media which equates to 184 spheres), as shown in Figure A.3a. The temperature and pressure were monitored using a Retsch sensing lid (PM GrindControl), which has capabilities of 273 – 473 K, 0 – 500 kPa, and can wirelessly send data at 200 Hz to a remote computer (Figure A.3b). The temperature

(measured by a thermistor) and pressure sensors are integrated into recessed locations in the steel sensing lid.

Figure A.3 Images of the 250 mL milling vessel loaded (a) with YSZ media and dysprosium filings in a 14:1 mass ratio with a total dysprosium mass of 5 grams and (b) after sealing with a lid consisting of gas purging and in situ temperature and pressure measuring capabilities. The in situ measuring capabilities allowed for a kinetics study on the nitridation reaction in the formation of DyN.

During each run, the milling vessels were loaded with media and dysprosium and sealed with the temperature and pressure monitoring lid in an argon atmosphere glovebox. It was then charged to approximately 450 kPa with oxygen-gettered UHP nitrogen (oxygen content less than 0.1 ppb as measured by a Neutronics OA-1 oxygen analyzer). The vessel was charged to 450 kPa and relieved (3 cycles) prior to a final charge of 450 kPa in order to ensure a pure nitrogen milling atmosphere.

The stages of the milling process were observed through mass measurements, SEM imaging, and powder X-ray diffraction (XRD) during a 500 rpm milling run. The 500 rpm milling run was periodically interrupted between 0 – 6 hours of milling. Each time the process was halted, the milling vessel was transferred into an argon atmosphere

glovebox where the lid was removed and the measurements or representative powders were taken. The same powder and media was then sealed, evacuated and charged with nitrogen, and secured to the mill for subsequent milling.

The effect of milling intensity was assessed by milling for 6 hours at different intensities from 350 – 650 rpm. After milling, the powder was separated from the milling media in the argon-filled glovebox and characterized using SEM imaging, laser-scattering particle size analysis (PSA), and XRD. Additionally, temperature and pressure data were used to assess the reaction kinetics at each milling intensity.

In each case, XRD was performed at room temperature on a Bruker D8 Discover using Cu-K_α radiation (λ = 0.15418 nm). However, some of the patterns were collected with a scintillation counter and some were collected with a 2-dimensional area detector. Due to the oxygen sensitivity of the material, the XRD samples were prepared in an argon glovebox and a semi- X-ray transparent film was placed over the powder filled sample holders in order to prevent oxidation during the XRD scans.

The particle morphology after 6 hours of milling at 350 – 650 rpm was investigated using a Hitachi (S-3400N) thermionic cathode scanning electron microscope (SEM) as well as a Horiba (LA-950) laser scattering particle size analyzer (PSA). The powders were first adhered to carbon tape prior to carbon coating in order to obtain SEM images with reduced electron charging. For PSA, the DyN powders were dispersed in an isoparaffinic fluid (Isopar V, ExxonMobil) by external ultrasonication using a 750 W sonication probe prior to loading into the mixing chamber of the Horiba analyzer. The refractive indices used for the free powder and the Isopar V were 2.5-0.43i and 1.452, respectively.

A.3 Results

Typical *in situ* temperature and pressure data (collected at 0.2 Hz) from milling dysprosium with a BPR of 14:1 at 500 rpm in UHP nitrogen is shown in Figure A.4. It is seen that the rate of change of both temperature and pressure reach a steady state after approximately 2.5 hours. An 8 kPa increase in the pressure was observed immediately upon starting the mill. The pressure peaked at 22 kPa above the initial pressure before decreasing and reaching a steady state decay rate (the constant decay is attributed to a slow leak in the seal between the milling vessel and sensing lid). Figure A.4 also shows systematic effects of the milling process on the temperature and pressure in the vessel when the mill is turned off (after 6 hours of milling). The pressure immediately drops 6 kPa and decays another 8 kPa between 0 – 9 minutes after stopping the mill. Additionally, as soon as the mill turns off, the temperature decreases by 1.1 K before increasing 0.6 K and then cooling to room temperature.

The temperature and pressure data was then used to calculate the amount of nitrogen consumed throughout the RM process (as shown in the inset of Figure A.4) using the ideal gas law:

$$n = \frac{PV}{RT} \qquad (2)$$

Where *n* is the number of moles of nitrogen gas consumed, *P* is the pressure, *V* is the volume of free space in the milling vessel, *R* is the ideal gas constant, and *T* is the temperature of the vessel.

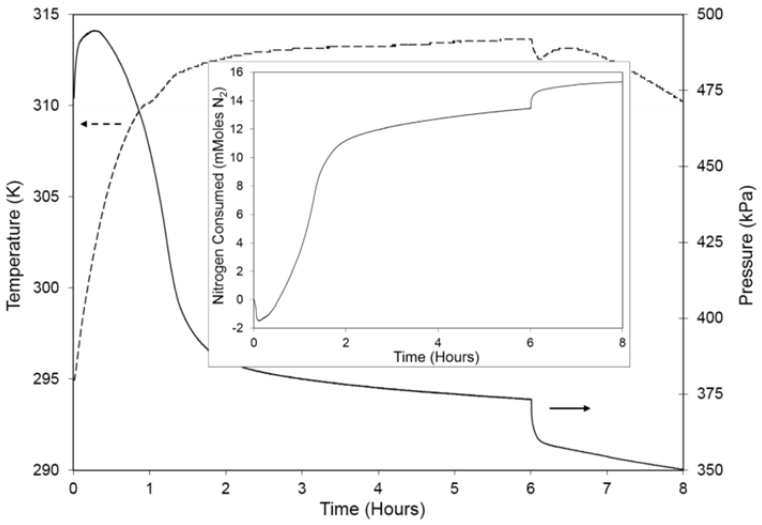

Figure A.4 Typical temperature and pressure data as recorded *in situ* (0.2 Hz) throughout the reactive ball milling of five grams of elemental dysprosium in dry nitrogen to form DyN at 500 rpm and a BPR of 14:1. The mill was shut off after 6 hours of milling. The inset shows the nitrogen consumption calculated using the *in situ* temperature and pressure data in the ideal gas law.

After approximately 1.5 hours of milling, the nitrogen consumption rate significantly slows, reaching steady state (with a slight leak) after approximately 2.5 hours. As described above, the effects of the milling process (when starting and ending the mill) on the temperature and pressure directly translate into the nitrogen consumption plot.

To better understand the distribution and morphology of the products and reactants as a function of RM time, a 500 rpm milling run, similar to that shown in Figure A.4, was periodically interrupted and the location of the powder within the mill was quantified. The bar chart in Figure A.5 shows the distribution of dysprosium within the milling vessel. Initially, all of the powder was of course free dysprosium filings.

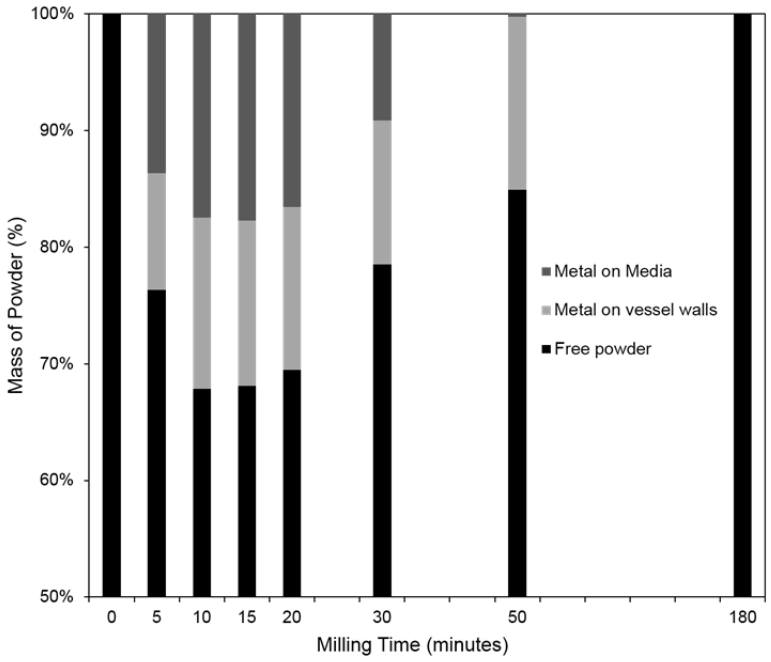

Figure A.5 Bar chart showing the distribution of dysprosium with time throughout planetary ball milling in dry nitrogen at 500 rpm. It is seen that the dysprosium initially "cold welds" to the vessel walls and milling media but after 50 minutes, nearly 85% of the original mass is recovered and after 180 minutes, all of the powder is free from the vessel walls and media in the form of a nitride.

After ten minutes of milling, approximately 30% of the dysprosium was cold welded to the media and the walls of the milling vessel. Following an additional 50 minutes, nearly 85% of the initial powder mass was recovered as free powder with the remainder still cold welded to the walls of the vessel. After 180 minutes of milling at 500 rpm, all of the dysprosium could be recovered as free powder within the milling vessel. In each case, the free powder was imaged using SEM (Figure A.6) and was characterized for phase distribution by XRD (Figure A.7).

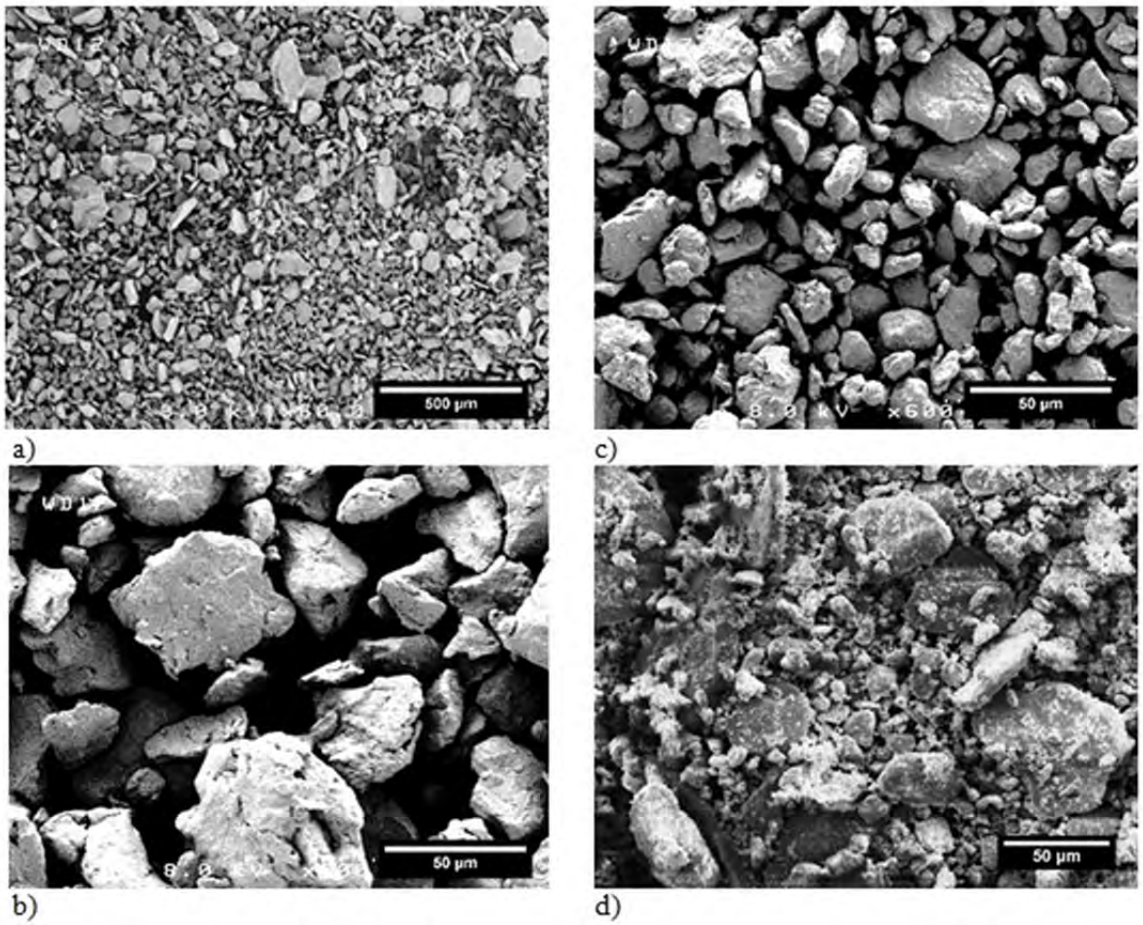

Figure A.6 SEM images of the free powder recovered throughout planetary ball milling elemental dysprosium in dry nitrogen at 500 rpm for a) 10 minutes, b) 30 minutes, c) 50 minutes, and d) 30 hours.

From the SEM images, it was seen that the free powder morphology changed with increased milling time from a large plate-like morphology to more uniform particles to a bimodal particle size after long milling times.

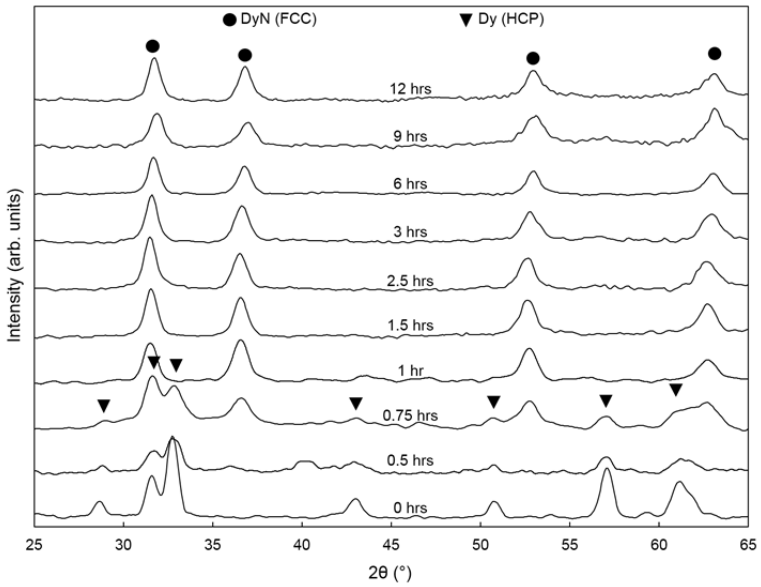

Figure A.7 X-ray diffraction patterns of the free powders resulting from reactive milling elemental dysprosium in dry nitrogen at 500 rpm up to 12 hours. After approximately 45 minutes of milling, the only crystalline phase is DyN.

As one might expect, XRD showed a transition from the hexagonal closed-pack (HCP) structure of dysprosium to the face-centered cubic (FCC) structure of DyN with increased milling time (Figure A.7). The diffraction intensity of the free powder after 30 minutes was very weak and an unidentified peak appears. However, after approximately 60 minutes, the HCP diffraction pattern caused by the elemental dysprosium diminishes and the FCC diffraction pattern of DyN dominates. As milling time was increased, there exists a slight shift in the lattice parameters, but no new phases appear to have formed.

The effect of milling intensity on the rate of nitrogen consumption after milling 5 grams of dysprosium for 6 hours is shown in Figure A.8. As previously described, the nitrogen consumption was calculated using the ideal gas law. However, the plot was generated after three distinct steps were completed to post process the acquired temperature and pressure data to allow for better comparison between milling runs: first,

a constant leak rate was subtracted from the pressure data, second, a shift was applied to the nitrogen consumption data, and third, the nitrogen consumption was normalized to the maximum amount of consumed nitrogen for each run. The leak rate between the milling vessel and the lid was determined by finding a linear fit to the constant nitrogen consumption rate (as noted above). The leak rates were determined after the mill was halted (in the 8 – 10 hour range, when the temperature had equilibrated) and were determined to be between 0.02 – 0.09 mMoles N_2 hr^{-1} for all milling runs. The shift of the nitrogen consumption data was to account for the effects of the milling process (described above) and was a simple positive linear shift to set the minimum nitrogen consumption value equal to zero (see the inset in Figure A.4). It is worth noting that the shift increased with milling intensity from 0.598 mMoles of N_2 at 350 rpm to 1.8 mMoles of N_2 at 650 rpm, which is 4 – 12% of the total theoretical nitrogen consumption in the nitridation reaction shown in Equation 1. The third fitting step, was to normalize the reaction extent in each milling run. This was completed by normalizing nitrogen consumption to the maximum apparent nitrogen consumption for each milling run, which was 92 ± 5% of the theoretical nitrogen consumption.

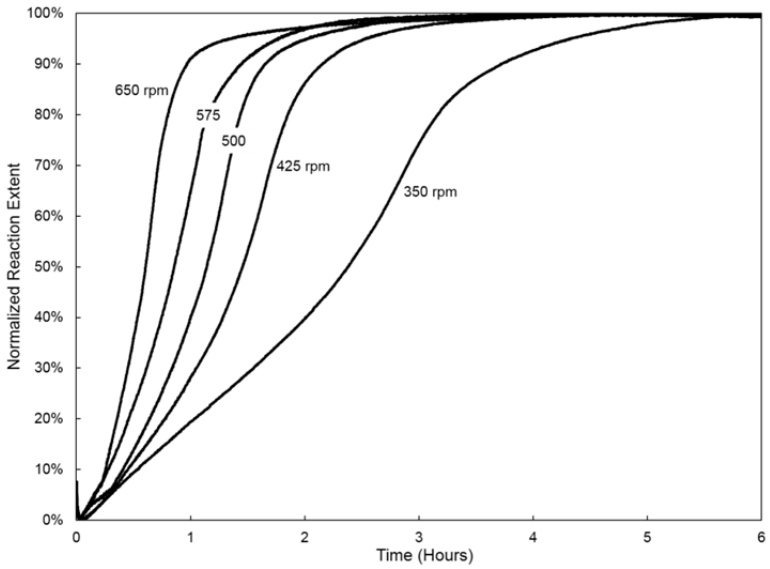

Figure A.8 Normalized nitrogen consumption during the reactive ball milling of five grams of elemental dysprosium in dry nitrogen for six hours in a planetary ball mill at various milling intensities. The uptake was calculated using the ideal gas law and the *in situ* temperature and pressure data recorded at 0.2 Hz. It is seen that the reaction kinetics decrease with milling intensity.

The effect of milling intensity on the resultant phase(s) of the free powder is shown in the XRD patterns in Figure A.9. From this figure, it appears to take longer than 6 hours of milling at 350 rpm to complete the dysprosium to DyN reaction, as evidenced by minor elemental HCP dysprosium peaks in the diffraction pattern. However, the reaction appeared to have reached completion at all greater milling intensities and a secondary, unidentified phase begins to appear after 6 hours of milling at 575 rpm.

The effect of milling intensity on the resultant powder morphology of the free powder is shown in the PSA and SEM images of Figure A.10. The volume-based particle size distribution plots of powders from each milling intensity are slightly bi-modal. There exists a mode at approximately 0.2 μm with a small volume fraction of powder but the mode at 2.6 μm dominates and contains a majority of the volume of the powder. All of the particles appeared to be less than 11 μm in size. Additionally, the powder retrieved

from the 650 rpm milling run had a narrower particle size distribution but is still centered at 2.6 μm. The SEM images show more irregular particle morphologies as the milling intensity is increased.

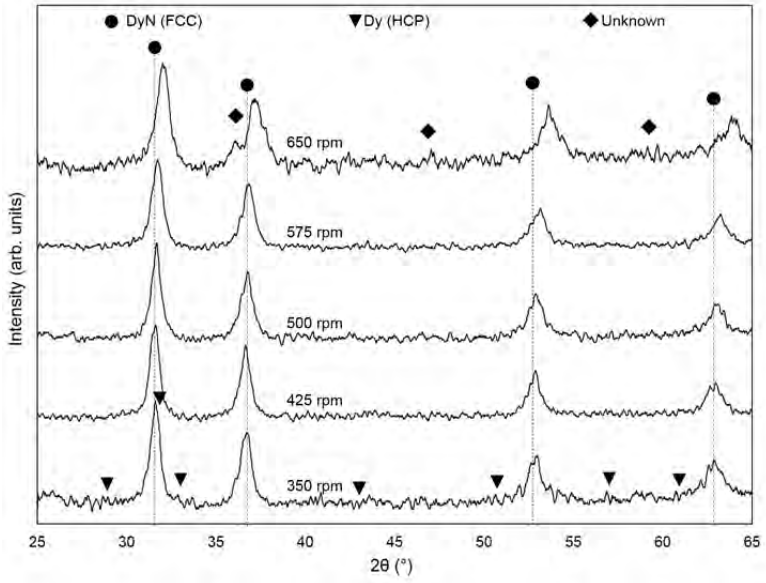

Figure A.9 X-ray diffraction patterns of the powders resulting from reactive milling elemental dysprosium in dry nitrogen for six hours at various milling intensities. In each case, a phase pure DyN was formed.

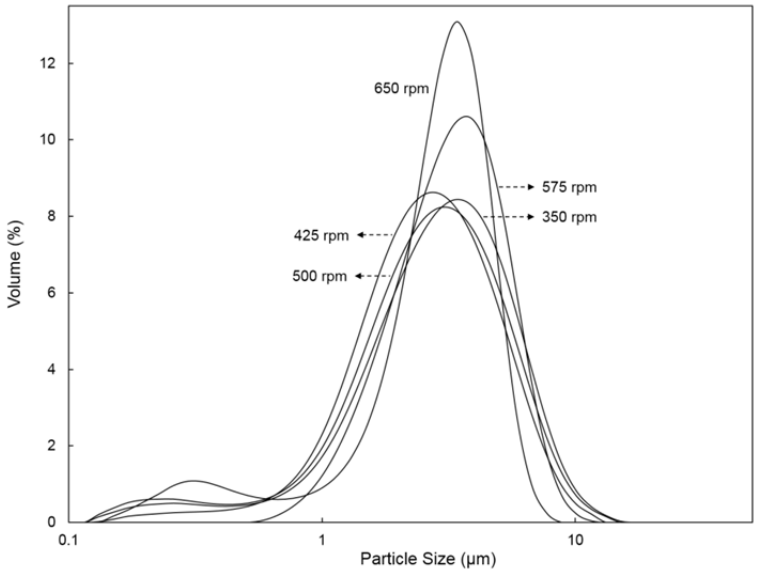

a)

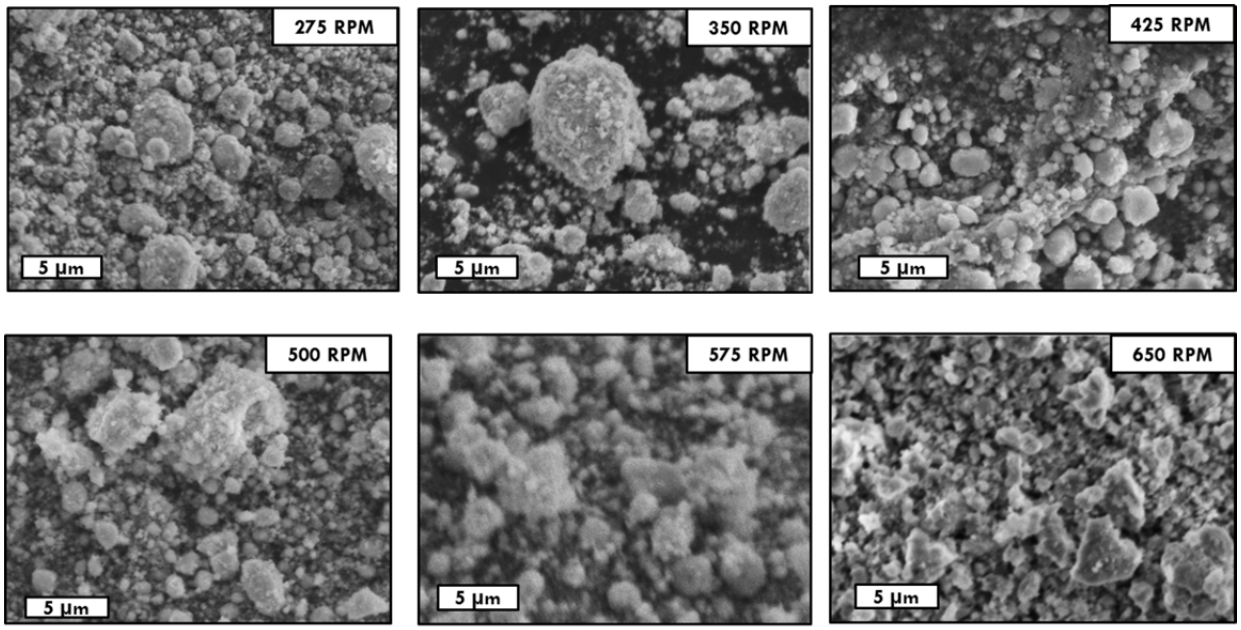

b)

Figure A.10 The particle size distribution (a) and morphology (b) obtained from free powder resulting from reactive milling elemental dysprosium in dry nitrogen for six hours at various milling intensities. The particle size distribution suggests that, regardless of the milling intensity, the average particle size was approximately 2.6 µm, which is supported by the SEM images.

A.4 Discussion

For the first time reported in literature, the rate of a nitridation reaction through RM in a PBM has been observed via *in situ* temperature and pressure measurements. Furthermore, RM in a PBM to form a lanthanide nitride has never been published other than previous work of this group [7-10]. Of other authors that have presented *in situ* pressure and temperature data, the ideal gas law was used to quantify the gas consumption in the milling vessel presumably because it is a robust and simple equation that is assumed to be valid with reasonable accuracies at the milling temperatures and pressures investigated [35, 37, 38, 40]. To be consistent with literature, the ideal gas law was also used for the work presented here. However, Cengel *et al.* [42] predict that the

Benedict-Webb-Rubin equation of state (BWREoS) will have a 0.0% associated error at 200-300 K and 200-1000 kPa, similar to the parameters of the studies presented here. The BWREoS, which has 8 empirical constants, is derived from virial equations to the following equation:

$$P = \frac{R_u T}{\bar{v}} + \left(B_0 R_u T - A_0 - \frac{C_0}{T^2}\right)\frac{1}{\bar{v}} + \frac{bR_u T - a}{\bar{v}^3} + \frac{a\alpha}{\bar{v}^6} + \frac{c}{\bar{v}^3 T^2}\left(1 + \frac{\gamma}{\bar{v}^2}\right) e^{-\gamma/\bar{v}^2} \quad (3)$$

where the P is pressure, R_u is the universal gas constant, T is the temperature, $\bar{v}$ is the molar volume, and the other variables are predetermined empirical constants specific to nitrogen, as defined in Table A.1 [42].

Table A.1 Empirical constants used in Eq. 3 [42] to estimate nitrogen consumption using in situ temperature and pressure data collected during the RM of dysprosium to form DyN.

a	A_0	b	B_0	c	C_0	α	γ
2.54	106.73	0.002328	0.04074	7.379E4	8.164E5	1.272E-4	0.0053

When the two equations of state are applied to the *in situ* temperature and pressure data from the PBM of dysprosium, a vertical shift in the calculated nitrogen consumption was observed. The maximum vertical shift, shown in Figure A.11 for a milling intensity of 500 rpm, increases nearly linearly with milling intensity and in each case, the BWREoS predicts a greater nitrogen consumption rate than does the ideal gas law, as shown in Table A.2. Table A.2 shows the time within each milling intensity that a maximum error is observed resulting from using the BWREoS versus the ideal gas law. The error is calculated as the difference between values predicted by each equation of state relative to the maximum theoretical nitrogen consumption of 5 grams of dysprosium, which is 15.4 mMoles of N_2. Table A.2 also shows the time at which the

maximum nitrogen consumption rate is observed for each milling intensity, which was found using the first derivative of the consumption data calculated using the ideal gas law. A nearly linear relationship was observed between the milling intensity, the maximum observed error, and the time where the maximum error was observed.

The observations presented here suggest that the ideal gas law tends to underestimate the amount of nitrogen consumed during RM by 2 – 3%. However, when considering reaction rates, the first derivative of the moles consumed versus time is the primary factor and small linear shifts of the amount of moles consumed due to the equation of state calculations (within the temperature range observed) are inconsequential.

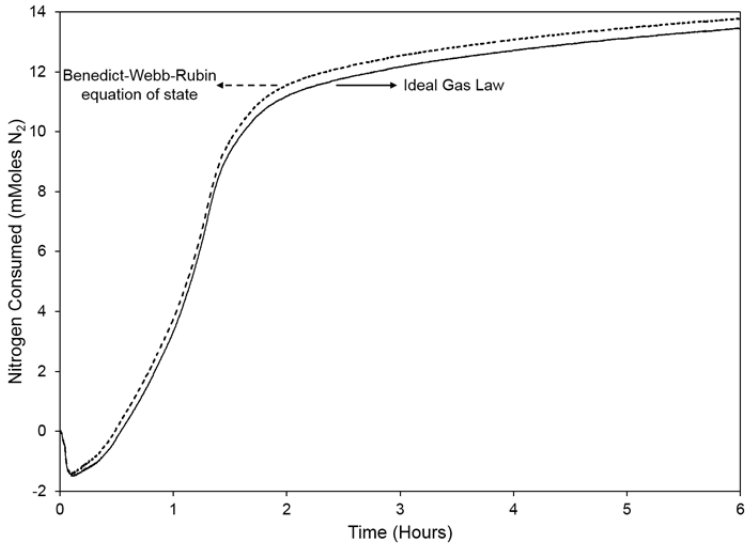

Figure A.11 Plot showing the variance in the nitrogen consumption calculated using the ideal gas law and the Benedict-Webb-Rubin equation of state throughout the reactive ball milling of five grams of elemental dysprosium in dry nitrogen to form DyN at 500 rpm and a BPR of 14:1. The variance from the two calculations varies from 1.9% at 350 rpm to 3.5% at 650 rpm, with the ideal gas law always predicting less nitrogen consumption.

Table A.2 Table showing the effects of calculating the nitrogen consumption using the in situ temperature and pressure data in the Benedict-Webb-Rubin equation of state versus the ideal gas law. It is seen that the maximum error observed between the two models occurs before the maximum nitrogen consumption rate is observed.

Milling intensity (rpm)	Time to maximum observed error (min)	Maximum error observed	Time to maximum N_2 consumption rate (min)
350	81	1.9%	175
425	66	1.8%	100
500	56	2.7%	78
575	38	3.1%	51
650	32	3.7%	39

The peculiar temperature and pressure behavior that is observed at the beginning of the milling process (Figure A.4), which also becomes more pronounced with milling intensity, was observed by a few authors studying the hydrogenation of magnesium and magnesium alloys [14, 35-37]. In this prior work, the temperature increase during the first 30 minutes of milling was attributed to the "mechanical action" of the mill. The initial behavior of pressure was attributed to an "incubation period," where a critical number of defects are created before the dissociation of H_2 and subsequent diffusion into the bulk magnesium can occur (marked by the onset of decreasing pressure). Doppiu *et al.* [36] present traces at hydrogen pressures ranging from 1 – 8 MPa which show a significant decrease in the "incubation period" and increase in the hydrogen absorption rate with increasing initial hydrogen pressure. The authors proposed two regions of hydrogen uptake: hydrogen absorption and nucleation of the hydride phase, with the latter of the two being much slower and only happening after a significant amount of hydrogen is absorbed and dissolved into the magnesium. However, in the case of rare earth elements, the tendency for nitrogen dissolution is low and it has been shown that diatomic nitrogen

will preferentially dissociatively chemisorb on clean dysprosium surfaces at 300 K rather than be adsorbed and subsequently dissolved into the metal [43]. It is therefore postulated that as fresh surface is created through the milling process, nitrogen will spontaneously dissociate on the dysprosium surfaces. Since it is thought that the dissolution of nitrogen in dysprosium is low, it will nearly instantaneously form DyN at a rate that is directly proportional to the creation of fresh, clean surfaces (which is a function of the number of media, the media impact frequency, and the media impact energy) and is further described and modeled in a concurrent publication [41].

To better understand the influence of the milling process on the apparent nitrogen consumption behavior, the effects observed in temperature and pressure traces during the early stages of RM were investigated. The first experiment to sort out discrepancies in the early stages of the milling process was to better understand the lag in sensing between the temperature and pressure monitors. It is assumed that a large fraction of the heat input into the milling vessel is contributed by the electrical motor and the mill itself via conduction through the bottom of the milling vessel where the mill and the vessel were in contact. Accordingly, a milling vessel that was loaded, sealed, and pressurized was placed on a hot plate preheated to 332 K while temperature and pressure data were recorded with the sensor lid. The resultant data from the sensing lid is shown in Figure A.12 (the apparent change in nitrogen content is shown in the inset and was calculated using the ideal gas law).

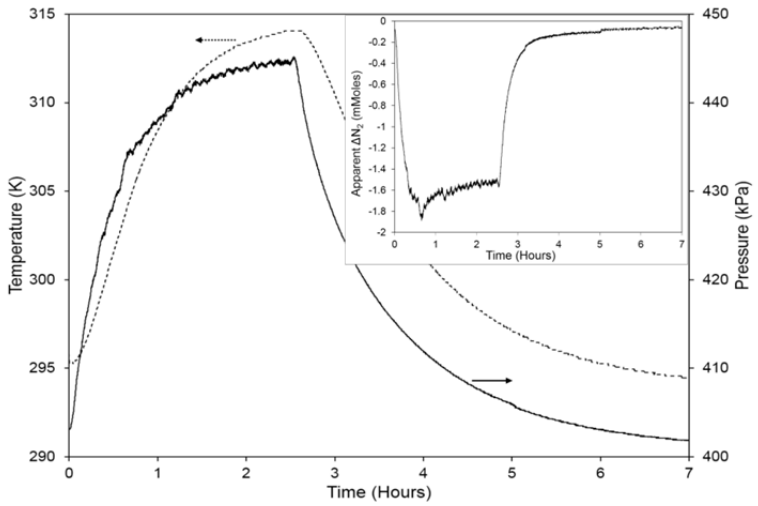

Figure A.12 Temperature and pressure behavior sensed by the sensing lid when the milling vessel assembly is placed on a constant heat source of 332 K and removed after 2.5 hours. The inset shows the effects of the readings on the apparent change in nitrogen content as calculated using the ideal gas law. Note: the effects are an order of magnitude less than the consumption in the Dy + N_2 → DyN reaction.

The temperature sensed at the top of the vessel (where the temperature sensor is located) reached an equilibrium in 2.5 hours at a temperature of 314 K, or 18 K cooler than the heat source. Once the temperature and pressure were both near equilibrium, the vessel was removed from the heat source and placed on an insulated bench at room temperature, where it took an additional 4.5 hours to cool back to room temperature. From the collected data, a 5 minute lag was observed in the temperature reading compared to the pressure reading even under static conditions. The temperature discrepancy between the source and the sensor is presumed to be due to natural convective losses to the surrounding environment causing a temperature gradient from the heat source at the bottom of the vessel to the temperature sensor at the top of the vessel. Additionally, by assuming the heat source is at the bottom of the vessel and that the convection is the main source of heat loss resulting in a temperature gradient, it is reasonable to assume that the temperature gradient will increase with milling intensity.

As the mill is rotating faster, a higher flow of air is passed over the milling vessel and convective cooling becomes more prominent. In any case, it is presumed that the temperature of the atmosphere within the milling vessel is at an intermediate temperature value that falls between the value at the heat source and that of the sensor.

The rise in pressure during the constant heat source experiment is the result of gas expansion with increasing temperature in a constant volume. The discrepancy in temperature (as described above and shown in the inset of Figure A.12) between the mean temperature of the vessel and that measured by the sensor in the milling lid results in an apparent consumption of nitrogen, as calculated by the ideal gas law. This apparent nitrogen consumption was solely the effect of non-equilibrium conditions (temperature) within the vessel.

To quantify the relative contributions of the mill, milling media impacts, and mechanical deformation of dysprosium to the heat generation measured by the pressure and temperature sensors, the milling process was duplicated with and without milling media and dysprosium. The results are shown in Table A.3, with the error determined from the standard deviation of at least 3 milling runs. When a sealed vessel was milled with no media and no dysprosium, the average temperature and pressure increases were 11 K and 1 kPa, respectively. The temperature and pressure both increased with the addition of milling media and again with addition of dysprosium. The data collected with the YSZ media and the 5 grams of dysprosium to create the 18 K and 22 kPa increases in temperature and pressure are seen in Figure A.4.

Table A.3 The effects of the media and dysprosium charge on the in situ temperature and pressure increase observed in the initial stages of milling dysprosium in nitrogen at 500 rpm with a 14:1 BPR of 5 mm diameter YSZ milling media (184 spheres) and dysprosium filings.

	Temperature increase (K)	Pressure increase (kPa)
Media and Dy	18 ± 1	22 ± 1
Media only	16.5 ± 0.2	16 ± 3
No charge	11 ± 1	1 ± 2

From these experiments, it was found that approximately 61% of the heat measured during milling is due to the mill itself balanced with the heat dissipation by convection and conduction during the milling process. The addition of media alone causes an additional 31% increase, and the addition of dysprosium to the milling process accounts for only the remaining 8% of the measured heat generation, or a statistical increase of approximately 1.5 K when 5 grams of dysprosium is added to the milling vessel. The additional heat increase from the addition of dysprosium can be explained by a decrease in coefficient of restitution of the milling media as dysprosium cold welds to the media and vessel walls in the early stages of milling, as shown in Figure A.5 (a concept that is more thoroughly explained and modeled in a concurrent publication [41]). As the coefficient of restitution of the milling media decreases, it suggests that collisions become less elastic and result in greater energy transfer to the milling vessel during media impact events, further increasing the temperature measured. These results indicate that, contrary to publications on hydrogenation of metals, most of the pressure and temperature increase at the beginning of a milling run may be attributed to the mill itself along with heat dissipation from milling media rather than any specific “mechanical action” on the milled material.

A.5 Conclusions

An experimental method has been developed and implemented to quantitatively assess the *in situ* nitrogen consumption during RM elemental dysprosium in a PBM to form DyN at ambient temperatures. To the best of the author's knowledge, *in situ* nitrogen consumption in a PBM has not been presented for *any* element in the literature to date; although there are publications that have used *in situ* monitoring to study hydrogen uptake in the synthesis of hydrogen storage materials in a PBM. This study presents an understanding of the effects of the mill on the apparent rate of nitrogen consumption at the beginning and end of the milling cycle to allow future researchers to deduce these effects from the RM process. The Dy-N system is a model system to develop an understanding of RM in a PBM due to the fact that no intermediate phases are known to exist in the Dy-N system other than stoichiometric DyN. However, the lack of thermodynamic data available in the literature for the Dy-N system complicates the assessment. It is presumed that the rate of the nitridation reaction of dysprosium is limited by the creation of fresh, reactive surfaces which catalyze the dissociation of diatomic nitrogen and allow for the spontaneous formation of DyN. The rate of creation of such fresh surfaces can be controlled by the milling intensity or the number of media, which are both related to the number of impacts per unit time.

The results of this investigation demonstrate that advanced nitride ceramics, which traditionally require long durations at high temperatures in hazardous atmospheres, can be synthesized in short times, at low temperatures, and in a closed system. This scalable process produces a final product that has a homogenous and fine microstructure that can be easily shaped and consolidated using conventional sintering processes.

A.6 Acknowledgements

This work was partially funded through a Nuclear Energy Research Initiative contract (NERI – DE-FC07 – 05ID14650).

A.7 References

[1] Thomason JS, Atwell RJ, Bajraktari Y, Bell JP, Barnett DS, Karvonides NSJ, Niles MF, Schwartz EL. From national defense stockpile (NDS) to strategic materials security program (SMSP): evidence and analytic support. vol. 1: Institute for Defense Analysis, 2010.

[2] Hoenderdaal S, Espinoza LT, Marscheider-Weidemann F, Graus W. Energy 2013;49:344.

[3] Kilbourn BT. A Lanthanide Lanthology: Part I, A-L. Fairfield, NJ USA: Molycorp, Inc., 1993.

[4] Zhou YK, Kim MS, Teraguchi N, Suzuki A, Nanishi Y, Asahi H. Phys. Status Solidi B-Basic Res. 2003;240:440.

[5] Thiede TB, Krasnopolski M, Milanov AP, de los Arcos T, Ney A, Becker HW, Rogalla D, Winter J, Devi A, Fischeri RA. Chem. Mat. 2011;23:1430.

[6] Li XJ, Zhou YK, Kim M, Kimura S, Teraguchi N, Emura S, Hasegawa S, Asahi H. Chin. Phys. Lett. 2005;22:463.

[7] Butt DP, Jaques BJ, Osterberg DD, Marx BM, Callahan PG, Hamdy AS. New routes to lanthanide and actinide nitrides. GLOBAL 2009: The Nuclear Fuel Cylcle: Sustainable Options and Industrial Perspectives, September 6, 2009 - September 11, 2009. Paris, France, 2009.

[8] Jaques B, Butt DP, Marx BM, Hamdy AS, Osterberg D, Balfour G. Synthesis and characterization of actinide nitrides. GLOBAL 2007: Advanced Nuclear Fuel Cycles and

Systems, September 9, 2007 - September 13, 2007. Boise, ID, United states: American Nuclear Society, 2007. p.591.

[9] Jaques BJ, Marx BM, Hamdy AS, Butt DP. Journal of Nuclear Materials 2008;381:309.311.

[10] Callahan PG, Jaques BJ, Marx BM, Hamdy AS, Butt DP. Journal of Nuclear Materials 2009;392:121.

[11] Takano M, Itoh A, Akabori M, Minato K. Journal of Physics and Chemistry of Solids 2005;66:697.

[12] Takano M, Tagami S, Minato K, Kozaki T, Sato S. Journal of Alloys and Compounds 2007;439:215.

[13] Suryanarayana C. Progress in Materials Science 2001;46:1.

[14] Huot J, Ravnsbæk DB, Zhang J, Cuevas F, Latroche M, Jensen TR. Progress in Materials Science 2013;58:30.

[15] Baláz P. Mechanochemistry in nanoscience and minerals engineering. Berlin; London: Springer, 2008.

[16] Calka A, Nikolov JI. Nanostructured Materials 1995;6:409.

[17] Liu L, Lu L, Chen L, Qin Y, Zhang LD. Metall. Mater. Trans. A-Phys. Metall. Mater. Sci. 1999;30:1097.

[18] Chen Y, Li CP, Chen H, Chen YJ. Sci. Technol. Adv. Mater. 2006;7:839.

[19] Chen Y, Fitz Gerald J, Williams JS, Bulcock S. Chemical Physics Letters 1999;299:260.

[20] Chen Y, Halstead T, Williams JS. Materials Science & Engineering A (Structural Materials: Properties, Microstructure and Processing) 1996;206:24.

[21] Sun JF, Wang MZ, Zhao YC, Li XP, Liang BY. Journal of Alloys and Compounds 2009;482:L29.

[22] Sun JF, Li XP, Liang BY, Zhao YC, Wang MZ. Journal of Inorganic Materials 2009;24:759.

[23] El-Eskandarany MS, Ashour AH. Journal of Alloys and Compounds 2000;313:224.

[24] Gotor FJ, Alcala MD, Real C, Criado JM. Journal of Materials Research 2002;17:1655.

[25] Real C, Roldan MA, Alcala MD, Ortega A. Journal of the American Ceramic Society 2007;90:3085.

[26] Roldan MA, Lopez-Flores V, Alcala MD, Ortega A, Real C. Journal of the European Ceramic Society 2010;30:2099.

[27] Qin Y, Liu L, Chen L. Journal of Alloys and Compounds 1998;269:238.

[28] Nikolov JI, Williams JS, Llewellyn DJ, Calka A. Phase evolution during ball milling of Al in NH3 and subsequent annealing. Warrendale, PA, USA: Mater. Res. Soc, 1998. p.649.

[29] Lee P-Y, Lin C-K, Chang C-L, Hwu Y, Chin T-S. Preparation of Iron nitride powders through mechanical alloying and atmospheric heat treatment. Kyongju, South Korea: IEEE, 1999. p.13.

[30] Lee M, Endoh S, Iwata H. Advanced Powder Technology 1997;8:291.

[31] Yuan Q, Zheng Y, Yu H. International Journal of Refractory Metals and Hard Materials 2009;27:121.

[32] Kano JY, Kobayashi E, Tongamp W, Saito F. Journal of Alloys and Compounds 2008;464:337.

[33] Kameshima Y, Irie M, Yasumori A, Okada K. Mechanochemical effect on low temperature synthesis of AlN by direct nitridation method. 15th International Symposium on the Reactivity of Solids (ISRS), 9-13 Nov. 2003, vol. 172. Netherlands: Elsevier, 2004. p.185.

[34] Trapp J, Kieback B. Acta Materialia 2013;61:310.

[35] Zhang JX, Cuevas F, Zaidi W, Bonnet JP, Aymard L, Bobet JL, Latroche M. J. Phys. Chem. C 2011;115:4971.

[36] Doppiu S, Schultz L, Gutfleisch O. Journal of Alloys and Compounds 2007;427:204.

[37] Deledda S, Hauback BC. Nanotechnology 2009;20:204010 (7 pp.).

[38] Deledda S, Hauback BC. Faraday Discussions 2011;151:315.

[39] Junxian Z, Pilette MA, Cuevas F, Charpentier T, Mauri F, Latroche M. J. Phys. Chem. C 2009;113:21242.

[40] Cuevas F, Korablov D, Latroche M. Physical Chemistry Chemical Physics 2012;14:1200.

[41] Alanko GA, Osterberg DD, Jaques BJ, Hurley MF, Butt DP. Acta Materialia 2014;Submitted.

[42] Çengel YABMA. Thermodynamics : an engineering approach. Boston: McGraw-Hill, 2002.

[43] Schreifels JA, Deffeyes JE, Neff LD, White JM. Journal of Electron Spectroscopy and Related Phenomena 1982;25:191.